UNDERSTANDING DROUGHT IN THE CARIBBEAN

A Dissertation

Presented to the Faculty of the Graduate School

of Cornell University

In Partial Fulfillment of the Requirements for the Degree of

Doctor of Philosophy

by

Dimitris Alexander Herrera Hernandez

May 2018

UNDERSTANDING DROUGHT IN THE CARIBBEAN

Dimitris Alexander Herrera Hernandez, Ph. D.

Cornell University 2018

ABSTRACT

This work analyzes drought variability, its trends, and its dynamics in the Caribbean, using instrumental records, reanalyses, and global climate model simulations for the periods 1950–2016 and 1979–2016. We use the self-calibrating Palmer Drought Severity Index (scPDSI) with the UN Food and Agriculture Organization (FAO) reference evapotranspiration to construct the first high-resolution (4 km) drought atlas for the Caribbean spanning 1950 to near-present. We find a significant drying in the Caribbean and Central America, which contrast with a relatively (but not-significant) wetting of Florida Peninsula during the period analyzed. We also find that the 2013–2016 "Pan-Caribbean drought" is the worst dry interval observed in the Caribbean during the period analyzed, and according to our results, anthropogenic warming contributed to 16–18% of its severity. Anthropogenic warming also contributed to ~7% of the Caribbean Islands that experienced drought conditions during the Pan-Caribbean drought, which roughly represents ~16,800 km^2. We also find that during droughts that occurred in 1997–1998, 2009–2010, and 2013–2016, a predominant moisture divergence over the Caribbean Sea and northeastern South America correlates to anomalous dry conditions and negative precipitation minus evaporation ($P–E$) values in the Caribbean. However, moisture convergence is also observed at local scales during these droughts, especially on the eastern coast of Central America and Florida Peninsula. These results are consistent with previous work that suggest a strong moisture divergence in northeastern South America as a critical driver of drought during El Niño events in northeastern South America and/or southeastern Caribbean Islands.

The results from this dissertation provides further insights into the nature of drought in the Caribbean and Central America, useful for researchers and stakeholders alike. This is especially important, since climate models consistently project a significant drying over the Caribbean and Central America the coming decades due to anthropogenic climate change.

BIOGRAPHICAL SKETCH

Dimitris Herrera was born and raised in the Dominican Republic, and since childhood, he has been curious and fascinated by hurricanes, convective storms, and seasonal haze from the Saharan dust. Dimitris also remembers his family struggling with drought many times, as they relied on the rainy season to irrigate their crops, making them susceptible to unexpected dry intervals. Witnessing his own family's climate vulnerability has motivated Dimitri's research on drought variability in the Caribbean and Central America, which he began during his M.S. at the National Autonomous University of Mexico (UNAM, Mexico), and continued with his Ph.D. in atmospheric science at Cornell, working with Dr. Toby Ault. Dimitris' doctoral dissertation aimed to understand hydroclimate variability and its dynamics in the Caribbean and Central America, and how climate change might increase drought risk across these regions. As part of his research, Dimitris published the first high-resolution (4 km) drought atlas for the Caribbean, which spans 1950–near present based on monthly estimates of the "self-calibrating" Palmer Drought Severity Index (scPDSI), and it is freely available at: http://ecrl.eas.cornell.edu/node/56. This atlas served as the high-resolution observational basis for his doctoral research on monitoring, diagnosing, and predicting the dynamics of drought in the Caribbean, in an effort to provide actionable information to families like his own and improve their resilience to climate extremes. Dimitris envisions himself as a climate scientist working on tropical hydroclimate variability and its dynamics, with especial emphasis in the Caribbean region.

To Keanu and Evan.

ACKNOWLEDGMENTS

Thank you God for your support during my Ph.D.; I would not have this done without you. I am thankful for the time, faith, and energy that my advisor, Dr. Toby Ault, had pushed on my research. I also want to thank my committee members, Drs. Arthur DeGaetano, Susan Riha, and Natalie Mahowald, for their valuable contributions to make this work better. I am especially grateful with Dr. John Fasullo, for his mentorship and advise during my doctoral stance at the National Center for Atmospheric Research (NCAR). I received the support of my working group members, Dr. Carlos Carrillo and Rick Moore, and my fellows Grace Li, Colin Evans, Brandon Benton, and Thomas Ehrmann. I further appreciate the love and encourage that I had received from my family, especially from my parents Rafael Herrera and Pilar Hernandez; my siblings, Hector and Anniola Herrera. Financial support to this work had come from the NSF grants EaSM2 AGS-1243125 and AGS-160256, the Fulbright Program, the Advanced Study Program (NCAR), the Warner Internship for Scientific Enrichment (NCAR), and the First Presbyterian Church Ithaca.

TABLE OF CONTENTS

LIST OF FIGURES

CHAPTER 1: INSIGHTS FROM A NEW HIGH-RESOLUTION DROUGHT ATLAS FOR THE CARIBBEAN SPANING 1950–2016

CHAPTER 2: EXACERBATION OF THE 2013–2016 PAN-CARIBBEAN DROUGHT BY ANTHROPOGENIC WARMING

LIST OF TABLES

INTRODUCTION

The Caribbean and Central America is home to more than 90 million people (CIA, 2013) who rely on the annual rainy season for agriculture, tourism, hydropower generation, and municipal water usage. These regions, in particular the Caribbean Islands, are vulnerable to drought due to their relatively small areas, inherent isolation, and a deficient large scale infrastructure for capturing and storing water. In fact, according to the UN Food and Agriculture Organization (FAO), the Caribbean holds seven of the 36 most water-stressed countries in the world, in which Barbados is among the world's top ten countries with less than 1,000 m^3 of freshwater per capita (FAO, 2016). Agriculture and tourism sectors—which provided ~73% of the shared gross domestic product (GDP) of the Caribbean in 2016[1]—are usually the most impacted by drought because they depend directly on rain to supply their freshwater needs. For example, according to the FAO, in 2016 over 80% of farms in the Caribbean and Central America used rainfed irrigation, making them highly vulnerable to unexpected severe and prolonged dry intervals. As compared to other drought-prone regions, such as the American Southwest, freshwater deficits in the Caribbean cannot be resolved by moving water large distances. Furthermore, technologies like desalination plants cannot be implemented as a long-term solution because of their elevated operational costs, given economical constrains of most countries in the Caribbean and Central America (FAO, 2016).

Although natural disasters associated with tropical cyclones (e.g., hurricanes Irma and Maria in 2017) in the Caribbean and Central America usually attract public attention, slow but persistent droughts have also caused losses comparable to hurricanes (e.g., OCHA 2015a,b; Peters 2015), and they often receive much less recognition. During the "Pan-Caribbean drought" between 2013 and 2016, for example, many staple crops were severely affected by the drought in both regions. In some cases, such as in El Salvador, Guatemala, and Honduras, crop yields of corn and beans were reduced by

[1] https://www.statista.com/statistics/699081/share-of-economic-sectors-in-gdp-in-latin-america-and-caribbean/

75–100% by October 2015 (OCHA 2015b). This drought further pushed more than 4 million people into food insecurity in the Caribbean and Central America, and worsened the situation of another 3.8 million food insecure people in Haiti. Similarly, droughts that occurred in 1997–1998 and 2009–2010 also caused important losses in agriculture, which resulted in significant increases of local food prices (Peters 2015; FAO 2016). These statistics indicate that, although hurricane-driven disasters can cause significant and rapid damage, gradual but persistent droughts can also wreak havoc in vulnerable countries like those of the Caribbean and Central America.

In addition to the current challenges that Caribbean and Central American nations confront in terms of freshwater availability, most of the current global climate models suggest an even worse scenario in the near future as a result of anthropogenic climate change (IPCC 2014). Climate models consistently project up to 50% less rain in certain areas of the Caribbean, while an increased evaporative demand of moisture by the atmosphere is also expected due to higher temperatures (IPCC 2014). This picture is further complicated by groundwater contamination due to higher saltwater intrusions and rising sea levels. Understanding drought variability, its trends, and its causes in the Caribbean and Central America is therefore critical to accurately assess future drought risk in these regions, to improve drought predictability across various spatial and temporal scales, and to improve societal resiliency and adaptation capacity.

This dissertation analyzes drought variability, its trends, and the dynamical and thermodynamical causes underpinning droughts in the Caribbean and Central America between 1950 and 2016 using various tools and climate datasets. This work is organized with the following sections: (i) the first chapter, in which we introduce our high-resolution the Caribbean drought atlas, (ii) the second chapter in which we analyze the relative contribution of anthropogenic warming to the Pan-Caribbean drought, (iii) the third chapter, where we assesses the dynamical and thermodynamical causes of three observed droughts in the Caribbean and Central America, and (iv) the conclusions, where we summarizes the major findings of this work and describes their implications.

In the first chapter—published in *Journal of Climate* (https://journals.ametsoc.-org/doi/abs/10.1175/JCLI-D-16-0838.1)—we describe and assess drought variability and its trends across the Caribbean and Central America. We introduce and use for such analyses our high-resolution drought atlas at 4 km lat/lon. A high-resolution drought product is needed in these regions to capture the influence of topography in modulating drought variation at local scales, as well as for resolving small islands of the Lesser Antilles, most of them invisible in the current global drought datasets (e.g., Dai, 2004; 2011; Vicente-Serrato et al. 2010; Sheffield et al. 2012; van der Schrier et al. 2013). Our drought atlas was developed using statistically downscaled products, and it spans from 1950 to 2016. We use monthly estimates of the "self-calibrating" Palmer drought severity index (scPDSI) (Palmer 1965; Wells et al. 2004) with the FAO reference potential evapotranspiration method (Allen et al. 1998). In this chapter, we also provide further insights into teleconnection patterns between the tropical Pacific and North Atlantic, specifically teleconnections with El Niño-Southern Oscillation (ENSO). Among other findings, we found that the 2013–2016 Pan-Caribbean drought is the most severe and extended drought during the period analyzed, and that the Caribbean and Central America have been experiencing a significant drying trend since 1950 as observed with scPDSI, although trends in precipitation anomalies are not significant.

Because of the unprecedented characteristic of the 2013–2016 Pan-Caribbean drought, in the second chapter we analyze the role of anthropogenic warmth on this drought. To do so, we use a modified method implemented in Williams et al. (2015), in which linearly-detrended temperature data are used to calculate the potential evapotranspiration and scPDSI. As in the first chapter, we use our Caribbean drought atlas and downscaled products to conduct this work. Results from observed climate data are then compared to climate models from the fifth phase of the Climate Model Intercomparison Project (CMIP5) to isolate the natural variability contribution from the anthropogenically-forced variability, and assessed for consistency with NASA Clouds and Earth's Radiant Energy System (CERES) (Loeb et al. 2012). Although climate models are consistent in showing a significant decrease in rain in the Caribbean with increased anthropogenic greenhouse gases, in this work we do not evaluate the

anthropogenic contribution to precipitation because anthropogenic-forced changes in precipitation are less certain than that for temperature. Nevertheless, our findings suggest that anthropogenic climate change is already increasing drought risk in the Caribbean through temperature effects on potential evapotranspiration, and that Pan-Caribbean drought-like dry intervals will be likely more common in the near future due to climate change. This chapter is an article currently under review in *Science Advances*.

In the third chapter, we evaluate the dynamical and thermodynamical processes underpinning three major droughts in the Caribbean and Central America between 1979 and 2016. Because of constrains in climate data required for such analyses, we could not evaluate droughts since 1950 but only from 1979. We calculated the moisture budgets, sea surface temperature, precipitation, and large-scale anomalies during droughts that occurred in 1997–1998, 2009–2010, and 2013–2016. The analysis from observations is complemented with the use of climate model outputs from the National Center for Atmospheric Research (NCAR) Community Earth System Model Large Ensemble (CESM–LENS). Our findings indicate that a persistent moisture divergence over the Caribbean Sea is present during the droughts analyzed, which is consistent with anomalies in vertically-integrated moisture transports. Furthermore, a "seesaw" pattern is also noticeable between the tropical Pacific and North Atlantic during drought in these regions. That it, a warmer than normal tropical Pacific is associated with drought in the Caribbean (especially the eastern portion) and Central America, and this usually occur along with colder temperatures in the tropical North Atlantic. The opposite is often observed with pluvials in these regions, in which tropical North Atlantic exhibits much warmer temperatures. This chapter is part of an article currently in preparation to be submitted to *Climate Dynamics*.

Finally, in the last section, the conclusions and implications of this dissertation, we summarize the major findings and contributions of this work, and describe its potential impacts for the Caribbean and Central America. In this section we further suggest future work required to fully understand the drying trend projected by climate models, as well as the dynamics behind such a trend.

CHAPTER 1
INSIGHTS FROM A NEW HIGH-RESOLUTION DROUGHT ATLAS FOR THE CARIBBEAN SPANING 1950–2016

DIMITRIS HERRERA AND TOBY AULT

Department of Earth, and Atmospheric Sciences, Cornell University, Ithaca, New York, 14853.

Abstract

Climate change is expected to increase the severity and frequency of drought in the Caribbean. Understanding drought variability and its trends is therefore critical for improving resiliency and adaptation capacity of this region, as well as for assessing the dynamics and predictability of regional hydroclimate across spatial and temporal scales. This work introduces a first of its kind high-resolution drought dataset for the Caribbean region from 1950 to 2016, using monthly estimates of the "self-calibrating" Palmer drought severity index (scPDSI), with the physically based Penman–Monteith approximation for the potential evapotranspiration. Statistically downscaled data products, including reanalysis, are employed to establish an historical baseline for characterizing drought from 1950 to the near present. Since 1950, the Caribbean has been affected by severe droughts in 1974–1977, 1997–1998, 2009–2010, and 2013–2016. Results indicate that the 2013–2016 drought is the most severe event during the time interval analyzed in this work, which agrees with qualitative reports of many meteorological institutions across the Caribbean. Linear trends in the scPDSI show a significant drying in the study area, averaging an scPDSI change of –0.09 decade^{-1} (p<0.05). However, this trend is not homogenous, and significant trends toward wetter conditions in portions of the study area were observed. Results further indicate a strong influence of both tropical Pacific and North Atlantic oceans in modulating drought variability across the study domain. Finally, this effort is the first step in building high-resolution drought products for the Caribbean to be updated regularly, with the purpose of drought monitoring and eventually seasonal drought prediction.

1. Introduction

Droughts are among the deadliest and costliest natural phenomena, leading to food shortages and annual losses of billions of dollars worldwide (e.g., Wilhite et al. 2007; Howitt et al. 2014). Although droughts do not unfold as rapidly as other meteorological hazards (e.g., hurricanes or floods), their duration can put food security, water storage, and even energy production at risk. A drought is usually characterized by below-normal precipitation, and often associated with above-normal temperatures that may span from several months to years and, in some cases, decades (Dai 2011; Cook et al. 2016). From observations and model simulations, previous studies have shown an increase of the global drought area since 1950 (Dai et al. 2004; Dai 2011, 2013; Dai and Zhao 2017; van der Schrier et al. 2013; Cook et al. 2015). These findings further correspond to increasing global temperatures and hence evaporative demand, which in turn has been identified as a crucial driver in the observed trend (Dai 2013; Dai and Zhao 2017; van der Schrier et al. 2013; Cook et al. 2015; Zhao and Dai 2015). Furthermore, projections from phases 3 and 5 of the Coupled Model Intercomparison Project (CMIP3 and CMIP5) have suggested a substantial increase in global aridity by the end of the twenty-first century as a consequence of rising concentrations of greenhouse gases (Dai 2013; IPCC 2014; Ault et al. 2014; Cook et al. 2015; Zhao and Dai 2015). Model simulations also indicate that the greatest decline in precipitation will occur in certain areas of the tropics and subtropics, where rainfall could be reduced by as much as 50% on average in regions like the Caribbean and Central America (IPCC 2014; Zhao and Dai 2015). In addition to these rainfall shortages, higher future temperatures could lead to even more severe droughts due to an increased atmospheric demand of moisture (Dai 2013; IPCC 2014; Cook et al. 2014, 2015; Zhao and Dai 2015). Consequently, this would drive or worsen drought risk even if precipitation does not change appreciably from historical averages (Cook et al. 2015; Ault et al. 2016).

Although many regional subtropical drying trends are robust across observational and model studies (IPCC 2014; Ault et al. 2014; Cook et al. 2015; Zhao and Dai 2015), large uncertainties in this picture originate from differences in data and models used for assessing drought. For example, Dai and Zhao (2017) calculated the Palmer drought

severity index (PDSI)—a widely used indicator of agricultural drought—using different underlying climate data products. They found that historical trends and variances of the PDSI are sensitive to differences between observational data products (especially precipitation, net radiation, and wind speed) and the calibration period used to normalize the index, although the latter has a smaller contribution than the underlying climate data. In terms of future projections of drought, both CMIP3 and CMIP5 are consistent in showing increased global aridity in the twenty-first century. Major differences among models are mostly due to discrepancies in projected precipitation (Zhao and Dai 2015, 2017). However, uncertainties in future projections of drought still persist on simulated regional trends and variances, which could be due to the dominant influence of the natural internal variability of drought at regional scales (Dai 2013; Zhao and Dai 2015, 2017).

The Caribbean region is vulnerable to climate change as a result of more severe and widespread droughts observed and projected at the end of the twenty-first century (IPCC 2014; Stephenson et al. 2014, 2016). The greatest decline in rainfall projected for the Caribbean might occur during boreal summer (June–August; Rauscher et al. 2008; Campbell et al. 2011; Karmalkar et al. 2011; IPCC 2014), a critical season for capturing and storing water in many countries of the region. In addition, the inherent insular nature of the Caribbean islands makes them especially vulnerable to drought because water cannot be collected, moved, or stored on large spatial scales (as it can be in the U.S. Southwest). Recent studies have also indicated that many of the small islands in the Caribbean Sea will face unprecedented freshwater and groundwater stresses because of climate change (e.g., Holding et al. 2016; Karnauskas et al. 2016). The region is made even more vulnerable by its dense population and limited economic growth, most of which depends on tourism and a poorly developed agricultural sector (Sahay 2005; Martin and Schumacher 2011; IPCC 2014).

Instrumental and historical records document the occurrence of multiyear droughts in the Caribbean and Central America during the last 60 years (e.g., Larsen 2000; Méndez and Magaña 2010; Peters 2015; Blunden and Arndt 2016). These events have

caused water shortages in agriculture, energy generation, and municipal usage, affecting the economies of many countries in the region (Larsen 2000; Peters 2015; OCHA 2015; FAO 2016). Some of those dry intervals have been linked to the warm phase of El Niño–Southern Oscillation (ENSO; Peters 2015; Blunden and Arndt 2016), including the 1997–1998, 2009–2010, and 2013–2016 droughts. The recent drought between 2013 and 2016 has been referred to as the most severe event in over 50–100 years in many countries of the Caribbean and Central America by some of their public institutions (e.g., DRNA 2016; IMN 2016), although this claim lacks firm quantitative backing because of the paucity of hydroclimatic data in the region. While the effects of this event have not yet been fully quantified, agricultural losses of over $200 million have been estimated in El Salvador and Guatemala (OCHA 2015; FAO 2016). For reference, the gross domestic product of these two countries was $25.85 and $63.79 billion, respectively, in 2015 according to the World Bank.

Although the Caribbean is likely to be affected by drought and freshwater stress in the future, there is currently no single study characterizing historical droughts and their trends at a spatial resolution appropriate for the topography of the region. A few studies have used data from weather stations, but they do not fully cover the entire region (e.g., Larsen 2000; Giannini et al. 2000, 2001a,b; Taylor et al. 2002; Jury et al. 2007; Peters 2015; Blunden and Arndt 2016). Regional and global station datasets, such as the National Oceanic and Atmospheric Administration (NOAA) Global Historical Climatology Network (GHCN), are missing a considerable amount of data in many sites in the Caribbean region and Central America, and many of the data that do exist are of inconsistent quality (Blunden and Arndt 2016). Furthermore, existing gridded drought products (e.g., Dai et al. 2004; Dai 2011; Vicente-Serrano et al. 2010; Sheffield et al. 2012; van der Schrier et al. 2013) are generated at spatial scales of 50–100km. At these scales, spatial variations in drought associated to the complex topography of many islands in the Caribbean Sea cannot be resolved. For example, a single grid cell of 0.5º, the highest resolution drought datasets currently available (Vicente-Serrano et al. 2010; van der Schrier et al. 2013) covers more than twice the area of Martinique (~1200 km^2). Therefore, products like this one are not suitable for assessing the effects of local

topography on enhancing or diminishing drought in the Caribbean or for evaluating how topography might influence the interannual variability and decadal trends of drought in the region. These products were also not designed to be regularly updated at monthly time scales while still providing an internally consistent picture of historical variations.

Given the limitations of existing products for characterizing and monitoring drought at small spatial scales in the Caribbean and Central America, here we introduce a high-resolution gridded drought dataset based on the "self-calibrating" PDSI (scPDSI; Wells et al. 2004) that spans 1950–2016. Our results yield an atlas that is relevant to stakeholders and researchers alike. It can further be updated on a monthly basis for ongoing drought monitoring and relief efforts. (Our atlas is available online at http://ecrl.eas.cornell.edu/products/caribbean-drought/index.html.)

2. Data and methods

2.1. Data

The climate data products used in this work are listed in Table 1. To calculate potential evapotranspiration (PET), we used statistically downscaled National Centers for Environmental Predication (NCEP)–National Center for Atmospheric Research (NCAR) reanalysis data (Kalnay et al. 1996) of monthly averages of temperature (T_{max}, T_{mean}, and T_{min}), cloud cover (to derive the net radiation), and wind speed that have native resolutions of approximately 1.8º and 2.5º in latitude and longitude (~200 and ~280 km, respectively). To assess the consistency of downscaled reanalysis temperature products, we also used gridded monthly temperature means from the 1º Berkeley Earth Surface Temperature (BEST) dataset (Mueller et al. 2013; Rohde et al. 2013). The BEST dataset incorporates approximately 400 land-weather stations in our study domain (defined as the region 6º–30ºN, 90º–60ºW; Fig. 1), including data from the GHCN and other global and regional climate data networks (Rohde et al. 2013). As compared to similar products, the number of records used by BEST is substantially higher. For example, the University of East Anglia Climatic Research Unit (CRU) Time Series, version 3.24 (TS3.24), dataset (Harris et al. 2014) currently uses less than a hundred temperature stations in the Caribbean and Central America. BEST further

differs from other global temperature datasets in the manner of treating temperature data, in which stations with discontinuities (e.g., missing data) are split and treated as different series, rather than undergoing a homogenization process (Mueller et al. 2013; Rohde et al. 2013). Split stations are then weighted based on their accuracy, as evaluated from nearby stations using a kriging approach (Rohde et al. 2013). The details of the method implemented to construct this dataset are available in Rohde et al. (2013). The BEST dataset is further updated on a regular basis, which is advantageous for drought monitoring.

Gridded monthly totals of precipitation were obtained from of the Global Precipitation Climatology Centre (GPCC), version 7 (V7), land surface dataset (Schneider et al. 2015a), which is based on 75000 quality-controlled rain gauges worldwide, including approximately 400 in the Caribbean and Central America. We used the GPCC V7 "combined product" (http://www.esrl.noaa.gov/psd/data/gridded/data.gpcc.html), with a native resolution of 1º (Schneider et al. 2015b). This version incorporates the full dataset from 1901 to 2014 with a monitoring product spanning from 2014 to the near present. Although various gridded precipitation products are currently available, we selected GPCC V7 for three reasons. First, GPCC data are updated on a regular basis, whereas most similar precipitation datasets (i.e., spanning since at least from 1950 to the near present) are not updated that frequently. This particular feature is essential to further building a high-resolution drought monitoring product for the Caribbean. Second, GPCC V7 has the highest station density in our study domain as compared to other datasets. As shown in Fig. 2, for example, the CRU TS3.24 station density is substantially lower in the Caribbean than in the GPCC V7. Third, GPCC data are one of the most reliable precipitation datasets currently available (Dai and Zhao 2017). For instance, in comparison to scPDSI derived from other precipitation products including the CRU TS3.24, GPCC data-based scPDSI estimates are more consistent with other independent drought metrics, such as soil moisture and runoff (Dai and Zhao 2017).

We used the global climate data suite WorldClim (Hijmans et al. 2005; http://www.worldclim.org/) and the Climate Hazards Group Infrared Precipitation with Station Data (CHIRPS; Funk et al. 2015) as target fields for downscaling and bias correcting the coarse resolution temperature and precipitation products described above. WorldClim is a long-term (1950–2000) high-resolution (~1 km^2 over the equator) global climatology of temperature (T_{max}, T_{mean}, and T_{min}) and precipitation, along with other derived bioclimatic variables. The dataset was developed by interpolating long-term monthly climatologies of weather stations using elevation, latitude, and longitude as predictors of climate variables (Hijmans et al. 2005). WorldClim includes climate data from the GHCN, the Food and Agriculture Organization of the United Nations (FAO), the World Meteorological Organization (WMO), the International Center for Tropical Agriculture (CIAT), and other additional minor databases from Central and South American countries (as well as others outside the study region) (Hijmans et al. 2005). Despite the scarcity of weather stations with high-quality climate data across our study domain, WorldClim used a relatively dense station network by incorporating climatological data from various sources, as well as by selecting stations with at least 10 years of monthly climate data during the 1950–2000 interval (Hijmans et al. 2005). For example, we estimated that WorldClim used approximately 5000 weather stations (for both temperature and precipitation) in our study domain, mainly distributed over northern South America[2]. However, those stations are not exempt from the problem of missing data; they simply satisfy the minimum requirement of having at least 10 years of climate data to be included in WorldClim. In spite of these obvious limitations, WorldClim is one of the very few high-resolution gridded climatologies currently available that make possible downscaling coarse temperature and precipitation datasets in regions with limited or missing continuous high-resolution data.

Because WorldClim solely provides high-resolution climatologies, we further used CHIRPS to correct monthly biases in variances and means of GPCC V7. This product

[2] See https://databasin.org/maps/new#datasets515a31dec689b4c 958ee491ff30fcce75.

spans from 1981 to the present, with a native resolution of 0.05º (~6 km) in the Caribbean. It integrates satellite imagery data with in situ weather station data from 50ºS to 50ºN. As with reanalysis and the GPCC monitoring product, CHIRPS is updated on a monthly basis with the purpose of drought monitoring (Funk et al. 2015). The number of stations used by CHIRPS to calibrate satellite precipitation estimates in our study domain is currently about 540[3], although this number was greater a decade or so ago. Most of the stations currently in use are concentrated in a portion of northern South America and the Florida Peninsula.

The available water holding capacity (AWC) data required for computing the scPDSI were obtained from the Global Gridded Surfaces of Selected Soil Characteristics of the International Geosphere–Biosphere Programme Data and Information Services (IGBP-DIS), through the Oak Ridge National Laboratory (ORNL; http://daac.ornl.gov/). This database provides information of various derived soil surfaces, including AWC, soil field capacity, and soil bulk density. It uses a statistical bootstrapping method to generate those surfaces from the FAO–United Nations Educational, Scientific and Cultural Organization (UNESCO) Digital Soil Map of the World (Global Soil Data Task Group 2000). Although the native resolution of this product is 5 arc min, we preprocessed using a bilinear interpolation routine to regrid the AWC data to a spatial resolution of 4 km.

2.2. Methods

For the purpose of facilitating the analysis of scPDSI trends and spatial variability, we divided the study area into four smaller regions based on physiographical settings (e.g., continentality vs insularity) and the total annual precipitation amount: 1) the Florida Peninsula (Fig. 1a), 2) Central America (Fig. 1b), 3) northern South America (Fig. 1c), and 4) the Caribbean (Fig. 1d). Previous studies have suggested dividing the Caribbean

[3] See ftp://ftp.chg.ucsb.edu/pub/org/chg/products/CHIRPS-2.0/ diagnostics/chirps-nstations_byCountry/.

into smaller regions based on climatic features such as seasonality (e.g., Giannini et al. 2000; Jury et al. 2007). We, however, examined the Caribbean as a single region because our domain not only includes the islands of the Caribbean, but also Central America and small portions of South and North America. We therefore compare hydroclimatic variations in the Caribbean along with other regions in our domain over the 1950–2016 interval.

2.2.1. Statistical downscaling and bias-correction

As previously mentioned, climate data products used in this work have native spatial resolutions ranging from 0.5º to 2.5º in latitude/longitude. At such scales, variations in drought related to local topography cannot be resolved. In the Caribbean, on islands like Hispaniola or Puerto Rico the spatial distribution and variances of precipitation are strongly conditioned by their highly complex topography (e.g., Izzo et al. 2010), with vertical gradients of up to 2700 m over just 15 km of horizontal distance. For reference, an 1º grid cell roughly covers an area larger than Puerto Rico (~9000 km^2). Accordingly, we applied statistical methods to downscale the coarse-resolution reanalysis, GPCC V7, and BEST datasets, as well as to correct biases in means and variances of downscaled fields. Furthermore, we selected a target resolution of 4 km to downscale climate data to make our product comparable with other high-resolution drought monitoring products, such as the West Wide Drought Tracker (https://wrcc.dri.edu/wwdt/current.php?folder5spi3&region5ww), which is forced with the Parameter-Elevation Relationships on Independent Slopes Model (PRISM) gridded datasets (Daly et al. 2002, 2008).

The downscaling method applied in this work is similar to the "delta method" implemented by Mosier et al. (2014). To downscale temperature, we first calculated the anomalies of the BEST dataset at its native resolution (1º in latitude/longitude). Anomalies of maximum, minimum, and mean monthly temperatures were calculated with respect to the 1950–2000 climatology because the same period was used to construct the WorldClim temperature products. These anomalies were then bilinearly interpolated to match with the target spatial resolution of 4 km. Finally, anomalies were

added to the WorldClim climatologies to generate downscaled temperature products with a spatial resolution of 4 km. It was necessary to regrid WorldClim to match our target resolution of 4 km because its native resolution is about 1 km at the equator (Hijmans et al. 2005). Since there are no high-resolution datasets of temperature to correct biases in spatial variances in the Caribbean (as there are for North America), we used the WorldClim temperature seasonality product to adjust annual seasonality of downscaled temperature fields, so they match the WorldClim annual cycle.

WorldClim temperature "seasonality" is the standard deviation of monthly means with respect to the annual average of temperature. We adjusted the annual cycle of our downscaled temperature products following a similar method as suggested by Leander and Buishand (2007):

$$T_{corr} = \overline{T}_{raw} + \left(\frac{\sigma(T_{obs})}{\sigma(T_{raw})}\right)(T - \overline{T}_{raw}) + (\overline{T}_{obs} - \overline{T}_{raw}) \quad (1)$$

where T_{corr} is the corrected temperature, T_{raw} is the annual mean temperature of uncorrected temperature data, and T_{obs} is the annual mean temperature from observations, which in this study is the mean from WorldClim climatology. The term $\sigma(T_{obs})$ is the standard deviation of WorldClim climatology (temperature seasonality), while $\sigma(T_{raw})$ is the annual standard deviation of the uncorrected temperature (i.e., the standard deviation with respect to the annual mean of every single year of the time series), and T is the uncorrected monthly time series of temperature over a specific grid cell. We modified Eq. (1), so that annual means and trends of the original downscaled data are maintained [Eq. (2)]:

$$T_{corr} = \overline{T}_{obs} + \left(\frac{\sigma(T_{obs})}{\sigma(T_{raw})}\right)(T - \overline{T}_{raw}) \quad (2)$$

If this step is done using just Eq. (1), we would be detrending downscaled fields by assigning a constant annual mean on each grid cell time series, hence the different formulation of Eq. (2).

Downscaling and bias-correcting of precipitation required a more sophisticated statistical approach than for temperature. Bias correction using the WorldClim coefficient of variation, as we did for temperature fields, fails to show spatial variations in precipitation not strictly related to local topography. For example, spatial variations in precipitation associated with frontal systems (which are common in the northwestern Caribbean during boreal winter) in areas with little topographic variability (e.g., Florida) are not captured using this method. Furthermore, we found annual variations in precipitation to be much higher than those in temperature. If we adjust downscaled precipitation to have the same coefficient of variation every year, this "correction" would affect the water balance of the scPDSI function, and consequently we might obtain scPDSI values that do not correspond to local conditions.

We applied a two-step statistical downscaling process using the CHIRPS precipitation dataset to correct monthly spatial variances and means of GPCC V7. As the first step, we regridded the original GPCC dataset to match the resolution of CHIRPS (0.05º or ~6 km). We then corrected the variances and means of GPCC V7 so that these statistics matched those of CHIRPS during the overlapping period from January 1981 to December 2015. This step was done using a quantile mapping approach following the method proposed by Panofsky and Brier (1968):

$$P_{corr,i} = F_{obs}^{-1}\left[F_{raw}\left[P_{raw,i}\right]\right] \quad i = 1, 2, 3 \ldots 12, \tag{3}$$

where $P_{corr,i}$ is the corrected precipitation for month, $P_{raw,i}$ is the uncorrected precipitation for month, F_{obs}^{-1} is the inverse cumulative distribution function (CDF) of observations, which in this case is the CHIRPS dataset, and F_{raw} is the corresponding CDF of uncorrected precipitation.

The second step is similar to the procedure we employed for temperature fields. We calculated precipitation anomalies as the fraction of each month with respect to its 1950–2000 climatology. Those anomalies were bilinearly interpolated and then aggregated to the WorldClim climatology to get a final downscaled product of 4 km. Again, it was necessary to regrid WorldClim precipitation climatologies to our target

resolution of 4 km. Last, we adjusted downscaled monthly mean values to match WorldClim's climatology from 1950 to 2000.

2.2.2. Evaluation of downscaled products

Where available, we used station data from GHCN versions 2 and 3 (V2 and V3), and homogenized weather station data from the Dominican Republic (from Izzo 2011) to evaluate and validate downscaled climate fields. We calculated root-mean-square errors (RMSEs) between 58 stations and underlying grid cells for precipitation, and 20 stations for temperature. We also computed Pearson correlation coefficients to evaluate whether downscaled products capture interannual station variability.

To evaluate the performance of WorldClim against other similar products in the Caribbean region, we also downscaled precipitation using the newly released (~1 km) data from the Climatologies at High Resolution for Earth's Land Surface Areas (CHELSA) product (Karger et al. 2016). The CHELSA suite uses a more sophisticated statistical approach than WorldClim to downscale climate fields from the European Centre for Medium-Range Weather Forecasts (ECMWF) interim reanalysis (ERA-Interim; Dee et al. 2011). CHELSA applies an algorithm that includes orographic predictors such as the wind effect, valley exposure, and the planetary boundary layer for downscaling both precipitation and temperature. It further corrects biases of ERA-Interim products using GPCC and GHCN station datasets (Karger et al. 2016).

As an additional test to evaluate the quality of downscaled products, we regridded GPCC V7 and BEST to match our downscaled precipitation and temperature products, respectively, using the "nearest neighbor" method to maintain their original spatial variations.

2.2.3. The self-calibrating Palmer Drought Severity Index

The PDSI, in its various forms, is the most widely used metric for drought monitoring in North America (Heim 2002; Dai et al. 2004; Dai 2011, 2013). The original PDSI (which we term PDSI-o) consists of a water balance model that uses precipitation and

PET as moisture supply and demand terms, respectively, integrated to a simple two-layer soil model (Palmer 1965). This makes the PDSI-o (and its variants) unique among drought indicators in its capacity to account for soil properties (i.e., AWC) to estimate drought severity. In contrast, the standardized precipitation index (SPI; McKee et al. 1993) and the standardized precipitation evapotranspiration index (SPEI; Vicente-Serrano et al. 2010) present alternative drought metrics to the PDSI-o, but are insensitive to underlying soil characteristics. Values of the PDSI-o smaller than –0.5 or greater than 0.5 indicate dry or wet conditions, respectively (Palmer 1965), while absolute values greater than 4 indicate an extreme event. Despite the success of the PDSI-o as a drought metric, it has also been criticized for showing inconsistent results across different climates (e.g., Alley 1984; Guttman et al. 1992; Wells et al. 2004).

Given the shortcomings of PDSI-o, we used the scPDSI, which makes drought severities comparable across different climate zones by tuning the index to local conditions (Wells et al. 2004). At its core, the scPDSI (X_i) is calculated as:

$$X_i = pX_{i-1} + qZ_i, \tag{4}$$

where X_i is a given month of the index, X_{i-1} is the index of the previous month, p and q are "duration factors" (which represent the importance of autocorrelation), and Z_i is the current moisture anomaly. As in Dai (2011), we used consecutive negative and positive moisture anomalies to calculate duration factors for dry and wet periods, respectively. Further details on how both the PDSI-o and the scPDSI are calculated are provided by Palmer (1965), Alley (1984), Guttman et al. (1992), and Wells et al. (2004).

Independent of the PDSI variant used, the index "calibration period" must be defined, which is the interval used as a benchmark to establish the normal hydroclimatic conditions for a specific location (Palmer 1965; Dai 2011; van der Schrier et al. 2013). Although previous studies have suggested a 1950–1980 interval as the optimum calibration period for computing the PDSI to capture the effect of anthropogenic climate change on drought (e.g., Dai and Zhao 2017), we used a 1950–2000 calibration interval to be consistent with the WorldClim climatology.

We arbitrarily set soil moisture initial conditions to have 50% of total AWC in each layer to initialize the calculations. Since the upper layer (S_s) has a fixed AWC of one inch, its initial moisture content was set at 0.5 in. (1 in. = ~2.54 cm); moisture content in the lower layer (S_u) depends on the total AWC as $S_u = AWC\text{-}S_s$ (Palmer 1965). In addition, we calculated the index beginning in January 1949 to minimize the influence of the initial conditions because our analysis spans the period from 1950 to 2016.

2.2.4. Potential evapotranspiration

In addition to using the self-calibrating version of the PDSI, we followed recent recommendations for "best practices" with the PDSI index (van der Schrier et al. 2011; Smerdon et al. 2015), using the Penman–Monteith (PM) method (Penman 1948; Monteith 1965) for calculating evapotranspiration, rather than the Thornthwaite equation (Thornthwaite 1948) used in PDSI-o. This approach is considered more physically realistic and more appropriate for evaluating the effects of climate change on drought severity (van der Schrier et al. 2011; Smerdon et al. 2015; Williams et al. 2015). Given the limited long-term climate data available for the Caribbean, we applied a variant of the PM that requires fewer climate fields for its computation [Eq. (5)] and is currently used by the FAO (Allen et al. 1998). Using this method, the PET is calculated as:

$$PET = \frac{0.408\Delta(Rn-G)+\gamma\frac{900}{T+273.16}U_2(e_s-e_a)}{\Delta+\gamma(1+0.34U_2)} \quad (5)$$

where,

$$U_2 = U_{10}\frac{\ln(128)}{\ln(661.3)},$$

and where the quantities are defined as follows: PET is the crop reference evapotranspiration (mm day^{-1}), Rn is the net radiation (MJ m^{-1} day^{-1}), G is the soil heat flux density (MJ m^{-2} day^{-1}), T is the average temperature at 2-m height (ºC), U_2 is the wind speed measured (or estimated from U_{10}) at 2-m height (m s^{-1}), U_{10} is the wind

speed measured at 10-m height (m s^{-1}), $e_s - e_a$ is the vapor pressure deficit for measurement at 2-m height (kPa), Δ is the slope of the vapor pressure curve (kPa $ºC^{-1}$), γ is the psychrometric constant (kPa $ºC^{-1}$), 900 is the coefficient for the reference crop (kJ^{-1} kg K day^{-1}), and 0.34 is the wind coefficient for the reference crop (s m^{-1}) (Allen et al. 1998). The concept behind this method stands from modeling an idealized grass surface with 0.12-m height, a constant water supply, and a soil resistance of 70 s m^{-1}. It also assumes a surface albedo of 0.23 (Allen et al. 1998). Although previous studies have shown a minimal impact on using either the PM or the Thornthwaite PET estimates for computing the PDSI (e.g., Dai 2011; van der Schrier et al. 2011) over the historical period, we suggest that variables included in the PM method, such as the vapor pressure deficit, might play a critical role on drought severity in the Caribbean during climate change (e.g., Williams et al. 2015).

With the method we used to calculate the PET, five climate variables are required: monthly averages of daily maximum, mean, and minimum temperature (T_{max}, T_{mean} and T_{min}), wind speed, and cloud cover. We used downscaled and bias-corrected temperature fields, while the other variables were bilinearly interpolated reanalysis products to match with the target resolution of 4km. Monthly averages of saturation vapor pressure (e_s) were estimated from vapor pressure:

$$e(T) = 0.6108 exp\left[\frac{17.27\,T}{T+237.3}\right] \quad (6)$$

where $e(T)$ is the vapor pressure (kPa) as a function of the air temperature, and T is the air temperature in degrees Celsius. To assess potential biases on saturation vapor pressure resulting from the nonlinearity of Eq. (6), we also calculated (e_s) using daily T_{max} and T_{min}, and then it was averaged to obtain monthly (e_s) estimates. We found minor differences on using both approaches, yielding a mean difference <0.002kPa $month^{-1}$. Equation (6) was also applied to calculate the actual vapor pressure (e_a), which requires the dew-point temperature rather than the air temperature. As suggested by Allen et al. (1998), the minimum temperature can be used to compute (e_a) when dew-point temperature and other humidity data are not available. Although there are reanalysis

products for both the relative and specific humidity, we derived (e_a) using our downscaled mean minimum daily temperature in place of the dew-point temperature because there is not a high-resolution dataset to further correct biases in means and variances of downscaled humidity fields from reanalysis in the Caribbean. We also used minimum temperature to be consistent with the saturated vapor pressure, which was calculated using our downscaled temperature products. In addition, uncertainties are high for humidity reanalysis products because they are largely based on simulated data (Kalnay et al. 1996; Williams et al. 2015). A similar approach was applied by Harris et al. (2014) to construct a 0.5º resolution vapor pressure dataset as part of the CRU TS3.10 climate suite. A caveat of using this approach is that we are assuming the dew-point temperature is never lower than the minimum temperature, which is not always realistic. However, this is mostly an issue for arid and semiarid regions (Allen et al. 1998). Although in the Caribbean there are few semiarid regions (e.g., southern Hispaniola and northern South America), we found that the method performs fairly well by qualitatively comparing our PET dataset with the CRU PET product.

Net radiation was calculated from reanalysis cloud cover (to derive sunshine hours) following Allen et al. (1998). Although this product has been classified as a category "C" variable, which indicates that it is derived solely from the model without observations (Kalnay et al. 1996), we found that it has a minimal impact on the scPDSI (Fig. 3). Finally, previous studies have reported major uncertainties in the reanalysis wind speed product because of the limited availability of high-quality observations (e.g., Dai 2011). To partially address this issue, we used the long-term wind speed monthly climatologies rather than the entire dataset, as in van der Schrier et al. (2013) with the CRU wind speed product. As with cloud cover, we compared the scPDSI forced with wind speed climatology, obtaining similar trends and variances of that in the Dai (2011) scPDSI dataset (Fig. 3).

2.2.5. Long-term trends and drought ranking

We calculated long-term trends in the scPDSI using the best-fit linear least squares method. Trends with *p*-values greater or equal to 0.05 at the 95% confidence level were

not considered in our analysis, although they are also described in the results. We calculated linear trends over the study area, as well as in each of the regions we divided our domain to identify changes at regional scales. Furthermore, given the strong autocorrelation of the scPDSI, we also calculated trends of the Palmer's moisture anomaly index (Z index; Palmer 1965) to contrast them against scPDSI trends. The Z index has very little (if any) autocorrelation and can serve as benchmark to assess the significance of the trends in the scPDSI.

To estimate the area where the recent 2013–2016 drought was record breaking, we ranked droughts by selecting the smallest monthly scPDSI values in each grid cell time series. In our analysis, the lower the ranking value the more severe the drought. That is, the most severe drought will be ranked as number one, while the wettest period of the same time series will occupy the last position.

2.2.6. Sea surface temperature

To identify large-scale climate patterns associated with Caribbean drought, we used the Extended Reconstructed Sea Surface Temperature, version 4 (ERSST.v4), dataset (Huang et al. 2015; Liu et al. 2015) to correlate sea surface temperature anomalies (SSTAs) with the scPDSI across the study domain. Correlations were done with SSTA averaged over the Niño-3.4 region (5ºN–5ºS, 170º–120ºW) in the tropical Pacific and over the tropical North Atlantic (0º–20ºN, 60º–20ºW) because these regions have been linked to the natural variability of precipitation in our study domain (e.g., Enfield and Alfaro 1999; Giannini et al. 2000, 2001a,b; Taylor et al. 2002; Jury et al. 2007). We further correlated regionally averaged scPDSI from our drought atlas with global SSTA to gain insights into the linkages between drought and remote patterns of SST variability. Since previous studies have shown seasonal changes in correlations between precipitation and SSTA from both tropical Pacific and North Atlantic (Giannini et al. 2000, 2001a,b; Taylor et al. 2002; Jury et al. 2007), we also conducted seasonal correlations using two seasons: 1) the early rainy season of May–July (MJJ), and 2) the late rainy season of August–October (ASO).

3. Results

3.1. Validation of downscaled products

Correlation coefficients between downscaled monthly precipitation and GHCN stations vary from 0.76 to 0.97, with an average of 0.89 over the study domain (Fig. 4a). The lowest correlations are found in the Caribbean and western Central America, as well as over coastal stations in northern South America (Fig. 4a). In terms of RMSE, the lowest value is 27 mm in the Maracaibo–Los Pozos station in Venezuela, while the highest is 79 mm in Caucagua, Venezuela (Fig. 4b). Both RMSEs account for less than 60% of the station standard deviation. Furthermore, correlations between the GPCC V7 regridded product and our downscaled precipitation product (4km) average over 0.92. Lower correlations are found on grids over the Andes in northern South America and Hispaniola Island (Fig. 5a).

Correlation coefficients and RMSE values between our BEST-downscaled temperature fields (T_{max}, T_{mean}, and T_{min}) and GHCN station data are similar to those of precipitation (Fig. 6). The higher biases in mean temperature are found over mountainous regions in Central America (RMSE = 1.08ºC), Hispaniola Island (RMSE = 0.91ºC), and northern South America (RMSE = 0.89ºC). The same pattern is also apparent in monthly minimum and maximum temperature means, with RMSE ranging from 0.79º to 1.12ºC. Similar correlations and RMSE are found between our reanalysis-downscaled temperature products and GHCN.

Downscaled BEST-based and reanalysis-based temperature products are very similar despite their differing spatial scales and underlying methodological assumptions (Fig. 6). Overall, correlations and RMSE are 0.88 and 0.40ºC, respectively, with the highest biases in northern South America, where correlations are below 0.6. However, grid cells with correlations below 0.85 only represent 20% of the study domain. Downscaled BEST products also correlate slightly better with some GHCN stations, as compared to downscaled reanalysis temperature products. For example, BEST mean temperature has a higher correlation (r = 0.85) than reanalysis (r = 0.78) with the Juan

Santamaria Airport station in Costa Rica.

The minor differences between BEST and reanalysis temperatures are also noticeable in the potential evapotranspiration. As shown in Fig. 7, both products perform similarly over the Caribbean and Central America. The largest biases are found, again, over northern South America, especially in the Orinoco River basin and the Andes (Fig. 7). Moreover, correlations between the BEST-based PET and reanalysis-based PET during the 1980–2016 interval (used as a benchmark of the satellite era) are lower than those calculated using the entire time series from 1950 to 2016 (Figs. 7c,d).

3.2. WorldClim versus CHELSA downscaled precipitation

While WorldClim and CHELSA climatologies might reflect somewhat different mean climate states because of their differing temporal coverage (1950–2000 vs 1979– 2013, respectively), we assume that major features such as rain shadows and regional spatial variations in precipitation are maintained over time. Overall, both downscaled precipitation products show similar long-term and spatial variances, as assessed using correlation coefficients and RMSE (Fig. 8). Averaged total annual precipitation differ in terms of their spatial variances, with the WorldClim-downscaled precipitation showing slightly higher contrast in rain shadows than with the CHELSA product. These differences are more noticeable in the Caribbean (particularly on Hispaniola Island) and Central America (Fig. 8). However, in spite of these differences, the averaged correlation between both products is 0.94.

CHELSA and WorldClim scPDSI estimates also show similar long-term trends and variations. Minor differences, mainly in the timing of some droughts and pluvials (i.e., the beginning and the end of dry and wet intervals), are observed in areas of complex topography in Central America and the Caribbean.

3.3. Major droughts and pluvials during the 1950–2016 interval

3.3.1. Major droughts

The worst droughts during the 1950–2016 interval (Fig. 9) were identified from the perspective of Caribbean islands (region in Fig. 1d). That is, we spatially averaged scPDSI over the Caribbean region and then selected the droughts using a scPDSI ≤ -1.5 threshold, with at least one year in duration. Because of this, major droughts identified in the Caribbean might not be the most extreme dry intervals in other regions such as northern South America, the Florida Peninsula, or Central America (Fig. 9), and in some instances they may not be correlated at all, as shown in Table 2.

We identified the first major drought in the Caribbean between 1974 and 1977. It was one of the most widespread and prolonged dry intervals in this region, and affected 49% of the study domain (as calculated from the percentage of grid cells with scPDSI ≤ -1) and 70% of the Caribbean (Figs. 9 and 10). In terms of severity, we calculated averaged scPDSI of –1.1 in the study domain (and much lower values locally), –1.5 in the Caribbean, –0.4 in northern South America, –0.6 in Central America, and –1.4 in the Florida Peninsula (Fig. 9). Localized wetter conditions occurred in the Andean region of northern South America, with scPDSI values indicating a slight wet spell (~1.0).

The 1997–1998 drought (Fig. 9) occurred during the strong El Niño of 1997–1998. Although dry conditions intensified across the region in the summer of 1997, they persisted until the summer and autumn of 1998. About 49% and 16% of the study area was affected by mild ($-1 \geq$ scPDSI ≥ -1.9) and severe ($-3 \geq$ scPDSI ≥ -3.9) drought conditions, respectively (Figs. 9 and 10), while at least 50% of the Caribbean was under mild drought (Fig. 10). Regions particularly affected by this event were northern South America, with a regional scPDSI average of –1.6, Central America (–1.4 scPDSI), and the Caribbean (–0.8 scPDSI). In contrast to the 1974–1977 dry interval, the Florida Peninsula experienced slightly wetter conditions during the 1997–1998 drought, with a regional scPDSI of 0.8.

Between mid-2009 and late 2010, a severe and widespread drought once again affected the domain, especially northeastern South America, the Caribbean (mostly the Lesser Antilles), and portions of Central America (Fig. 9). During this event, 68% of the study area was under mild drought conditions, and 28% was under severe drought (Fig. 10). Furthermore, over 85% of northern South America as well as 99% of the Lesser Antilles were severely affected by the drought (Fig. 10). In contrast to other major droughts in the Caribbean, this dry interval did not appreciably affect the Greater Antilles, with approximately 59% of land area under mild drought conditions. In terms of severity, regional scPDSI averages vary across the study domain, from –0.9 scPDSI in the Caribbean to –3.0 in South America. For the rest of the regions, scPDSI averaged –1.5 in Central America and 0.4 in the Florida Peninsula.

More recently, between late 2013 and early 2016, the Caribbean and most of the study domain further struggled with a severe drought. As in the 1997–1998 period, part of this period occurred during a strong El Niño. However, this drought was considerably more severe and widespread, affecting 80% of the study area, and almost 95% of the Caribbean with a mild drought (Figs. 9 and 10). The drought peaked in 2015, and during this year almost the entire Caribbean experienced mild drought conditions, while 51% of the islands were in severe drought (Fig. 10). In terms of regional averages, this drought reached scPDSI of –2.6 in the Caribbean, –3.1 in northern South America, and –2.2 in Central America. In contrast, Florida Peninsula received above normal precipitation, with a mean scPDSI of 0.8 (a similar pattern to the 1997–1998 drought). However, unlike the 1997–1998 drought, the 2013–2016 event affected the southern portion of the Florida Peninsula (Fig. 9), as well as northwestern Cuba.

3.3.2. Major pluvials

Major pluvials were selected by repeating the method we used to choose major droughts in the Caribbean. We found that some pluvials coincided with active hurricane seasons in the North Atlantic, including those in 1979, 2008, and 2012. A brief analysis of this result is provided in section 4b. Furthermore, it was found that very wet conditions (i.e., scPDSI $\geq$ 3) occur on more localized scales as compared to severe droughts (i.e., scPDSI

≤ 3), at least in the Caribbean (Fig. 11).

One of the most prominent pluvials occurred between 2012 and 2013 (Fig. 11), when 60% of our domain and 50% of the Caribbean were under wet conditions (scPDSI ≥ 1) (Fig. 12). We calculated a regionally averaged scPDSI of 1.4, which is considered slightly wet (Palmer 1965). This wet interval was most pronounced in northern South America, with a regionally averaged scPDSI of 2.9. Furthermore, most of the Caribbean and the Pacific coast of Central America experienced mild wet conditions as well, with a mean scPDSI of 1.9 and 1.3, respectively. In contrast, the Florida Peninsula and the Caribbean coast of Central America were experiencing a moderate drought, with an average scPDSI of –2.0.

Other major pluvials also occurred during 1958–1962, 1977–1981, and 2007–2009, but they were not as widespread as the 2012–2013 wet period. In some cases, a "seesaw pattern" between northern South America and the Florida Peninsula is particularly pronounced, where pluvials in one region are usually paired with dry conditions in the other, and vice versa (Fig. 11). During the wet periods in 1958–1962, 1977–1981, and 2007–2009, 27%, 51%, and 59%, respectively, of the study domain was under slightly wet conditions (Fig. 12).

3.4. Long-term trends

Linear trends in the scPDSI vary markedly across the study area, even at local scales (Fig. 13). We calculated scPDSI trends during the 1950–2008 interval to compare our results with trends previously reported by Dai (2011) in the Caribbean (Fig. 13a). In general, results reveal a statistically significant decline in the scPDSI—indicating a drying trend—from 1950 to 2008 ($p < 0.05$), with an average trend of –0.09 scPDSI decade^{-1}. It is important to mention, however, that this is the spatially averaged trend across the study area, which means that in specific locations drying trends are more pronounced. Sectors of Central America (e.g., in Nicaragua and Honduras), for example, have linear trends of –0.25 scPDSI decade^{-1} ($p < 0.05$) (Fig. 13a).

We further calculated linear trends including the full time interval of our drought product (1950–2016), which depict a similar pattern as from 1950 to 2008 (Fig. 13b). Differences were observed in the intensity of the trends, but in general the spatial patterns were consistent. Significant positive trends prevailed in northern South America (10ºN, 75ºW) with scPDSI trends averaging 0.15 scPDSI decade^{-1} ($p < 0.05$). Positive trends were also found in Puerto Rico (average change of 0.15 scPDSI decade^{-1}) and the highlands of Hispaniola Island (average change of 0.07 scPDSI decade^{-1}) but they were not statistically significant ($p = 0.12$). A similar result was also observed in the trends of the Z index, although they are slightly lower than those in the scPDSI ($\pm$0.04 units decade^{-1}).

3.4.1. Regional trends

Regional trends calculated using the full interval of 66 years are shown in Fig. 14. As with our selection of the worst dry and wet intervals, we spatially averaged the scPDSI over the regions we divided our study domain. Results reveal that scPDSI declined significantly in three of the four regions, with the highest drying trend in northern South America with –0.1 scPDSI decade^{-1} ($p < 0.05$). The linear trend in northern South America is closely followed by trends in the Caribbean (–0.09 scPDSI decade^{-1}; $p < 0.05$) and Central America (–0.087 scPDSI decade^{-1}; $p < 0.05$). Although results also indicate a drying trend in the Florida Peninsula (–0.06 scPDSI decade^{-1}), this is not statistically significant ($p = 0.15$).

3.5. Sea surface temperature correlations

Seasonal correlations between SSTA and scPDSI time series vary during seasonal cycles (Fig. 15). Negative correlations associate above-normal SST with drought, and positive correlations with wetter conditions. For example, Fig. 15 shows the correlations between scPDSI in the Caribbean with global SSTA during MJJ. A non-statistically significant correlation is observed with the tropical Pacific region during this season (r = –0.2), while it is significant over the tropical North Atlantic (r = 0.5). In contrast, during ASO (Fig. 15) both oceanic basins are significantly correlated with scPDSI in

the Caribbean (r = ±0.5). Furthermore, correlation patterns between SSTAs and the Florida Peninsula scPDSI are quite the opposite from those observed in the Caribbean, Central America, and northern South America (Fig. 15). This region is significantly correlated with the tropical Pacific in both seasons, while a non-statistically significant correlation is observed with the tropical North Atlantic (Fig. 15).

4. Discussion

4.1. Evaluation of downscaling and bias-correction methods

Our drought atlas underscores the advantage of using high-resolution climate products for calculating the scPDSI in insular regions like the Caribbean. This is not only because high-resolution datasets allow us to evaluate variations in drought at local scales, but also because the smallest insular states in the region are resolved. For example, some of the Lesser Antilles do not appear in the current drought datasets (e.g., Dai et al. 2004; Dai 2011; Vicente Serrano et al. 2010; van der Schrier et al. 2013), simply because those islands are much smaller than a single grid cell of such products. From our drought atlas, islands even smaller than 100 km^2 (such as some of the British Virgin Islands) are represented. Furthermore, we assessed the consistency of our drought product with two approaches. First, we used statistical tools to compare the forcing climate datasets—especially precipitation—with station data before calculating the scPDSI. Even though correlation coefficients may not fully capture the differences among datasets, we ensured a more realistic comparison by combining correlations with RMSE. Both approaches indicate that our downscaled products are consistent with station data in terms of trends and variability. Second, we contrasted our drought atlas with reports issued by local public institutions describing some of their historical droughts. We compared, for example, spatial variations of the recent 2013–2016 drought in Puerto Rico in our atlas against reports issued by the Puerto Rican Department of Natural and Environmental Resources (DRNA). In these reports, the evolution of the drought was documented using various indicators, including the United States Drought Monitor (USDM; http://droughtmonitor.unl.edu), and precipitation anomalies estimated from satellite products (DRNA 2016). Although some biases were observed in our drought

atlas, especially in the western side of the island, it captured the persistent drought in southern Puerto Rico as described in those reports.

We found that the delta method implemented here is appropriate in light of limitations in high-resolution gridded climate products in our study region, and for being computationally inexpensive. A key advantage of this method is the relatively low volume of climate data required for its implementation, as compared to more sophisticated statistical methods like bias-corrected constructed analogs (BCCA; Maurer et al. 2010) or bias correction and spatial disaggregation (BCSD; Wood et al. 2004). For example, while ideally it might be better to downscale using BCCA (because of its sophisticated statistical approach), high-resolution historical products are required for the constructed analog (CA) step used in this method. This issue in particular prevented us from applying such a method. While BCCA and BCSD require high-resolution climate datasets, the delta method used here only needs high-resolution climatologies of the variables to downscale. This is especially important for the Caribbean because there is no a single high-resolution product that resolves for local topography from 1950 to near-present. Although CHIRPS may be used to downscale precipitation using the BCSD method, it only spans from 1981 to the present, and we required consistency in our downscaling approach for both temperature and precipitation going back to 1950.

4.2. Characteristics of droughts and pluvials

The eight extreme events we analyzed help us to characterize some key features of dry and wet intervals in our study area. For example, spatial variations in drought are characterized by a seesaw pattern between northern South America and the Florida Peninsula, where droughts in northern South America are accompanied by wet periods in Florida, and vice versa (e.g., Figs. 9 and 11). This pattern is particularly apparent with droughts and pluvials during ENSO events, and it is also observed when comparing the drought area index in each region (Fig. 10). During the 1997–1998, 2009–2010, and 2013–2016 droughts in northern South America and the Caribbean, wetter conditions prevailed in the Florida Peninsula, and in some cases in western Cuba (Fig. 9). These

findings are consistent with previous studies (e.g., Schultz et al. 1998; Giannini et al. 2001a,b) in which warm phases of the ENSO have been associated with drought in northern South America, and above-normal precipitation in the Florida Peninsula. The wetter conditions observed in Florida correlate with a higher intrusion of frontal systems during the boreal winter when El Niño peaks. In contrast, a persistent subsidence over northern South America could be responsible for the drier conditions observed during El Niño in this region (Giannini et al. 2001a,b).

Some pluvials occurred during active hurricane seasons in the North Atlantic. Although the scPDSI smooths the influence of extreme precipitation events like those associated with tropical cyclones, we examined some of the most intense hurricanes that affected Hispaniola Island in 1979, 1998, and 2008. In some instances, like after Hurricanes David (1979) and Georges (1998), we found scPDSI changes of 1.6 and 1.8, respectively, in a single month. Hispaniola was also affected by two tropical cyclones in August 2008, including Hurricane Gustav. Averaged scPDSI across the island changed from –1.8 in July 2008 (mild drought conditions) to 2.9 in August (moderately wet), representing a change of 4.2 scPDSI units in one month. Although tropical cyclones last for a few days, they often bring substantial amounts of precipitation (on the order of hundreds of millimeters in few days) that eventually contribute to a major change in the scPDSI, even in a short period of time. For example, the greatest accumulated monthly precipitation in Barahona (Dominican Republic, during 1939–2008) is 945 mm (Izzo 2011)[4]. This extreme event occurred in October 1963 and coincided with the landfall of major Hurricane Flora in southwestern Hispaniola. In fact, this amount is 7 times the average precipitation for October in this station (~160mm) and virtually equal to its annual mean (~950 mm). As estimated from Roth (2008), the contribution of Flora to this event was approximately 800 mm, or roughly 85% of total precipitation in this month. These results highlight the role that tropical cyclones might play in ending droughts or worsening pluvials at local scales in the Caribbean. However,

[4] Station data provided by the National Meteorological Office of the Dominican Republic (ONAMET).

based on these findings we cannot argue that pluvials in the Caribbean are solely caused by the natural variability of tropical cyclones. Hence, this warrants further research that might include dynamical downscaling of landfalling hurricanes in the region to provide insights into the possible interplay between tropical cyclones and local topography in modulating drought variability.

Our atlas is also consistent with previous studies connecting SSTA to drought variability in the region (e.g., Enfield and Alfaro 1999; Giannini et al. 2000, 2001a,b; Taylor et al. 2002; Jury et al. 2007). As shown in Fig. 15, regional scPDSI time series are significantly correlated with SSTA, especially in the tropical Pacific and North Atlantic Oceans. However, correlation patterns with indices from these basins vary across the study area, and are even anticorrelated. For example, while scPDSI in the Florida Peninsula is positively correlated with above normal tropical Pacific SSTs, the correlations are negative in Central America, northern South America, and the Caribbean (Fig. 15). This means that during El Niño events, wetter conditions are usually observed in Florida and drought observed in the rest of the domain. These findings are also consistent with the seesaw pattern seen in the most extreme hydroclimatic intervals, and highlight the influence of both the tropical Pacific and North Atlantic in modulating drought variability in our study area. Furthermore, correlations not only vary across space but also through the seasonal cycle. For example, scPDSI in the Caribbean is significantly correlated with the tropical Pacific during early boreal autumn (ASO), while there is no correlation in boreal spring–summer (MJJ) (Fig. 15). In contrast, the same region is positively correlated with the tropical North Atlantic in both seasons, which means that above normal temperature in this sector of the North Atlantic ocean is usually associated with higher precipitation in the Caribbean (e.g., Giannini et al. 2000, 2001a,b; Taylor et al. 2002; Jury et al. 2007).

Correlations further vary at local scales across the study domain, and even in the same region. Regionally averaged scPDSI in Central America is, for example, negatively correlated with the tropical Pacific (Fig. 15), but this pattern is not equally strong across the region (Fig. 16). The Pacific coast of Central America appears to be

more sensitive to variations in the Niño-3.4 region, while the Caribbean coast is not correlated at all ($p > 0.05$), and indeed positive correlations are observed in some grid cells (Fig. 16). Similarly, statistically significant correlations are observed in western Cuba with the Niño-3.4 during MJJ, while the eastern side of the island is negatively correlated. These patterns suggest the role topography might have in modulating drought variation in our study domain by modulating the spatial variation of precipitation, although dynamical downscaling may be required to fully understand this picture.

4.3. The 2013–2016 Caribbean drought

Results from this work indicate that during the 2013–2016 interval, the Caribbean faced the most severe and widespread drought since 1950. This drought has caused major water shortages in agriculture, municipal consumption, and energy generation[5], mainly affecting Hispaniola, Cuba, Puerto Rico, and Jamaica, as well as the Lesser Antilles. We call this dry interval a "Pan-Caribbean drought" because virtually all Caribbean islands were affected by it. As the Caribbean, Central America, and northern South America also confronted serious problems with water shortage in agriculture and municipal consumption due to this drought.

The drought was record breaking in the summer of 2015, when 99% of the Caribbean, 98% of northern South America, and 87% of Central America were under drought conditions (Fig. 17). In terms of severity, it was also record breaking in 17% of the domain in 2015. These findings indicate that this event was not only the most severe in terms of scPDSI values (below –6 scPDSI in the Caribbean and Central America) but it was also the most widespread drought since at least 1950.

El Niño has been identified as the culprit of some major droughts in the Caribbean, Central America, and northern South America (e.g., Giannini et al. 2000, 2001a,b;

[5] See http://reliefweb.int/disaster/dr-2015-000091-hti.

Taylor et al. 2002; Jury et al. 2007), including the 1997–1998 and the recent 2013–2016 event (Amador et al. 2016). However, as compared to the 1997–1998 drought, when even northwestern Cuba and Florida experienced wetter conditions, the 2013–2016 dry interval was extremely dry in both locations. This aridity not only extended across the entire island of Cuba, but also affected portions of Florida that usually receive above normal precipitation during El Niño (Giannini et al. 2001a,b). Other particular difference between these "El Niño droughts" was their duration. Whereas the 1997–1998 event lasted a year, the 2013–2016 drought extended for at least three years, since it is still (at the time of writing) ongoing in some locations of the study area[6].

To assess the potential role of temperature anomalies on this anomalous drought, we ranked annual PET anomalies using our PET product. We found the highest anomalies in both PET and temperatures in 2015, which coincides with the driest year in the Caribbean during the 2013–2016 drought (Fig. 18). We therefore argue that temperature anomalies during the drought might have been a major contributor to the severity of this event, in addition to lower precipitation. Nevertheless, further studies are required to fully evaluate the details of this picture.

5. Conclusions

We have documented the first high-resolution scPDSI-based drought atlas for the Caribbean and Central America, spanning 1950–2016. We argue that high-resolution drought products are required for the Caribbean region, not only because of its complex topography and inherent insularity, but also because of its unique exposure to the impacts of climate change across these gradients. This atlas delivers critical information to researchers and stakeholders by providing insight into the historical backdrop of drought variability in the region. This is especially important for the Caribbean, since many of its nations have been recognized as some of the most vulnerable countries to severe droughts and pluvials (Stephenson et al. 2014, 2016). We summarize the main

[6] See http://rcc.cimh.edu.bb/spi-monitor-january-2017/.

findings of this work as follows:

- Downscaling and bias-correction methods applied in this work are robust in capturing spatial and temporal variations of the underlying climate data. For example, correlations and root-mean-square errors indicate that our downscaled products capture the interannual variability of stations, as well as major droughts and pluvials. Furthermore, comparing the scPDSI derived from station-based precipitation and temperature records against our downscaled fields shows that these two approaches yield consistent results.

- A seesaw pattern in droughts and pluvials is observed between the Florida Peninsula and northern South America. These findings are consistent with previous studies (Giannini et al. 2000, 2001a,b; Taylor et al. 2002; Jury et al. 2007) but have not been documented at such high spatial resolution until now. Likewise, both the tropical Pacific and North Atlantic appear to have the highest influence in modulating drought variations in our study domain.

- Linear trends in the scPDSI vary substantially across the study area, and even at local scales. For example, in general, a significant drying trend is prevalent in the Caribbean (-0.09decade^{-1}, $p < 0.05$) whereas a wetting trend is observed in the highlands of Hispaniola and Puerto Rico ($0.15\ \text{decade}^{-1}$, $p \geq 0.05$). Regional trends in Central America, northern South America, and the Florida Peninsula also show a predominant drying trend. We also found that, even though trends in the scPDSI across the study area are tied to the decline in precipitation, the increasing trend in temperature might also have a substantial effect.

- Finally, the 2013–2016 Caribbean drought is the worst multiyear period of aridity in the Caribbean and Central America since at least 1950. It was both more severe and more extensive than any other event in our dataset. This dry interval appears to be related not only to El Niño-driven precipitation deficits, but also to temperature-driven increases in PET. Furthermore, our results agree with station-based reports from many meteorological institutions across the

Caribbean that recognized the 2013–2016 drought as the worst event in decades, or even in the last 100 years in some countries.

In conclusion, we consider this effort to be the first step in building a high-resolution drought product for the Caribbean and Central America that can be updated regularly, and made available to the public for ongoing monitoring and modeling efforts. Further applications of this atlas could include quantifying potential predictability across multiple temporal or spatial scales, targeting it for paleoclimate reconstructions, or applying rigorous detection and attribution analysis to the historical trends. Regardless, our results document—for the first time, to our knowledge—that the 2013–2016 drought was indeed the worst on record in terms of both its severity and spatial extent since at least 1950. Future work could therefore help clarify the contribution of anthropogenic warming to this extreme anomaly, as well as help constrain future risks in a changing climate.

REFERENCES

Allen, R., and Coauthors, 1998: Crop evapotranspiration: Guidelines for computing crop water requirements. FAO Irrigation and Drainage Paper 56, 300 pp.

Alley, W. M., 1984: The Palmer Drought Severity Index: Limitations and assumptions. *J. Climate Appl. Meteor.*, 23, 1100–1109, doi:10.1175/1520-0450(1984)023,1100:TPDSIL.2.0.CO;2.

Amador, J. A., H. G. Hidalgo, E. J. Alfaro, A. M. Durán-Quesada, and B. Calderón, 2016: Regional climates: Central America and the Caribbean [in "State of the Climate in 2015"]. *Bull. Amer. Meteor. Soc.*, 97, S178–S181, doi:10.1175/ 2016BAMSS-tateoftheClimate.1.

Ault, T. R., J. E. Cole, J. T. Overpeck, G. T. Pederson, and D. M. Meko, 2014: Assessing the risk of persistent drought using climate model simulations and paleo-climate data. *J. Climate*, 27, 7529–7549, doi:10.1175/JCLI-D-12-00282.1.

——, J. S. Mankin, B. I. Cook, and J. E. Smerdon, 2016: Relative impacts of mitigation, temperature, and precipitation on 21st-century megadrought risk in the American Southwest. Sci. Adv., 2, e1600873, doi:10.1126/sciadv.1600873.

Blunden, J., and D. S. Arndt, Eds., 2016: State of the Climate in 2015. *Bull. Amer. Meteor. Soc.*, 97, S1–S275, doi:10.1175/ 2016BAMSStateoftheClimate.1.

Campbell, J. D., M. A. Taylor, T. S. Stephenson, R. A. Watson, and F. S. Whyte, 2011: Future climate of the Caribbean from a regional climate model. *Int. J. Climatol.*, 31, 1866–1878, doi:10.1002/joc.2200.

Cook, B. I., J. E. Smerdon, R. Seager, and S. Coats, 2014: Global warming and 21st century drying. *Climate Dyn.*, 43, 2607–2627, doi:10.1007/s00382-014-2075-y.

——, T. R. Ault, and J. E. Smerdon, 2015: Unprecedented 21st century drought risk in the American Southwest and Central Plains. Sci. Adv., 1, e1400082, doi:10.1126/sci-adv.1400082.

——, E. R. Cook, J. E. Smerdon, R. Seager, A. P. Williams, S. Coats, D. W. Stahle, and J. V. Díaz, 2016: North American megadroughts in the Common Era: Reconstructions and simulations. Wiley Interdiscip. Rev.: *Climatic Change*, 7, 411– 432, doi:10.1002/wcc.394.

Dai, A., 2011: Characteristics and trends in various forms of the Palmer Drought Severity Index during 1900–2008. *J. Geophys. Res.*, 116, D12115, doi:10.1029/2010-JD015541.

——, 2013: Increasing drought under global warming in observations and models. *Nat. Climate Change*, 3, 52–58, doi:10.1038/ nclimate1633.

——, and T. Zhao, 2017: Uncertainties in historical changes and future projections of drought. Part I: Estimates of historical drought changes. *Climatic Change*, doi:10.-1007/s10584-016-1705-2, in press.

——, K. Trenberth, and T. Qian, 2004: A global dataset of Palmer Drought Severity Index for 1870–2002: Relationship with soil moisture and effects of surface warming. *J. Hydrometeor.*, 5, 1117–1130, doi:10.1175/JHM-386.1.

Daly, C., W. P. Gibson, G. H. Taylor, G. L. Johnson, and P. Pasteris, 2002: A knowledge-based approach to the statistical mapping of climate. *Climate Res.*, 22, 99–113, doi:10.3354/ cr022099.

——, and Coauthors, 2008: Physiographically sensitive mapping of temperature and precipitation across the conterminous United States. *Int. J. Climatol.*, 28, 2031–2064, doi:10.1002/ joc.1688.

Dee, D. P., and Coauthors, 2011: The ERA-Interim reanalysis: Configuration and performance of the data assimilation system. *Quart. J. Roy. Meteor. Soc.*, 137, 553–597, doi:10.1002/ qj.828.

DRNA, 2016: Informe sobre la sequía de 2014–2016en Puerto Rico. Departamento de Recursos Naturales y Ambientales del Estado Libre Asociado de Puerto Rico (DRN-A),

División de Monitoreo del Plan de Aguas, San Juan, Puerto Rico, 92 pp.

Enfield, D. B., and E. J. Alfaro, 1999: The dependence of Caribbean rainfall on the interaction of the tropical Atlantic and Pacific Oceans. *J. Climate*, 12, 2093–2103, doi:10.1175/ 1520-0442(1999)012,2093:TDOCRO.2.0.CO;2.

FAO, 2016: Situation report: Dry corridor in Central America. Food and Agriculture Organization of the United Nations, 3 pp. [Available online at http://www.fao.org/-emergencies/resources/documents/resources-detail/en/c/422097/.]

Funk, C., and Coauthors, 2015: The climate hazards infrared precipitation with stations—A new environmental record for monitoring extremes. *Sci. Data*, 2, 150066, doi:10.1038/sdata.2015.66.

Giannini, A., Y. Kushnir, and M. Cane, 2000: Interannual variability of Caribbean rainfall, ENSO, and the Atlantic Ocean. J. Climate, 13, 297–311, doi:10.1175/1520-0442(2000)013,0297: IVOCRE.2.0.CO;2.

——, M. A. Cane, and Y. Kushnir, 2001a: Interdecadal changes in the ENSO teleconnection to the Caribbean region and the North Atlantic Oscillation. *J. Climate*, 14, 2867–2879, doi:10.1175/1520-0442(2001)014,2867:ICITET.2.0.CO;2.

——, J. C. Chiang, M. A. Cane, Y. Kushnir, and R. Seager, 2001b: The ENSO teleconnection to the tropical Atlantic Ocean: Contributions of the remote and local SSTs to rainfall variability in the tropical Americas. *J. Climate*, 14, 4530–4544, doi:10.1175/1520-0442(2001)014,4530:TETTTT.2.0.CO;2.

Global Soil Data Task Group, 2000: Global Gridded Surfaces of Selected Soil Characteristics (IGBP-DIS). Distributed Active Archive Center, Oak Ridge National Laboratory, doi:10.3334/ ORNLDAAC/569.

Guttman, N. B., J. R. Wallis, and J. R. M. Hosking, 1992: Spatial comparability of the Palmer Drought Severity Index. *J. Amer. Water Resour. Assoc.*, 28, 1111–1119, doi:-10.1111/ j.1752-1688.1992.tb04022.x.

Harris, I., P. D. Jones, T. J. Osborn, and D. H. Lister, 2014: Updated high-resolution grids of monthly climatic observations: The CRU TS3.10 dataset. *Int. J. Climatol.*, 34, 623–642, doi:10.1002/joc.3711.

Heim, R. R., 2002: A review of twentieth-century drought indices used in the United States. *Bull. Amer. Meteor. Soc.*, 83, 1149–1165, doi:10.1175/1520-0477(2002)08311-49:AROTDI.2.3.CO;2.

Hijmans, R. J., S. E. Cameron, J. L. Parra, P. G. Jones, and A. Jarvis, 2005: Very high resolution interpolated climate surfaces for global land areas. *Int. J. Climatol.*, 25, 1965–1978, doi:10.1002/joc.1276.

Holding, S., D. M. Allen, S. Foster, A. Hsieh, I. Larocque, J. Klassen, and S. C. Van Pelt, 2016: Groundwater vulnerability on small islands. *Nat. Climate Change*, 6, 1100–1103, doi:10.1038/nclimate3128.

Howitt, R. E., J. Medellín-Azuara, D. MacEwan, J. R. Lund, and D. Sumner, 2014: Economic analysis of the 2014 drought for California agriculture. Tech. Rep., Center for Watershed Sciences, University of California, Davis, 20 pp. [Available online at https://watershed.ucdavis.edu/2014-drought-report.]

Huang, B., and Coauthors, 2015: Extended Reconstructed Sea Surface Temperature version 4 (ERSST.v4): Part I. Upgrades and intercomparisons. *J. Climate*, 28, 911–930, doi:10.1175/ JCLI-D-14-00006.1.

IMN, 2016: Pronóstico: Fenómeno ENOS y estación lluviosa 2016. Instituto Meteorológico Nacional de Costa Rica (IMN), San José, Costa Rica, 14 pp. [Available online at https://www.imn. ac.cr/web/imn/43.]

IPCC, 2014: Climate Change 2014: Synthesis Report. R. K. Pachauri and L. A. Meyer, Eds., IPCC, 151 pp.

Izzo, M., 2011: Analisi del clima e delle dinamiche climatiche nella Repubblica Dominicana e delle relative influenze sul territorio. Ph.D. thesis, University of Molise, Italy,

162 pp.

——, C. M. Rosskopf, P. P. C. Aucelli, A. Maratea, R. Méndez, C. Pérez, and H. Segura, 2010: A new climatic map of the Dominican Republic based on the Thornth-waite classification. *Phys. Geogr.*, 31, 455–472, doi:10.2747/0272-3646.31.5.455.

Jury, M., B. A. Malmgren, and A. Winter, 2007: Subregional precipitation climate of the Caribbean and relationships with ENSO and NAO. *J. Geophys. Res.*, 112, D16107, doi:10.1029/ 2006JD007541.

Kalnay, E., and Coauthors, 1996: The NCEP/NCAR 40-Year Reanalysis Project. *Bull. Amer. Meteor. Soc.*, 77, 437–471, doi:10.1175/1520-0477(1996)077,0437:TNYRP.-2.0.CO;2.

Karger, D. N., and Coauthors, 2016: Climatologies at High Resolution for the Earth's Land Surface Areas. 20 pp. [Available online at https://arxiv.org/abs/1607.00217.]

Karmalkar, A. V., R. S. Bradley, and H. F. Díaz, 2011: Climate change in Central America and Mexico: Regional climate model validation and climate change projections. *Climate Dyn.*, 37, 605–629, doi:10.1007/s00382-011-1099-9.

Karnauskas, K. B., J. P. Donnelly, and K. J. Anchukaitis, 2016: Future freshwater stress for island populations. *Nat. Climate Change*, 6, 720–725, doi:10.1038/nclimate-2987.

Larsen, M. C., 2000: Analysis of 20th century rainfall and streamflow to characterize drought and water resources in Puerto Rico. *Phys. Geogr.*, 21, 494–521.

Leander, R., and T. A. Buishand, 2007: Resampling of regional climate model output for the simulation of extreme river flows. *J. Hydrol.*, 332, 487–496, doi:10.1016/j.-jhydrol.2006.08.006.

Liu, W., and Coauthors, 2015: Extended Reconstructed Sea Surface Temperature version 4 (ERSST.v4): Part II. Parametric and structural uncertainty estimations. *J. Climate*, 28, 931–951, doi:10.1175/JCLI-D-14-00007.1.

Martin, E. R., and C. Schumacher, 2011: Modulation of Caribbean precipitation by the Madden–Julian oscillation. *J. Climate*, 24, 813–824, doi:10.1175/2010JCLI3773.1.

Maurer, E. P., and Coauthors, 2010: The utility of daily large-scale climate data in the assessment of climate change impacts on daily streamflow in California. *Hydrol. Earth Syst. Sci.*, 14, 1125–1138, doi:10.5194/hess-14-1125-2010.

McKee, T. B., N. J. Doesken, and J. Kleist, 1993: The relationship of drought fre-quency and duration to time scales. Preprints, Eighth Conf. on Applied Climatology. Anaheim, CA, Amer. Meteor. Soc., 179–184.

Méndez, M., and V. Magaña, 2010: Regional aspects of prolonged meteorological droughts over Mexico and Central America. *J. Climate*, 23, 1175–1188, doi:10.1175/-2009JCLI3080.1.

Monteith, J. L., 1965: Evaporation and environment. 19th Symp. of the Society for Experimental Biology, Swansea, England, Society for Experimental Biology, 205–234.

Mosier, T. M., D. F. Hill, and K. V. Sharp, 2014: 30-arcsecond monthly climate surfaces with global land coverage. *Int. J. Climatol.*, 34, 2175–2188, doi:10.1002/joc.-3829.

Mueller, R., and Coauthors, 2013: Berkeley Earth temperature averaging process. *Geoinfo. Geostat. Overview*, 1 (2), doi:10.4172/2327-4581.1000103.

OCHA, 2015: Drought in Central America in 2015: Situation report (as of October 6, 2015). United Nations Office for the Coordination of Humanitarian Affairs (OCHA). [Available online at http://www.redhum.org/uploads/documentos/pdf/Sitrep_OCHA-ROLAC_Drought_in_CA_EN_061015- 20151006-AL-17144.pdf.]

Palmer, W. C., 1965: Meteorological drought. U.S. Weather Bureau Research Paper 45, 58 pp.

Panofsky, H. A., and G. W. Brier, 1968: Some Applications of Statistics to Meteorolo-

gy. Pennsylvania State University Press, 224 pp.

Penman, H. L., 1948: Natural evaporation from open water, bare soil and grass. Proc. Roy. Soc. London, 193, 120–145, doi:10.1098/ rspa.1948.0037.

Peters, E. J., 2015: The 2009/2010 Caribbean drought: A case study. Disasters, 39, 738–761, doi:10.1111/disa.12123.

Rauscher, S. A., and Coauthors, 2008: Extension and intensification of the Meso-American mid-summer drought in the twenty-first century. *Climate Dyn.*, 31, 551–571, doi:10.1007/ s00382-007-0359-1.

Rohde, R., and Coauthors, 2013: A new estimate of the average Earth surface land temperature spanning 1753 to 2011. *Geoinfo. Geostat.* Overview, 1 (1), doi:10.4172/2327-4581.1000101.

Roth, D. M., 2008: Hurricane Flora (1963) rainfall graphic. Tropical cyclone point maxima, National Weather Service. Accessed 9 June 2012. [Available online at http://www.wpc.ncep. noaa.gov/tropical/rain/flora1963filledrainblk.gif.]

Sahay, R., 2005: Stabilization, debt, and fiscal policy in the Caribbean. International Monetary Fund, Working Paper 05/26, 43 pp. [Available online at https://www.imf.org/external/pubs/ft/ wp/2005/wp0526.pdf.]

Schneider, U., A. Becker, P. Finger, A. Meyer-Christoffer, B. Rudolf, and M. Ziese, 2015a: GPCC full data reanalysis version 7.0 at 1.08: Monthly land-surface precipitation from rain-gauges built on GTS-based and historic data, doi:10.5676/ DWD_GPCC/FD_M_V7_100.

——, ——, ——, ——, and M. Ziese, 2015b: GPCC monitoring product: Near real-time monthly land-surface precipitation from rain-gauges based on SYNOP and CLIMAT data, doi:10.5676/DWD_GPCC/MP_M_V5_100.

Schultz, D. M., W. E. Bracken, and L. F. Bosart, 1998: Planetary and synoptic-scale

signatures associated with Central American cold surges. *Mon. Wea. Rev.*, 126, 5–27, doi:10.1175/ 1520-0493(1998)126,0005:PASSSA.2.0.CO;2.

Sheffield, J., E. F. Wood, and M. L. Roderick, 2012: Little change in global drought over the past 60 years. Nature, 491, 435–438, doi:10.1038/nature11575.

Smerdon, J. E., B. I. Cook, E. R. Cook, and R. Seager, 2015: Bridging past and future climate across paleoclimatic reconstructions, observations, and models: A hydroclimate case study. J. Climate, 28, 3212–3231, doi:10.1175/JCLI-D-14-00417.1.

Stephenson, T. S., and Coauthors, 2014: Changes in extreme temperature and precipitation in the Caribbean region, 1961– 2010. *Int. J. Climatol.*, 34, 2957–2971, doi:10.1002/joc.3889.

——, and Coauthors, 2016: Regional climates: The Caribbean [in "State of the Climate in 2015"]. Bull. Amer. Meteor. Soc., 97, S181–S182, doi:10.1175/2016BAMSStateoftheClimate.1.

Taylor, M. A., D. B. Enfield, and A. A. Chen, 2002: Influence of the tropical Atlantic versus the tropical Pacific on Caribbean rainfall. *J. Geophys. Res.*, 107, 3127, doi:10.1029/2001JC001097.

Thornthwaite, C. W., 1948: An approach toward a rational classification of climate. Geogr. Rev., 38, 55–94, doi:10.2307/210739.

van der Schrier, G., P. D. Jones, and K. R. Briffa, 2011: The sensitivity of the PDSI to the Thornthwaite and Penman–Monteith parameterizations for potential evapotranspiration. *J. Geophys. Res.*, 116, D03106, doi:10.1029/2010JD015001.

——, J. Barichivich, K. R. Briffa, and P. D. Jones, 2013: A scPDSI-based global data set of dry and wet spells for 1901–2009. *J. Geophys. Res. Atmos.*, 118, 4025–4048, doi:10.1002/ jgrd.50355.

Vicente-Serrano, S. M., S. Beguería, and J. I. López-Moreno, 2010: A multiscalar

drought index sensitive to global warming: The standardized precipitation evapotranspiration index. *J. Climate*, 23, 1696–1718, doi:10.1175/2009JCLI2909.1.

Wells, N., S. Goddard, and M. J. Hayes, 2004: A self-calibrating Palmer drought severity index. *J. Climate*, 17, 2335–2351, doi:10.1175/1520 0442(2004)017,2335:ASPDSI.2.0.CO;2.

Wilhite, D. A., M. D. Svoboda, and M. J. Hayes, 2007: Understanding the complex impacts of drought: A key to enhancing drought mitigation and preparedness. *Water Resour. Manage.*, 21, 763–774, doi:10.1007/s11269-006-9076-5.

Williams, A. P., R. Seager, J. T. Abatzoglou, B. I. Cook, J. E. Smerdon, and E. R. Cook, 2015: Contribution of anthropogenic warming to California drought during 2012–2014. *Geophys. Res. Lett.*, 42, 6819–6828, doi:10.1002/2015GL064924.

Wood, A. W., L. R. Leung, V. Sridhar, and D. P. Lettenmaier, 2004: Hydrologic implications of dynamical and statistical approaches to downscaling climate model outputs. Climatic Change, 62, 189–216, doi:10.1023/B:CLIM.0000013685.99609.9e.

Zhao, T., and A. Dai, 2015: The magnitude and causes of global drought changes in the twenty-first century under a low– moderate emissions scenario. *J. Climate*, 28, 4490–4512, doi:10.1175/JCLI-D-14-00363.1.

——, and ——, 2017: Uncertainties in historical changes and future projections of drought. Part II: Model-simulated historical and future drought changes. *Climatic Change*, doi:10.1007/ s10584-016-1742-x.

FIGURES

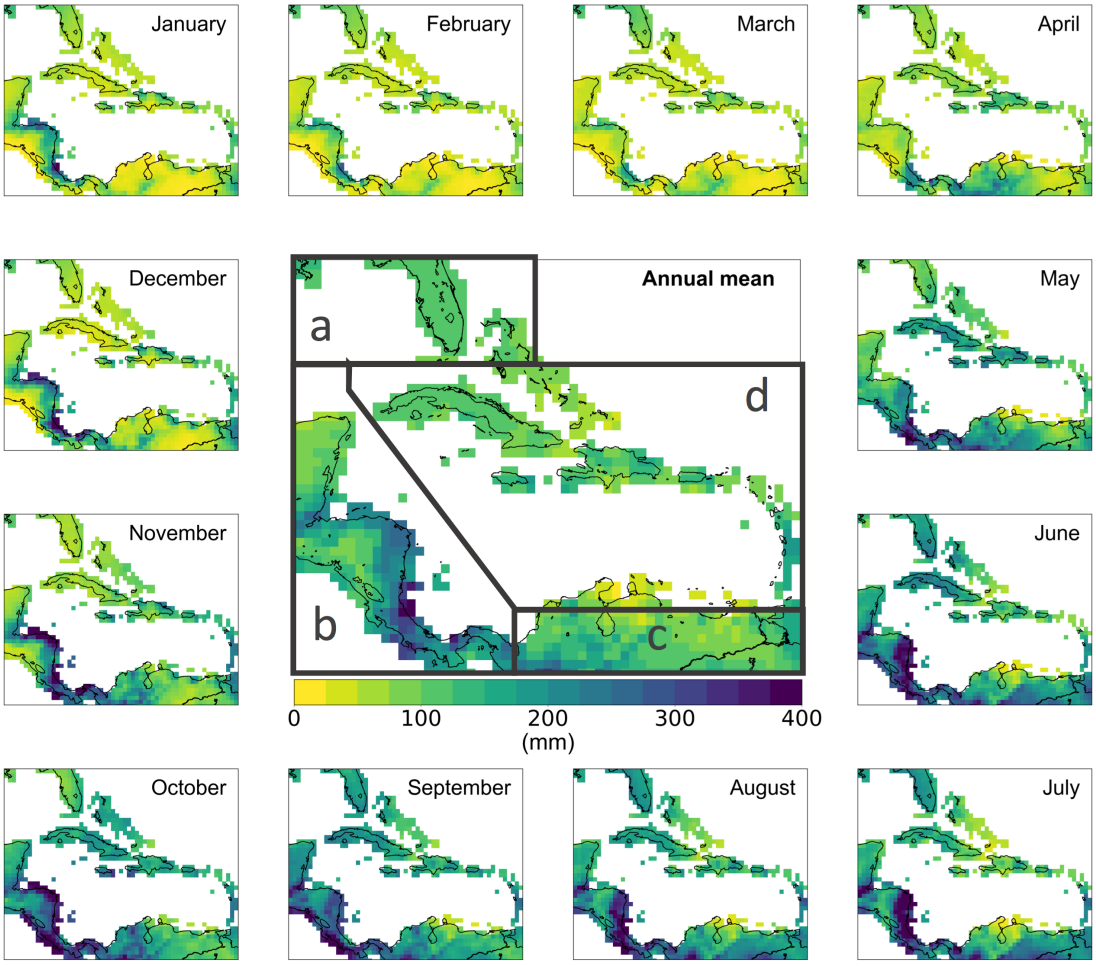

FIG. 1. Monthly precipitation climatology of the study domain (1950–2000) from the GPCC V7 at 0.58 resolution and the annual mean and four focus regions of this work: (a) the Florida Peninsula, (b) Central America, (c) northern South America, and (d) the Caribbean.

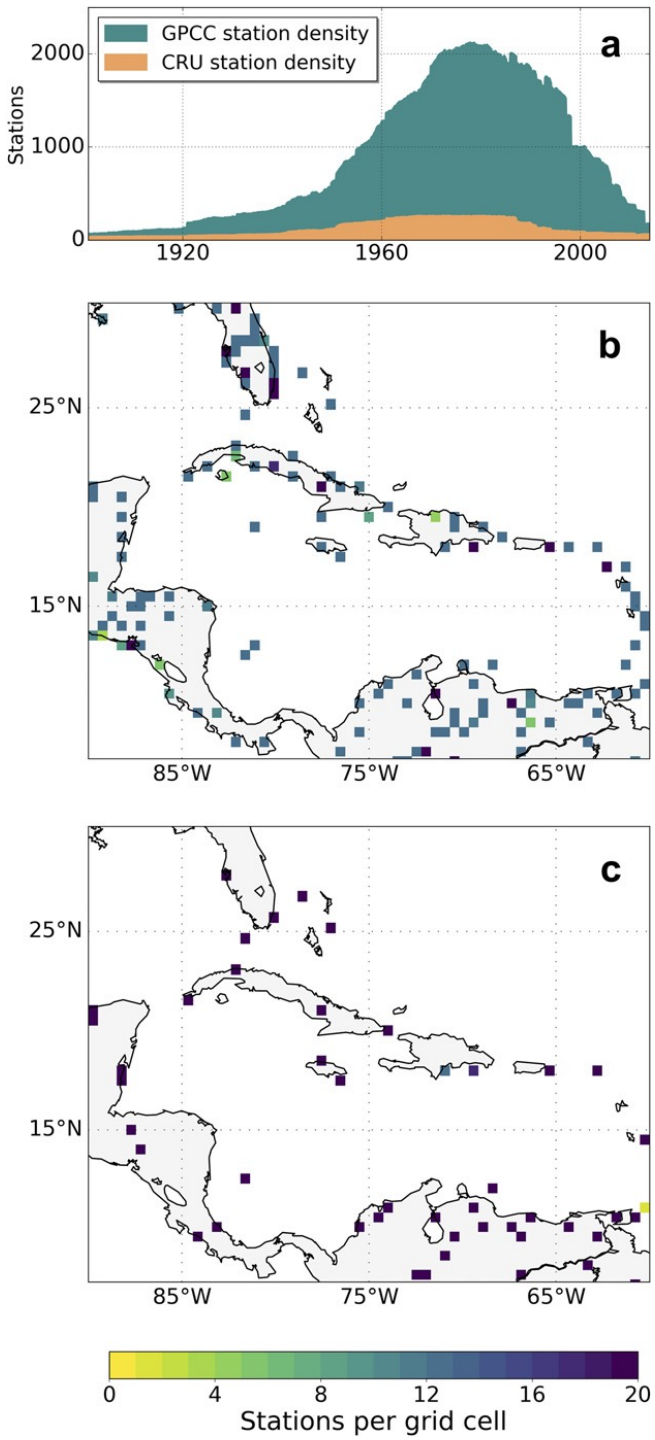

FIG. 2. Number of stations used by GPCC V7 and CRU TS3.24 in our study domain: (a) station density time series during the 1901– 2013 interval, (b) number of station of GPCC, and (c) CRU TS 3.24 in 2013.

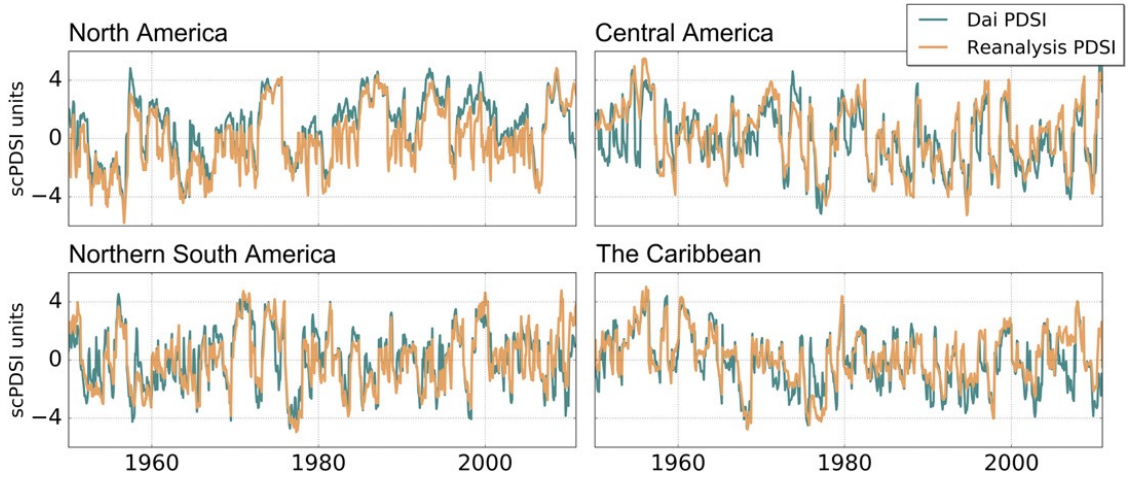

FIG. 3. Comparison between the coarse-resolution PDSI calculated using the NCEP–NCAR reanalysis data (regridded to 18) and the Dai PDSI dataset (Dai 2011) on few selected grids from North America, Central America, northern South America, and the Caribbean. The "reanalysis PDSI" was computed using the GPCC V7 dataset for precipitation and reanalysis products of temperature, total cloud cover, and wind speed climatology.

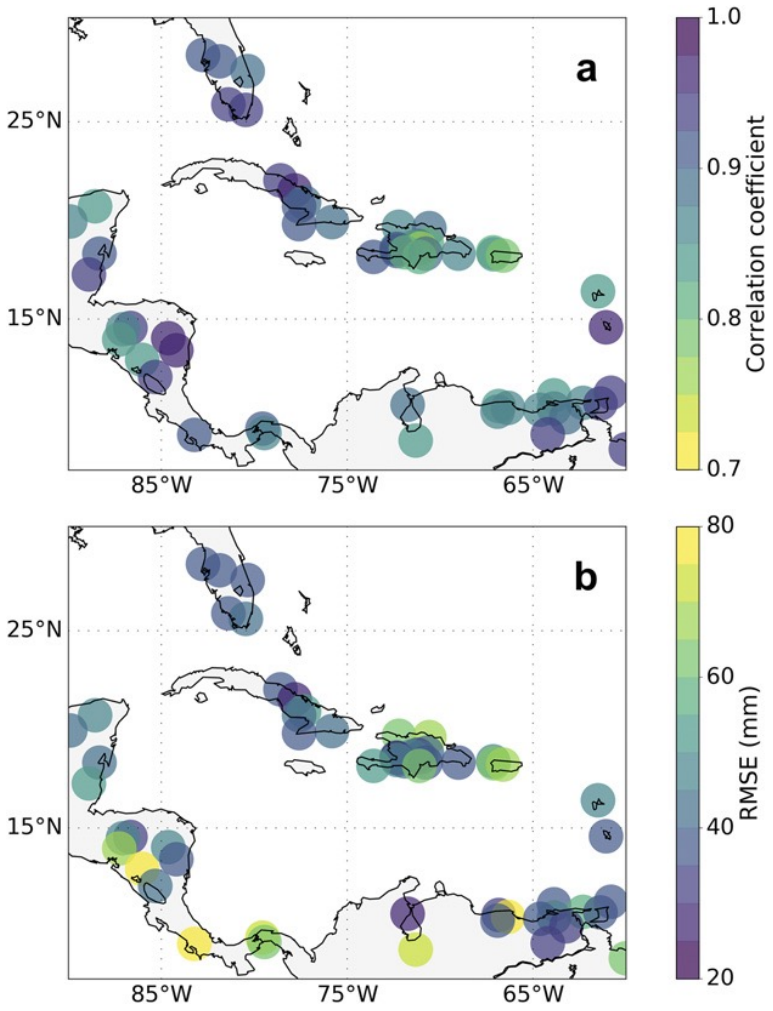

FIG. 4. (a) Correlation coefficients and (b) RMSEs between our downscaled precipitation product and GHCN station data. We selected GHCN stations with at least 15 years with continuous data during the 1950–2016 interval.

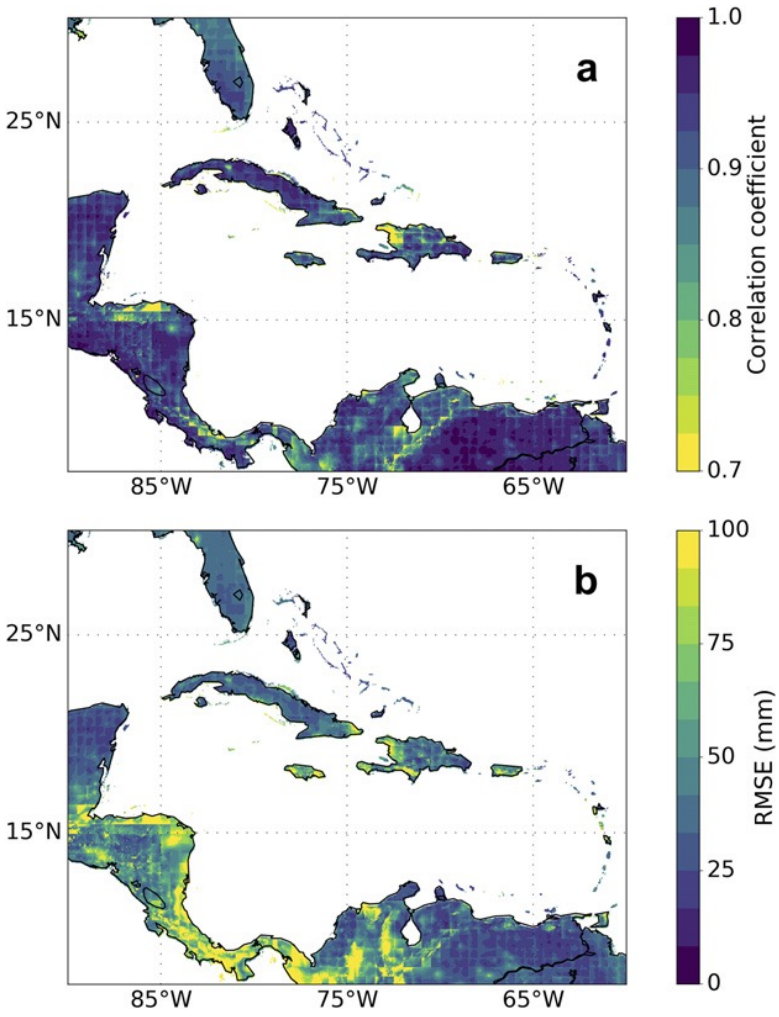

FIG. 5. (a) Correlation coefficients and (b) RMSEs between our downscaled precipitation product and the GPCC V7 interpolated to 4 km (using the nearest-neighbor method) during the 1950–2016 interval. The largest biases are observed over Central America and the Andes in South America.

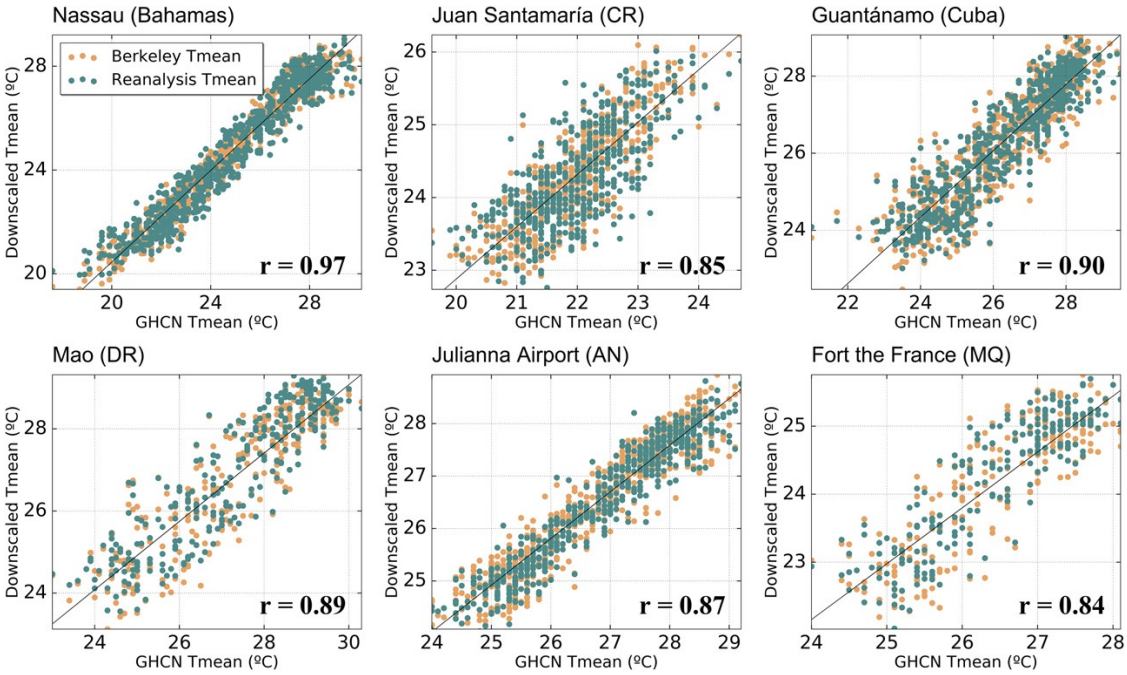

FIG. 6. Scatterplots of monthly mean temperatures of six GHCN stations and downscaled data from BEST (brown) and reanalysis (cyan) data during the 1950–2016 interval. We selected weather stations with at least 10 years without missing data located in the Bahamas, Costa Rica (CR), Cuba, Dominican Republic (DR), Netherlands Antilles (AN), and Martinique (MQ, France). The values of both axes differ in each panel because of differences in the average temperature among stations. Diagonal lines in each panel represent the 1:1 correlation line.

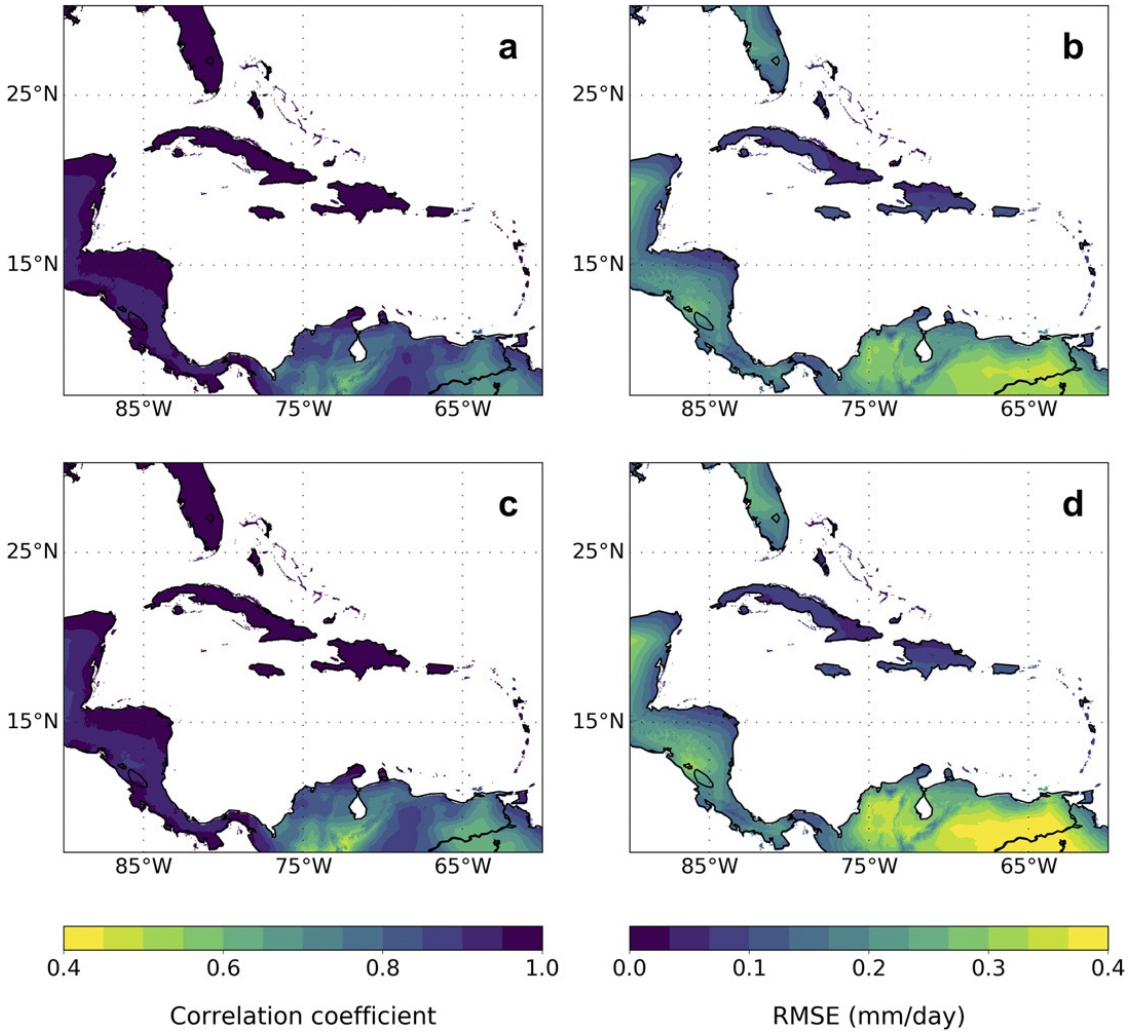

FIG. 7. (a), (c) Correlation coefficients and (b), (d) RMSEs between PET calculated using BEST and NCEP– NCAR reanalysis surface temperature products. Lower correlations were observed over northern South America, while the highest RMSEs were also observed on the same region. Note that (a) and (b) show correlations and RMSE, respectively, using the full time series (from 1950 to 2016), while (c) and (d) are the same metrics as computed after 1980 to assess the skill of reanalysis for the satellite era.

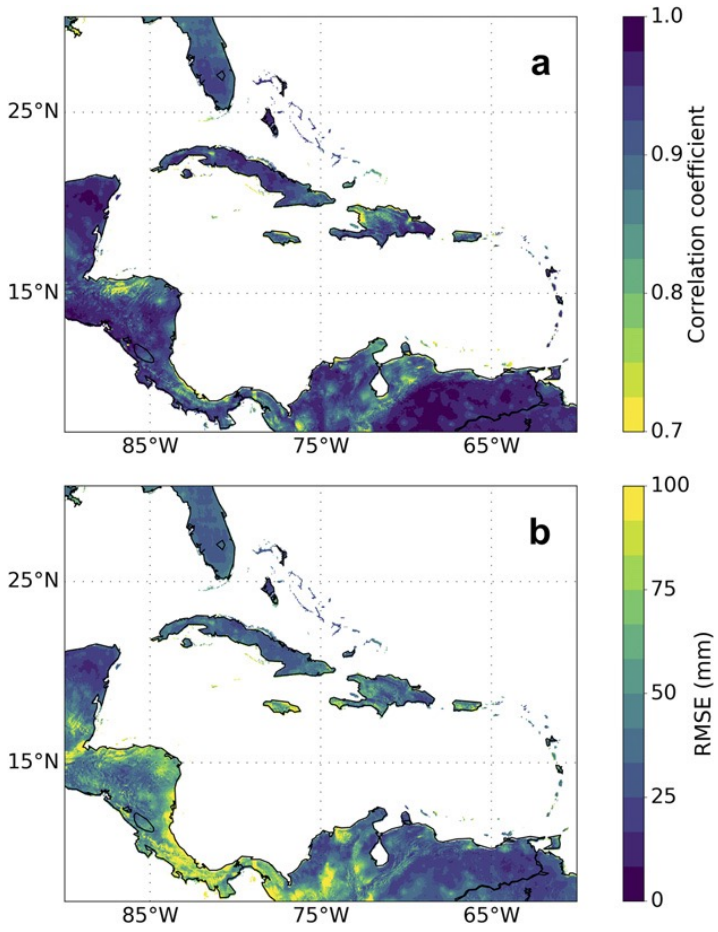

FIG. 8. (a) Correlation coefficients and (b) RMSEs between downscaled precipitation products using WorldClim and CHELSA. Both downscaled products span the 1950–2016 interval.

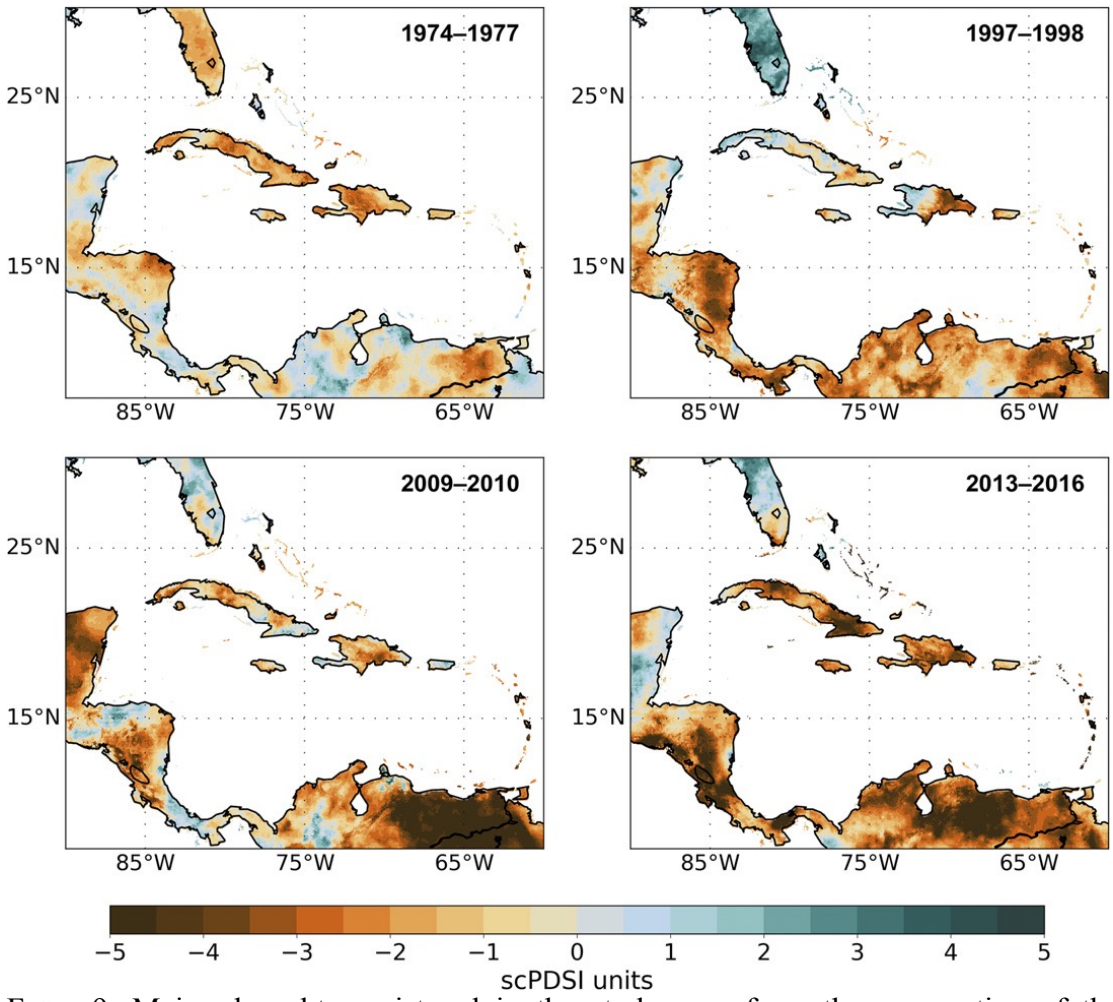

FIG. 9. Major droughts registered in the study area from the perspective of the Caribbean between 1950 and 2016 of at least one year in duration.

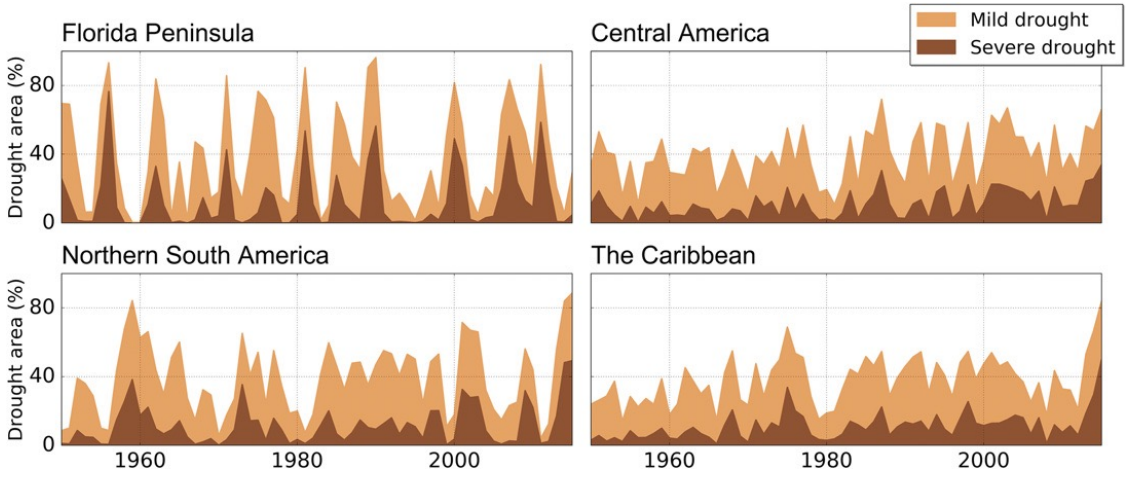

FIG. 10. Drought area index time series of the four focus regions used in this work, calculated based on the percentage of grid cells with scPDSI # 21 (mild drought) and with scPDSI # 23 (severe drought).

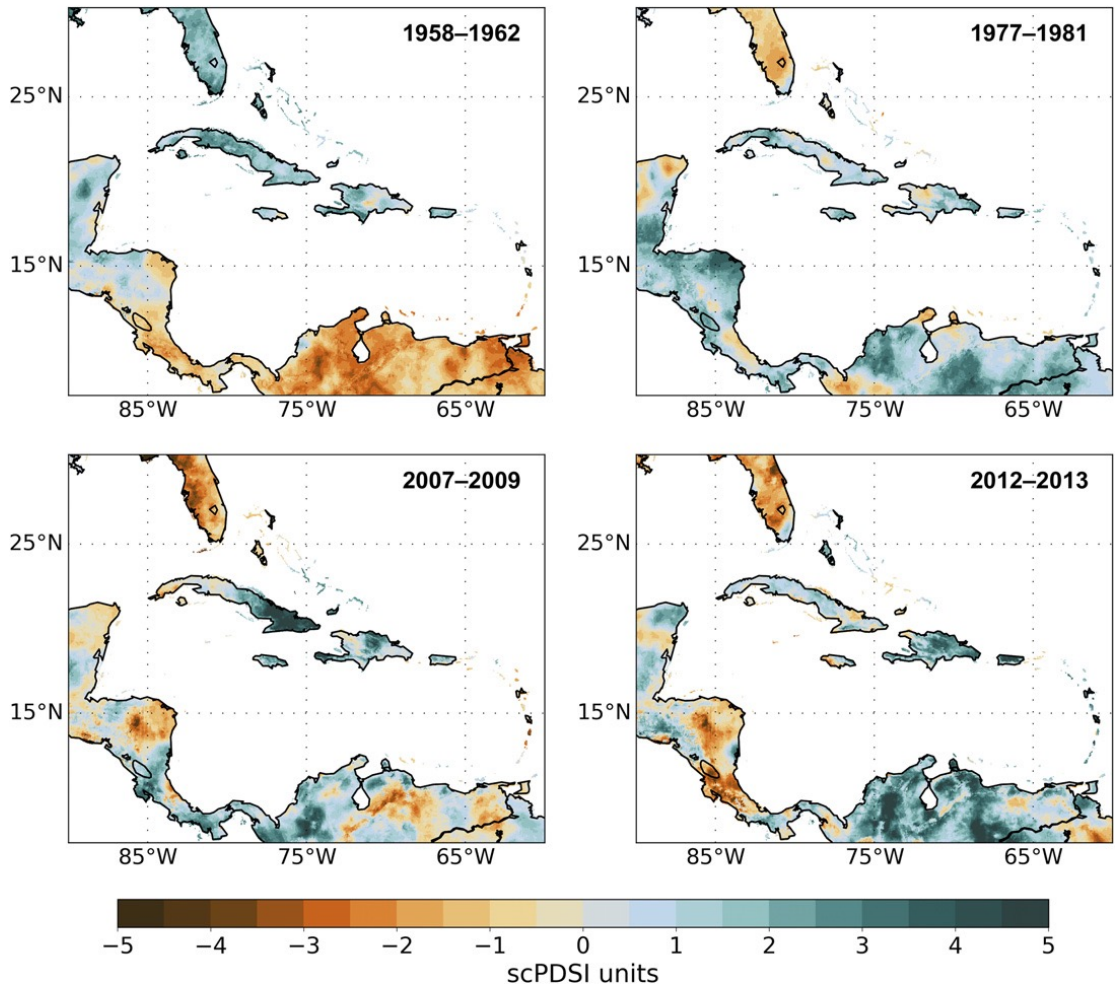

FIG. 11. As in Fig. 9, but for pluvials.

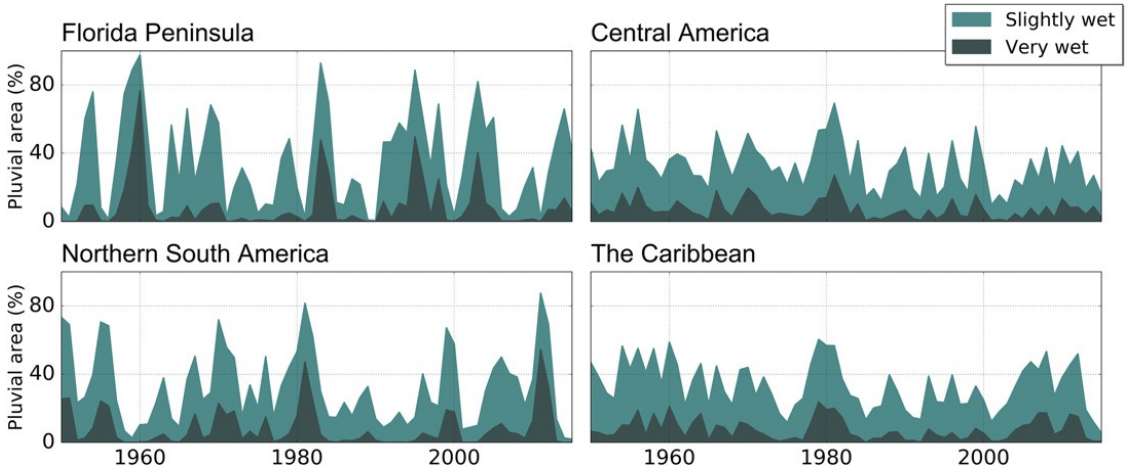

FIG. 12. As in Fig. 10, but for pluvials.

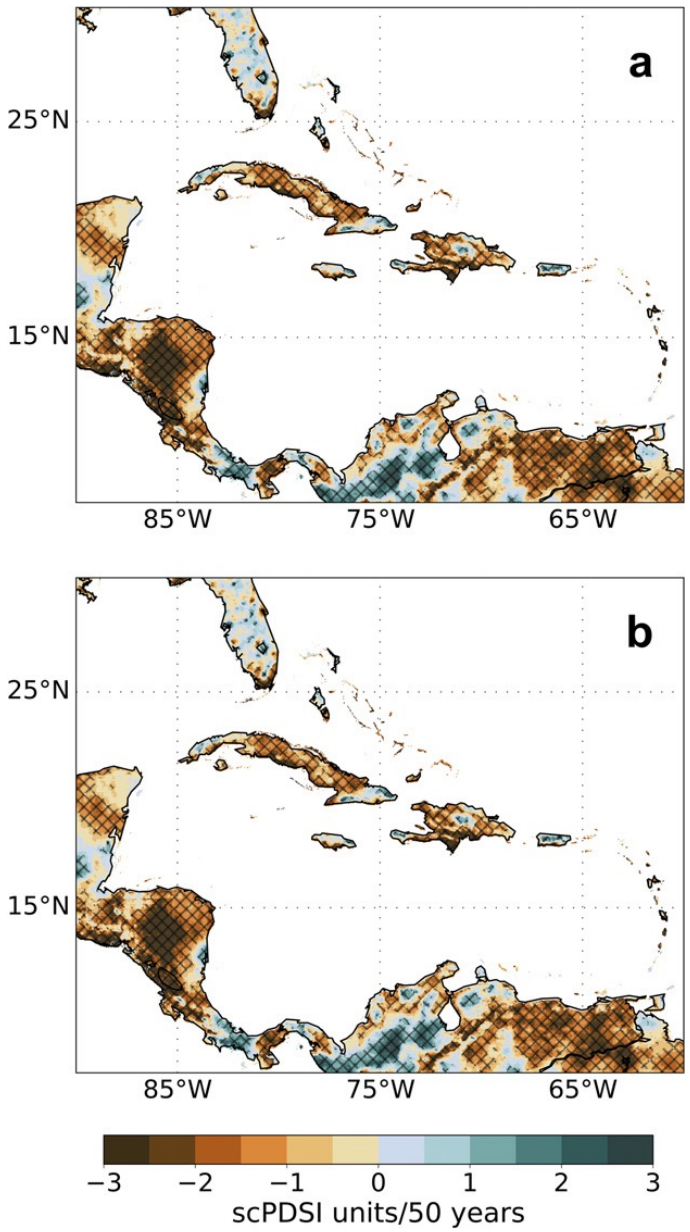

FIG. 13. Linear trends showing (a) the change of the scPDSI during the 1950–2016 interval and (b) in 1950–2008. Brown colors represent a drying trend, and cyan colors a wetting trend. In (a) and (b), the hatching means a significant trend ($p < 0.05$) at the 95% level.

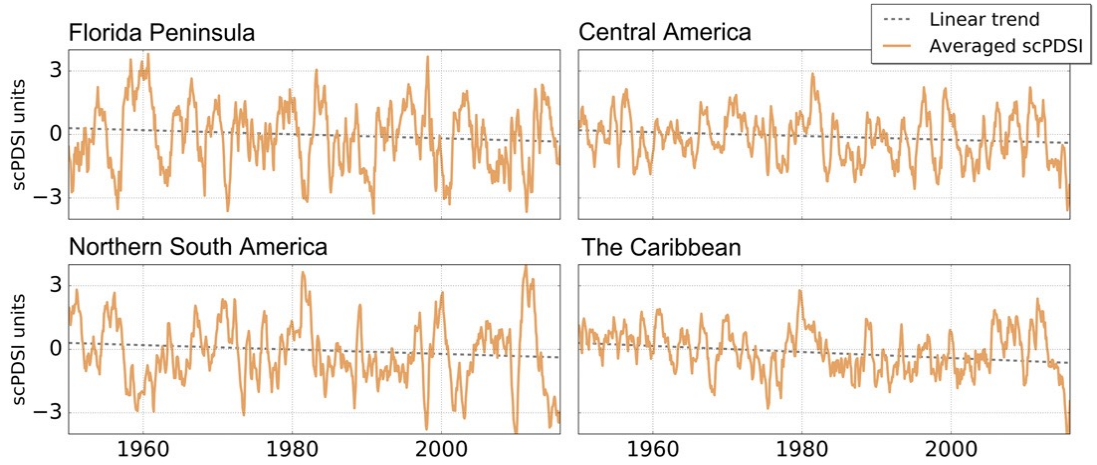

FIG. 14. Linear trends of spatially averaged scPDSI over the four key regions. Note the seesaw pattern between the Florida Peninsula and northern South America.

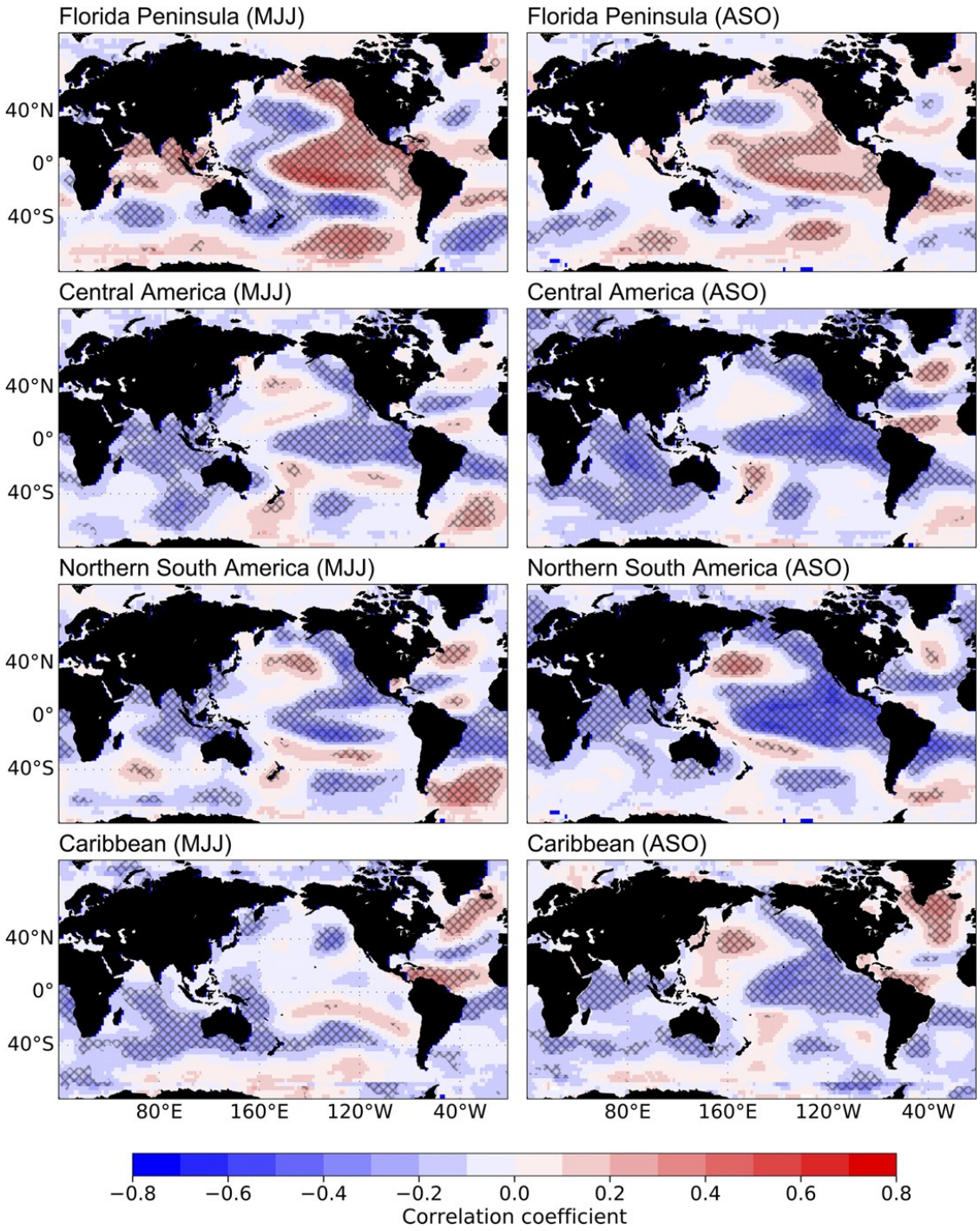

FIG. 15. Seasonal correlations between regionally averaged scPDSI time series in our study domain and global SSTAs during the 1950–2016 interval. The hatched areas are statistically significant correlations at the 95% level.

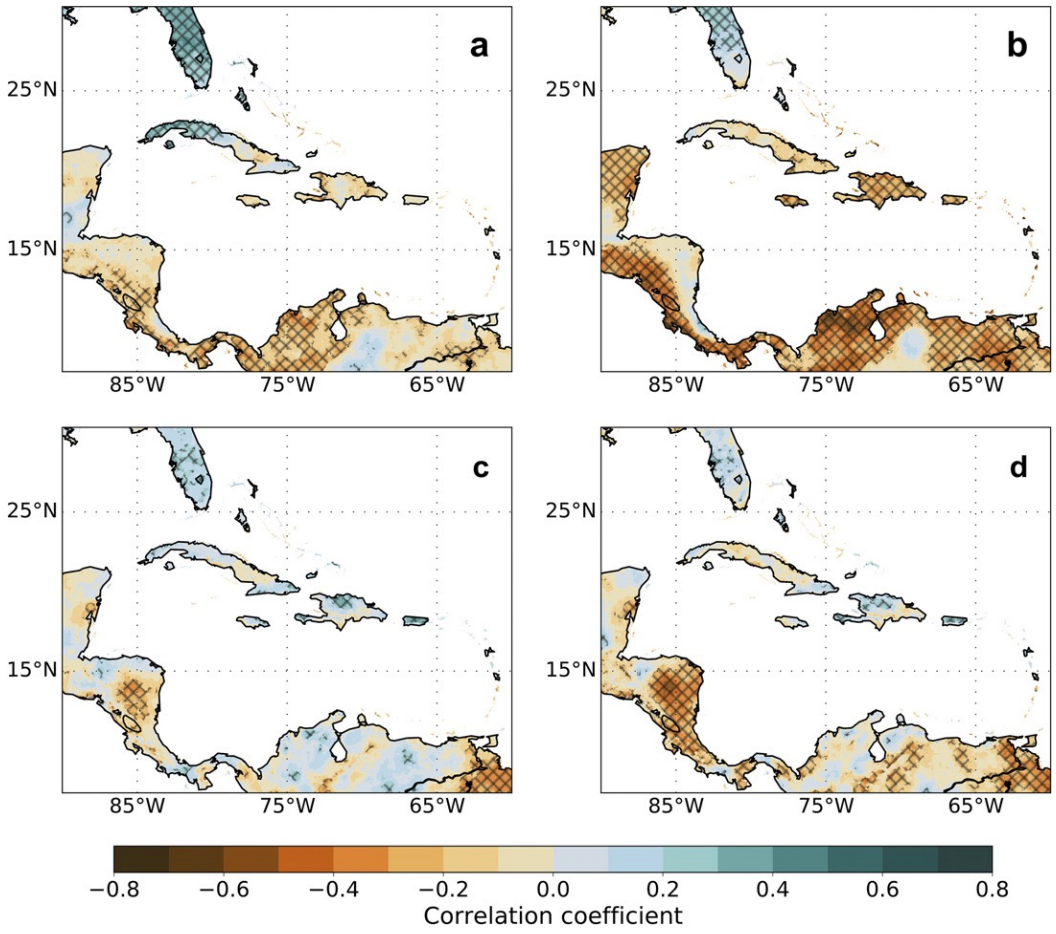

FIG. 16. Correlations between scPDSI and SSTAs over the Niño-3.4 region during the (a) MJJ and (b) ASO periods. (c),(d) As in (a),(b), but with SSTAs over the tropical North Atlantic. The hatched areas are statistically significant correlations at the 95% level.

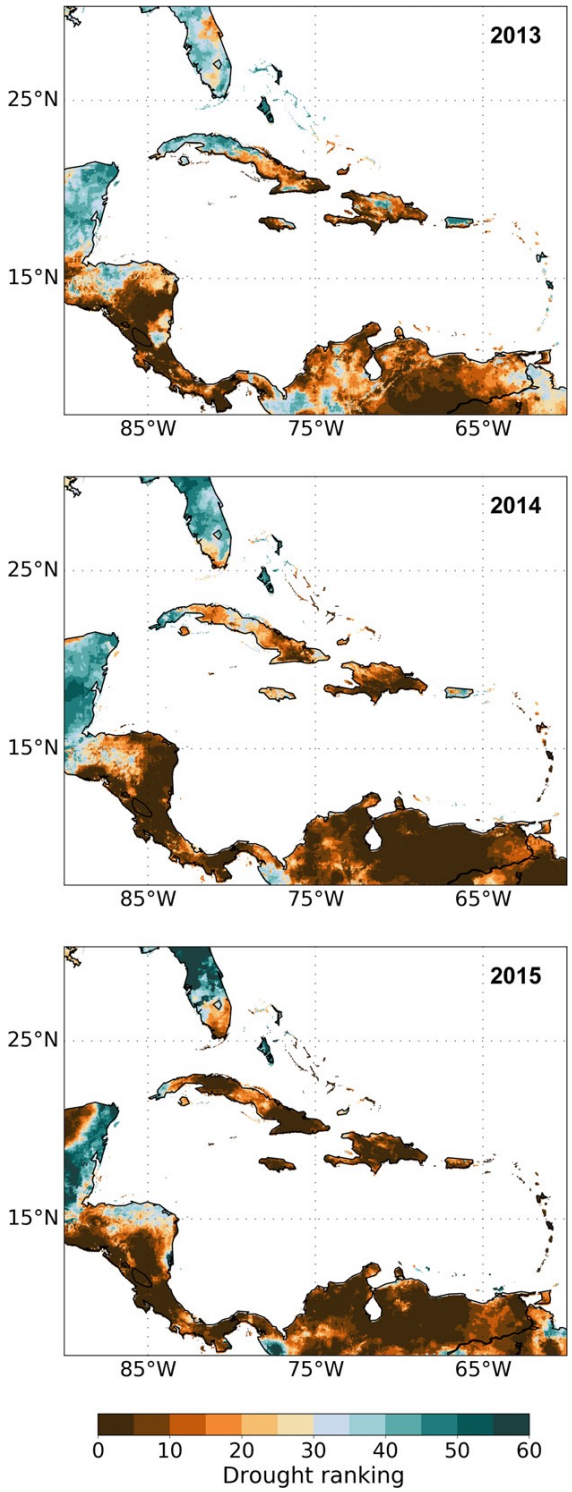

FIG. 17. Annual drought rankings between 2013 and 2015. Drought conditions in 2014 ranked as the most severe since 1950 in a greater area than in 2015. However, in the Caribbean, 2015 ranks as the driest year during the 2013–2016 drought.

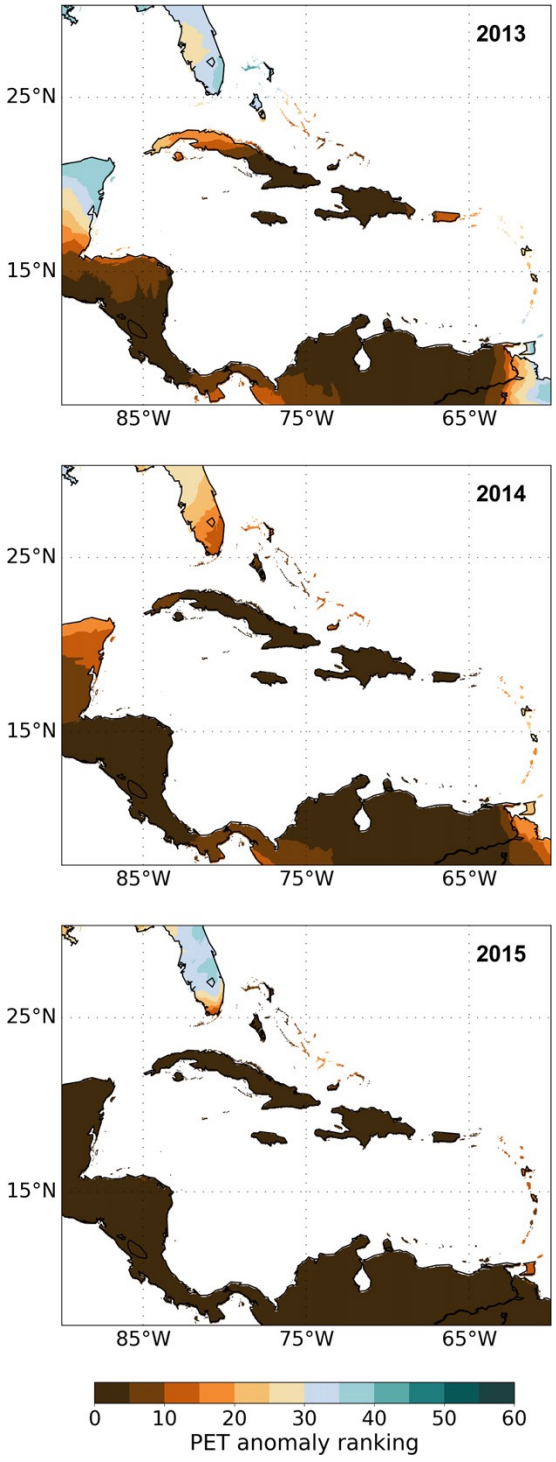

FIG. 18. As in Fig. 17, but for annual PET anomalies.

TABLES

TABLE. 1. Monthly climate datasets used in this work.

Variable	Dataset	Native resolution	Period used	Reference
Precipitation	*GPCC	1º	1949–2016	Schneider et al. (2014)
	*CHIRPS	0.05º	1981–2016	Funk et al. (2015)
	*CRU TS4.01	0.5º	1949–2016	Harris et al. (2014)
	WorldClim (Climatology)	~1 km	1950–2000	Hijmans et al. (2005)
	*CHELSA (Climatology)	~1 km	1979–2013	Karger et al. (2016)
Temperature	*BEST	1º	1949–2016	Rohde et al. (2013)
	*NCEP–NCAR Reanalysis	2.5º	1949–2016	Kalnay et al. (1996)
	*CRU TS4.01	0.5º	1949–2016	Harris et al. (2014)
	WorldClim (Climatology)	~1 km	1950–2000	Hijmans et al. (2005)
Net radiation	*JRA-55 Reanalysis	~1.25º	1958–2016	Ebita et al. (2011)
	*NCEP–NCAR Reanalysis	~1.8º	1949–2016	Kalnay et al. (1996)
	*CRU TS4.01	0.5º	(Climatology)	Harris et al. (2014)
	*CERES	1º	2001–2016	Loeb et al. (2012)
Wind speed	*NCEP–NCAR Reanalysis	2.5º	1981–2010 (Climatology)	Kalnay et al. (1996)
	*CRU TS4.01	0.5º	1949–2016	Harris et al. (2014)
Vapor pressure	Derived from *BEST	1º	1949–2016	Rohde et al. (2013)
	*CRU TS4.01	0.5º	1949–2016	Harris et al. (2014)
Elevation	WorldClim	~1 km	- -	Hijmans et al. (2005)
Available Water Holding Capacity	*IGBP–DIS	0.08º	- -	Global Soil Data Task Group (2000)
Radiative fluxes	*CERES	1º	2001–2016	Loeb et al. (2012)

***GPCC: Global Precipitation Climatology Centre Version 7.**
***CRU: Climatic Research Unit version TS4.01**
***CHIRPS: Climate Hazards Group InfraRed Precipitation with Station data.**
***CHELSA: Climatologies at High resolution for Earth's land Surface Areas.**
***BEST: Berkeley Earth Surface Temperature.**
***NCEP–NCAR: National Centers for Environmental Predictions–National Center for Atmospheric Research.**
***IGBP–DIS: International Geosphere-Biosphere Programme Data and Information Services.**
***CERES: Clouds and Earth's Radiant Energy Systems.**
***JRA-55: Japanese 55-year Reanalysis.**

TABLE. 2. Correlations between spatially averaged scPDSI time series of the regions shown in Fig. 1. Bold numbers indicate a statistically significant correlation ($p < 0.05$) at the 95% level.

	Central America	**Northern South America**	**The Caribbean**
Florida Peninsula	**–0.3**	**–0.5**	**0.06**
Central America		**0.7**	**0.46**
Northern South America			**0.4**

CHAPTER 2

EXACERBATION OF THE 2013–2016 PAN-CARIBBEAN DROUGHT BY ANTHROPOGENIC WARMING

DIMITRIS HERRERA[1], TOBY AULT[1], JOHN T. FASULLO[2], SLOAN J. COATS[2], CARLOS M. CARRILLO[1], BENJAMIN I. COOK[3,4], A. PARK WILLIAMS[4]

[1]Department of Earth and Atmospheric Sciences, Cornell University, Ithaca, 14853, NY, USA.

[2] Climate and Global Dynamics Division, National Center for Atmospheric Research, 3090 Center Green Dr., Boulder, CO, 80301, USA.

[3] NASA Goddard Institute for Space Studies, 2880 Broadway, New York, NY, USA.

[4] Lamont-Doherty Earth Observatory of Columbia University, 61 Route 9W, Palisades, 10964, NY, USA.

Abstract

The Caribbean islands are expected to see more frequent and severe droughts due to reductions in precipitation and increases in evaporative demand as a result of anthropogenic climate change. Between 2013 and 2016 the region experienced a "Pan-Caribbean" drought that was the most severe and widespread event since at least 1950, due in part to El Niño in 2015, but it is unknown whether its severity was exacerbated by increased evaporative demand due to anthropogenic warmth. We examine the role of recent warming on this drought, using new high-resolution self-calibrating Palmer Drought Severity Index (scPDSI) datasets. Anthropogenic warmth accounted for 16–18% of drought severity, and between 7% and 20% of the Pan Caribbean drought's spatial extent. Our findings suggest that anthropogenic warming is already increasing drought risk in the Caribbean and is likely to continue to do so in the near future with major implications for more than 43 million people living in this region.

1. Introduction

Since at least 1950, the Caribbean has seen a gradual drying trend (Neelin et al.2006; Dai, 2011; van der Schrier et al. 2013; Herrera and Ault, 2017) with several multi-year droughts, the most severe and widespread of which occurred between 2013 and 2016 (Herrera and Ault, 2017). Given its extensive spatial scale, we refer to this event as the "Pan-Caribbean Drought" (Fig. 1). This drought affected the entire region and pushed more than two million people into food insecurity (OCHA, 2015). The effects were particularly acute in Haiti, where one million people (~10% of its population) were severely affected by food insecurity and required immediate assistance, and further worsened the situation of an additional 3.8 million food-insecure people (OCHA, 2015). The Pan-Caribbean drought occurred in conjunction with precipitation deficits, which were driven in part by a strong El Niño in 2015 (OCHA, 2015; Blunden et al. 2016), and some of the highest temperature and potential evapotranspiration (PET) anomalies observed in the region (Herrera and Ault, 2017). As compared to the 1997–1998 drought, which also occurred during a strong El Niño, the Pan-Caribbean drought was considerably more severe (see Methods), and it affected regions usually associated with wet conditions during El Niño, such as western Cuba (Jury et al. 2007; Herrera and Ault, 2017). Further details about El Niño-Caribbean drought teleconnections are described in the Supporting Information.

Given the warming and drying trends projected for the Caribbean over the coming decades (Dai, 2011; IPCC, 2014; Hayhoe, 2013), and because the Pan-Caribbean drought co-occurred with unprecedented high temperatures (Herrera and Ault, 2017), assessing the role of anthropogenic warmth on this drought is critical to better project drought risk in the Caribbean. In this work, we quantify the contribution of anthropogenic warming to the Pan-Caribbean drought using climate data from observations and model simulations for the period 1949–2016 (see Methods and Tables S1, S2). To address the inherent limitations of coarse resolution datasets for characterizing drought in the Caribbean, the observed gridded products are statistically-downscaled following Herrera and Ault (2017) (see Methods).

We estimate the effect of anthropogenic warming on the Pan-Caribbean drought by comparing the observed record of PET and self-calibrating Palmer Drought Severity Index (scPDSI) (Palmer, 1965; Wells et al. 2004) to an alternate record calculated after removal of observed warming trends since 1950, as in Williams et al. (2015). We refer to the alternate PET and scPDSI records that do not include warming trends as "adjusted" records. In both calculations, we use unadjusted precipitation, net radiation, and wind speed data. The anthropogenic contribution is estimated as the difference between scPDSI calculated using adjusted temperature (T_{min}, T_{mean}, and T_{max}) against scPDSI using unadjusted temperature. Results are compared to PET and scPDSI estimates using multi-model ensembles of T_{min} and T_{max} and net radiation data from the Coupled Model Intercomparison Project phase 5 (CMIP5) (Taylor et al. 2012). CMIP5 simulations account for the influence of anthropogenic-forced and natural variability of temperature to PET; thus, CMIP5 archives can be used as a benchmark to assess the consistency of our methodology. We compare, for example, scPDSI estimated using fully-forced and naturally-forced historical simulations of temperature, against scPDSI using pre-industrial control simulations. This allows us to evaluate the effects of the ~2 Wm^{-2} anthropogenic radiative forcing after the pre-industrial era to the Pan-Caribbean drought. These results are further assessed for consistency with observed monthly surface radiative fluxes and cloud data from NASA's Clouds and Earth's Radiant Energy System (CERES) (Loeb et al. 2012) (see Methods for further details).

We use the UN Food and Agriculture Organization (FAO) reference PET (Allen et al. 1998) because it is more physically realistic (Smerdon et al. 2015; Williams et al. 2015; Abatzoglou et al. 2016) than the Thornthwaite equation (Thornthwaite, 1948) used in the original PDSI (Palmer, 1965). A key drawback of the Thornthwaite approach—especially for climate change applications—is the use of temperature as the only climate variable to estimate PET, which leads to an exacerbation of the sensitivity of PET to temperature variations (Smerdon et al. 2015; Williams et al. 2015; Abatzoglou et al. 2016). The FAO formulation that we use, in contrast, is calculated using temperature, vapor pressure, wind speed, and net radiation (Allen et al. 1998).

2. Data and Methods

2.1. Climate data

The climate products we used to calculate potential evapotranspiration (PET) and self-calibrating Palmer Drought Severity Index (scPDSI) are listed in the Table S1. Because of the relatively coarse horizontal resolution of the current gridded climate products, which varies from 0.5º to 2.5º (~55 km to ~280 km, respectively) and fails to resolve many of the Lesser Antilles (Jury et al. 2007; Dai, 2011; 2013; van der Schrier et al. 2013; Cook et al. 2015), we used statistically-downscaled monthly precipitation data from the Global Precipitation Climatology Centre (GPCC) "combined product" (available at: https://www.esrl.noaa.gov/psd/data/gridded/data.-gpcc.html) (Schneider et al. 2015a,b), and temperature fields (T_{min}, T_{mean}, and T_{max}) from the Berkeley Earth Surface Temperature (BEST) (Rohde et al. 2013). Wind speed and net radiation data were obtained from National Centers for Environmental Predictions–National Center for Atmospheric Research (NCEP–NCAR) (Kalnay et al. 1996) and the Japanese 55-year (JRA-55) (Ebita et al. 2011) reanalyses, and were bi-linearly interpolated to a common resolution of 4 km. The validation of downscaled products and further details of the downscaling and bias-correction procedures we used are described in the Supporting Information and in Herrera and Ault (2017). We also computed alternate PET and scPDSI records based on data from the Climatic Research Unit version TS4.01 (CRU vTS4.01) (Harris et al. 2014) and found that results were nearly identical to those reported here. To carefully assess the role of radiative flux on drought variability, we used observed surface radiation (up and down, shortwave and long wave) and cloud-cover data from the Clouds and Earth's Radiant Energy System (CERES) (Loeb et al. 2012) at 1º geographic resolution spanning January 2001–December 2016. CERES data were not used to calculate PET nor scPDSI, but rather to conduct a complementary analysis of observed radiative fluxes during the Pan-Caribbean drought.

Simulated temperature data (T_{min} and T_{max}) were obtained from the Coupled Model Intercomparison Project Phase 5 (CMIP5) (Taylor et al. 2012) and are listed in Table S2. Models were selected based solely on the availability of monthly T_{min} and T_{max} data

during the study interval. We used temperature data from the archive's historical simulations from 1950 to 2005, appended to the Representative Concentrations Pathway 8.5 (RCP8.5) to cover 2006–2016. Pre-industrial control and naturally-forced historical simulations were used as a benchmark to estimate the contribution of anthropogenic-forcing to scPDSI and PET-anomalies. CMIP5 data of precipitation, net radiation, wind speed, and soil moisture were further used to assess the consistency of scPDSI with simulated soil moisture in terms of interannual variability and long-term trends.

2.2. The "self-calibrating" Palmer Drought Severity Index (scPDSI)

Since it was introduced in the mid-1960s, PDSI (Palmer, 1965), and more recently the scPDSI (Wells et al. 2004), has been widely used in North America for drought monitoring and research (Dai, 2013; van der Schrier et al. 2013; Cook et al. 2015). PDSI has been also used as a metric in hydroclimate reconstructions over the last thousand years in North America, southern Asia, and Europe (Cook et al. 2004; 2015). The index can be computed on a weekly and monthly basis for the purposes of drought monitoring and research. The original PDSI consists of a simple water balance model that uses precipitation and PET as moisture supply and demand, respectively, coupled with a two-layer soil model (Palmer, 1965). Despite its successful use in diagnosing drought during recent decades, the PDSI has been criticized for a lack of coherence across different climates (Alley, 1984). This issue is largely due to the constant duration factors in the original PDSI formulation, which were empirically derived from stations in the central US (Palmer, 1965; Alley, 1984; Wells et al. 2004). scPDSI addresses this limitation by automatically calculating duration factors based on local climate conditions during a determined calibration period (Wells et al. 2004). The PDSI's calibration period is the interval used to establish the normal hydroclimatic conditions for a specific location (Palmer, 1965), and hence partially controls the variance of the index. scPDSI is calculated with the same basic formulation as the original PDSI as:

$$X_i = pX_{i-1} + qZ_i, \quad (1)$$

where X_i is the index value in month i, X_{i-1} is the index of the previous month, p and q

are the duration factors, and Z_i is the current moisture anomaly. The duration factors determine the autocorrelation of the PDSI by assigning different weights to X_{i-1} and Z_i to determine the current index. As suggested in Dai (2011; 2013), we used a 1950–1980 calibration period in our scPDSI computations because the anthropogenic signal is more pronounced after the 1980s. However, because the JRA-55 reanalysis spans 1958–near present, we used a 1958–1980 period in our estimations with JRA-55. Further details on how we calculated scPDSI are described by Herrera and Ault (2017).

2.3. The Penman-Monteith (PM) potential evapotranspiration (PET) method.

We used a modified version of the original Penman-Monteith (PM) method, as used by the UN Food and Agricultural Organization (FAO) (Allen et al. 1998). We selected this method because it requires fewer inputs for its computation as compared to the original PM method (Penman, 1948; Monteith, 1965; Allen et al. 1998), which is advantageous for regions where climate data are sparse such as the Caribbean. The theoretical basis of the FAO-PM method lies in an idealized grass-surface with a permanent water supply and 0.12 m height. It also assumes a soil resistance of 70 s m^{-1}, and a surface albedo of 0.23 (Allen et al. 1998). Formally, PET is calculated with the following equation:

$$PET = \frac{0.408\Delta(Rn-G)+\gamma\frac{900}{T+273.16}U_2(e_s-e_a)}{\Delta+\gamma(1+0.34U_2)}, \quad (2)$$

where,

$$U_2 = U_{10}\frac{\ln(128)}{\ln(661.3)}$$

PET is the crop reference evapotranspiration (mm day^{-1}), Rn is the net radiation (MJ m^{-2} d^{-1}), T is the average temperature at 2 m height (ºC), G is the soil heat flux density (MJ m^{-2} d^{-1}), U_2 is the wind speed measured (or estimated from U_{10}) at 2 m height (m s^{-1}), U_{10} is the wind speed measured at 10 m height (m s^{-1}), $e_s - e_a$ is the vapor pressure deficit measured at 2 m height (kPa), Δ is the slope of the vapor pressure curve (kPa $ºC^{-1}$), γ is the psychrometric constant (kPa $ºC^{-1}$), 900 is the numerator coefficient

for the reference crop (kJ^{-1} kg K d^{-1}), and 0.34 is the denominator coefficient for the reference crop (s m^{-1}) (Allen et al. 1998). In contrast to previous studies that used this method for calculating PET (Cook et al. 2015; 2016; Karnauskas et al. 2016), we estimated gridded saturated vapor pressure (e_s) using our downscaled and bias-corrected T_{max} and T_{min} products with the following equation (Allen et al. 1998):

$$e(T) = 0.6108exp\left[\frac{17.27\,T}{T+237.3}\right], \quad (3)$$

where $e(T)$ is the vapor pressure (kPa) as a function of the air temperature, and T is the air temperature in degrees Celsius (ºC). The actual vapor pressure (e_a) was also obtained with Eq. (3) but using our downscaled T_{min} instead of dew-point temperature because we wanted to be consistent with (e_s), which was estimated with our downscaled temperature datasets. Also, we found that this simplification did not have meaningful impact on the results, as, when we calculated PET from reanalysis data, the Caribbean PET record was similar regardless of whether we calculated (e_a) from T_{min} or specific humidity. Furthermore, since we used our downscaled temperature datasets for these computations, the topographic influence to vapor pressure was therefore taken into account. This PET dataset is the same we used in Herrera and Ault (2017), and is currently available upon request.

2.4. Estimation of anthropogenic contribution

For the anthropogenic contribution estimates, we used a suite of observations and simulations to calculate PET and scPDSI as in Williams et al. (2015). Because there is not observed temperature data without the anthropogenic fingerprint, we used linearly-detrended temperatures to estimate scPDSI without the impact of anthropogenic forcing. We therefore assume the anthropogenic-forced component solely as the linear trend observed in temperature during the period 1950–2016 in the Caribbean. Despite its simplicity, we used this approach—rather than an alternative formal detection and attribution (D&A) methodology—because we aimed to specifically evaluate the effect of the warming trend on the Pan-Caribbean drought, which models probably more accurately characterize than anthropogenic-forced effects on interannual variability and

magnitude of extremes on a single observed event. In addition, we used CMIP5 outputs of fully-forced and naturally-forced historical simulations to validate the performance and accuracy of our linear-detrending method for temperature in the Caribbean. In contrast to Williams et al. (2015), we only used this method and not a low-pass filter to find the anthropogenic trend because our estimates did not span the whole 20th century. Further, we did not attempt to identify the anthropogenic component of other variables used in the calculation of scPDSI (such as precipitation) because of the difficulty of separating forced and internal variability in these variables (Deser et al. 2012; Cook et al. 2014; Williams et al. 2015).

Estimates from the CMIP5 multi-model ensemble were conducted by comparing scPDSI calculated using historical simulations (1950–2005) appended to the Representative Concentration Pathway 8.5 (RCP8.5) scenario (2006–2016), against scPDSI calculated with naturally-forced historical (1950–2005) and pre-industrial control simulations (1950–2016). Along with temperature, we evaluated net radiation data to determine the change in drought severity due to the ~2 Wm^{-2} anthropogenic radiative forcing after the pre-industrial era. Similarly, given that scPDSI does not account for CO_2 effects on drought via physiological effect on plant stomatal resistance, we compared simulated scPDSI with simulated soil moisture data as in Cook et al. (2015). We finally used observed surface radiation data between 2001 and 2016 from CERES to evaluate the observed radiative signatures associated with the drought. Collectively, these sensitivity experiments emphasize that temperature, not radiation, is the primary driver of interannual variability in Caribbean drought severity and spatial extent.

2.5. Statistical significance.

Given the relatively small size of our sample (n=48 months from January 2013 to December 2016), and because the data are not normally distributed, we implemented a resampling (with replacement), or "bootstrap", method to estimate the statistical significance of our findings. Here, the null-hypothesis states that "anthropogenic warmth did not increase the Pan-Caribbean drought severity and the observed trends in

temperature and scPDSI are random", while the alternative hypothesis states that "anthropogenic warmth has intensified the drought". We selected the mean as the statistic to test using the unadjusted-temperature scPDSI means to contrast with the adjusted-temperature scPDSI means. We followed these steps to conduct such a test: (i) we adjusted the means of the observed scPDSI samples to match the unadjusted scPDSI means, (ii) the modified observed scPDSI data were randomly resampled 10000 times, (iii) we then calculated the mean of each of the 10000 simulated scPDSI series to obtain the normal distribution of the 10000 scPDSI means, (iv) finally, we calculated the *p*-values as the probability of proportion of means equal or below the observed scPDSI mean. We repeated this procedure on each gridcell of our domain to further generate the statistical significance maps used in this work.

3. Results

Observed annual PET anomalies during 2013–2016 were significantly higher than PET anomalies with the detrended temperatures, increasing PET rates from 20 mm/year to 68 mm/year in the Caribbean on average (Fig. 2). The CMIP5 multi-model ensemble supports a similar contribution of higher temperatures to these PET-anomalies, increasing from 9 mm/year with the pre-industrial control to 33 mm/year with the RCP8.5 scenario (Fig. 2B). However, the magnitude of simulated PET-anomalies was lower than that from observations, likely because multi-model ensemble temperatures were also lower in the Caribbean. Changes in PET-anomalies on each island were comparable to those observed in the Caribbean as a whole, with the lowest change in the Lesser Antilles (38 mm/year), and the highest in Hispaniola Island (48 mm/year) (Fig. 2C).

Anthropogenic warmth accounted for approximately 16% of the Pan-Caribbean drought severity across the region, which was significant against the null hypothesis that these trends in scPDSI were random (see Methods and Supporting Information) (Fig. 3). Consistent with observations, estimations from the CMIP5 multi-model ensemble indicated an ~18% ($p < 0.05$) contribution to drought severity with the RCP8.5 scenario during this period as compared to the pre-industrial control However, there was

substantial geographic variability in these contributions across the Caribbean (Fig. 3A). For example, the greatest changes in scPDSI were observed in Cuba, where drought severity with 32% ($p < 0.05$) contribution, while in the Lesser Antilles it was only 6% and not statistically significant. Anthropogenic contributions to drought severity in Hispaniola Island were 13% ($p < 0.05$), yet drought severity changes were only statistically significant on parts of the island (Fig. 3A). In Jamaica, anthropogenic warmth contributed to ~16% of drought severity ($p < 0.05$), while in Puerto Rico the contribution was 12% and not statistically significant ($p > 0.05$) (Fig. 3C).

Higher temperatures also enhanced the geographic extent of the drought (Fig. 3D). In the Caribbean, for example, anthropogenic warmth accounted for 7% of the area affected by mild-drought (scPDSI values between –1.9 and –1.0) and for ~20% of the area under severe-drought (scPDSI values between –3.9 and –2.0) (Table 1). These changes encompass areas of nearly 16,000 km^2 and 13,000 km^2, respectively. Consistent with changes in drought severity, the greatest change in dry area was observed over Cuba, where the warming trend accounted for 16% and 25% of areas under mild and severe drought, respectively (Fig. 3D). For comparison, a 16% contribution to drought area in Cuba corresponds to ~10,400 km^2 more land under mild-drought, which roughly comprises 10% of the total area of the country (109,820 km^2 (CIA, 2013); Table 1), or almost the area of Jamaica (10,991 km^2) (CIA, 2013). In Hispaniola Island, Puerto Rico, Jamaica, and the Lesser Antilles, contributions to mild-drought area ranged from approximately 6% to 19% (Table 1).

We found that drought severity, as estimated with scPDSI, does not respond linearly to changes in PET-anomalies at local scales. By comparing Fig. 2A with 3A, for example, this nonlinearity is noticeable in southern Hispaniola Island and parts of central-eastern Cuba, where the largest anthropogenic contributions to PET-anomalies were observed. These areas, however, do not corresponded to those with the highest anthropogenic contributions to scPDSI. This apparent discrepancy is likely related to how scPDSI is calibrated. For example, the scPDSI's sensitivity to both precipitation and PET varies across the region because it is calibrated to local climate conditions.

Consequently, relative contributions of precipitation and PET to scPDSI vary depending on the climate of a specific location. During the Pan-Caribbean drought, we found that regions with the lowest coefficients of variation in precipitation anomalies coincided with those areas where the anthropogenic contribution to drought was higher (Fig. S1). This result suggests that the effect of anthropogenic warming on drought severity is stronger in areas where precipitation is less variable.

4. Discussion

Our estimates of anthropogenic warmth contributions to the Pan-Caribbean drought severity are likely conservative for several reasons. For example, we treated anthropogenic warming as an approximately linear trend from 1950 onward, but in reality the rate of anthropogenic warming may have been higher during the latter part of that time period (e.g., Williams et al. 2015). We further did not consider anthropogenic effects on precipitation trends and variability and how these affected the Pan-Caribbean drought, as these effects are likely too complex to be approximated by an empirical trend since 1950 (Deser et al. 2012; Williams et al. 2015; Abatzoglou et al. 2016). Notably, climate models consistently simulate significant decreases in precipitation in the Caribbean as anthropogenic greenhouse-gas concentrations increase in the future (Neelin et al. 2006; IPCC, 2014), and if those impacts are already present in the precipitation data we employed, then the total contribution of anthropogenic climate change would be greater than the temperature-only part we have estimated here.

During the Pan-Caribbean drought, precipitation anomalies were not the lowest on record in the Caribbean. By comparing precipitation anomalies of some of the worst droughts in the region (Fig. 4B), it is evident that the 1974–1977 and 1968–1969 droughts had larger rainfall deficits. However, drought rankings calculated with scPDSI (Fig. S2) indicate the Pan-Caribbean drought as the most severe drought in ~32% of the Caribbean islands, but when removing the warming trend this area changed to 21% (Fig. S2).

Although inherent uncertainties in our estimations arise from our statistical downscaling method, the paucity of long-term high quality weather station data and the relatively low resolution of CMIP5 data relative to the size of the Caribbean Islands precluded a more accurate evaluation. Nevertheless, our results indicate that anthropogenic warmth almost certainly increased drought severity and the area experiencing record-breaking drought in the Caribbean. This is similar to what was found for California during the 2012–2014 drought (Williams et al. 2015). We further validated our downscaled products with station data from the Global Historical Climatology Network (GHCN) (Supporting Information). As shown in Figure S3, our products correlated well with the GHCN stations we selected in the Caribbean and northern South America. However, these stations could not be integrated in our downscaling nor bias-correction procedures because most of them have less than 20 years of continuous climate data.

scPDSI does not account for the effect of increased atmospheric CO_2 concentration on plant physiology, which is hypothesized to diminish PET-induced soil drying by increasing water use efficiency of plants (Cook et al. 2016). To assess the impact of not accounting for these vegetation feedbacks, we compared scPDSI from CMIP5 with soil moisture from CMIP5 during 1950–2016 over the Caribbean as in Cook et al. (2015). Simulated soil moisture in the coupled land surface models of CMIP5 is a more explicit and physically based representation of the surface moisture balance than the simple bucket model used in scPDSI, and includes responses of vegetation to climate and CO_2. If CO_2 effects on water use efficiency do have a large water savings effect, we would expect the model soil moisture to show substantially less drying than scPDSI. For each CMIP5 model considered in the Caribbean, there was a significant correlation between scPDSI and soil moisture anomalies (ranging from $r = 0.23$ to $r = 0.85$, $p < 0.01$), with an average correlation of $r = 0.69$ ($p < 0.01$), and drying trends in scPDSI are not systematically more severe than in the soil moisture. This suggests that scPDSI accurately reflects surface moisture balance in these models, in spite of the simple water balance formulation it uses, and that CO_2 effects on plant physiology and PET-induced drying trends were small in the Caribbean over the period analyzed.

5. Conclusions

The Pan-Caribbean drought of 2013–2016 was appreciably more severe as a result of anthropogenic warmth, a finding that is robust across a range of models and observational datasets. This result supports the idea that anthropogenic climate change is already impacting the Caribbean through temperature effects on PET, and that the recent drought is likely to be a prelude to future episodes under anthropogenic change. That is, we expect future droughts in the region to be increasingly severe because of higher temperatures alone, regardless of changes in precipitation.

As is the case for many of the Small Island Developing States around the world (Holding et al. 2016; Karnauskas et al. 2016), freshwater resources in the Caribbean are already facing a growing number of pressures ranging from saltwater intrusion from sea level rise to demands from the municipal, energy, and agricultural and touristic sectors. Importantly, in the Caribbean Islands freshwater cannot be moved around at large scales as it can in the US southwest. Although, new technologies such as desalination have recently provided relief in some Caribbean Islands, particularly in the Lesser Antilles and the Bahamas (UNESCO, 2016), the operational cost of desalination plants in many cases outweighs their benefits. Moreover, the economic limitations of many Caribbean nations preclude the implementation of such an option (UNESCO, 2016). Finally, though the 2013–2016 Pan-Caribbean drought was unprecedented in an historical context, our work suggests that it might be a good analogue for the nature of future droughts because of the important role temperature played in exacerbating its severity and extent. Further study of the 2013–2016 drought can help inform strategic policy and water management decisions across the region.

REFERENCES

Abatzoglou J. T., A. P. Williams, 2016: Impact of anthropogenic climate change on wildfire across western US forests. *Proc Natl Acad Sci USA* 113(42):11770–11775.

Allen, R., and Coauthors, 1998: Crop evapotranspiration: Guidelines for computing crop water requirements. FAO Irrigation and Drainage Paper 56, 300 pp.

Alley, W. M., 1984: The Palmer Drought Severity Index: Limitations and assumptions. *J. Climate Appl. Meteor.*, 23, 1100–1109, doi:10.1175/1520-0450(1984)023,1100:TPDSIL.2.0.CO;2.

Blunden, J., and D. S. Arndt, Eds., 2016: State of the Climate in 2015. *Bull. Amer. Meteor. Soc.*, 97, S1–S275, doi:10.1175/ 2016BAMSStateoftheClimate.1.

Central Intelligence Agency (CIA), The World Factbook 2013-2014. Washington, DC, USA, 2013; https://www.cia.gov/library/publications/the-world-factbook/index.html.

Cook, B. I., and Coauthors, 2014: Global warming and 21st century drying. *Clim Dyn* 43:2607–262.

Cook, B. I., and Coauthors, 2016: North American megadroughts in the Common Era: reconstructions and simulations. *WIREs Clim Chang* 7:411–432.

——, T. R. Ault, and J. E. Smerdon, 2015: Unprecedented 21st century drought risk in the American Southwest and Central Plains. Sci. Adv., 1, e1400082, doi:10.1126/sci-adv.1400082.

Cook E. R., C. A. Woodhouse, C. M. Eakin, D. M. Meko, D. W. Stahle, 2004: Long-term aridity changes in the western United States. *Science*, 306, 1015–1018.

Cook E. R., and Coauthors, 2015: Old World megadroughts and pluvials during the Common Era. *Sci. Adv.* 1:e1500561.

Dai, A., 2011: Characteristics and trends in various forms of the Palmer Drought Severity Index during 1900–2008. *J. Geophys. Res.*, 116, D12115, doi:10.1029/2010-

JD015541.

——, 2013: Increasing drought under global warming in observations and models. *Nat. Climate Change*, 3, 52–58, doi:10.1038/ nclimate1633.

Deser C., and Coauthors, 2012: Uncertainty in climate change projections: the role of internal variability. *Clim Dyn* 38, 527–546.

Ebita A., and Coauthors, 2011: The Japanese 55-year Reanalysis "JRA-55": an interim report. *SOLA*, 7, 149–152.

Harris, I., P. D. Jones, T. J. Osborn, and D. H. Lister, 2014: Updated high-resolution grids of monthly climatic observations: The CRU TS3.10 dataset. *Int. J. Climatol.*, 34, 623–642, doi:10.1002/joc.3711.

Hayhoe K (2013) Quatifying Key Drivers of Climate Variability and Change for Puerto Rico and the Caribbean. (Tech. Report: G10AC00582, 2013) https://s3.amazonaws.com/IndividualGISdata/PDFs/KatherineHayhoe_CaribbeanFinalReport.pdf.

Herrera D, Ault T (2017) Insights from a new high-resolution drought atlas for the Caribbean spanning 1950 to 2016. *J Clim* 30:7801–7825.

Holding, S., D. M. Allen, S. Foster, A. Hsieh, I. Larocque, J. Klassen, and S. C. Van Pelt, 2016: Groundwater vulnerability on small islands. *Nat. Climate Change*, 6, 1100–1103, doi:10.1038/nclimate3128.

IPCC, 2014: Climate Change 2014: Synthesis Report. R. K. Pachauri and L. A. Meyer, Eds., IPCC, 151 pp.

Jury M, Malmgren BA, Winter A (2007) Subregional precipitation climate of the Caribbean and relationships with ENSO and NAO. *J Geophys Res* 112:D16107.

Kalnay, E., and Coauthors, 1996: The NCEP/NCAR 40-Year Reanalysis Project. *Bull. Amer. Meteor. Soc.*, 77, 437–471, doi:10.1175/1520-0477(1996)077,0437:TNYRP.-2.0.CO;2.

Karnauskas, K. B., J. P. Donnelly, and K. J. Anchukaitis, 2016: Future freshwater stress for island populations. *Nat. Climate Change*, 6, 720–725, doi:10.1038/nclimate-2987.

Loeb N. G., and Coauthors, 2012: Observed changes in top-of-the-atmosphere radiation and upper-ocean heating consistent within uncertainty. *Nat Geosci* 5:110–113.

Monteith, J. L., 1965: Evaporation and environment. 19th Symp. of the Society for Experimental Biology, Swansea, England, Society for Experimental Biology, 205–234.

Neelin J. D., H. Münnich, H. Su, J. E. Meyerson, C. E. Holloway, 2006: Tropical drying trends in global model and observations. *Proc Natl Acad Sci USA* 103:6110–6115.

Palmer, W. C., 1965: Meteorological drought. *U.S. Weather Bureau Research Paper* 45, 58 pp.

Penman, H. L., 1948: Natural evaporation from open water, bare soil and grass. *Proc. Roy. Soc. London*, 193, 120–145, doi:10.1098/ rspa.1948.0037.

Rohde, R., and Coauthors, 2013: A new estimate of the average Earth surface land temperature spanning 1753 to 2011. *Geoinfo. Geostat.* Overview, 1 (1), doi:10.4172/2327-4581.1000101.

Schneider, U., A. Becker, P. Finger, A. Meyer-Christoffer, B. Rudolf, and M. Ziese, 2015a: GPCC full data reanalysis version 7.0 at 1.08: Monthly land-surface precipitation from rain-gauges built on GTS-based and historic data, doi:10.5676/ DWD_GPCC/FD_M_V7_100.

——, ——, ——, ——, and M. Ziese, 2015b: GPCC monitoring product: Near real-time monthly land-surface precipitation from rain-gauges based on SYNOP and CLIMAT data, doi:10.5676/DWD_GPCC/MP_M_V5_100.

Taylor KE, Stouffer RJ, Meehl GA, 2012: An overview of CMIP5 and the experiment design. *Bull Am Meteorol Soc* 93:485–498.

Thornthwaite, C. W., 1948: An approach toward a rational classification of climate.

Geogr. Rev., 38, 55–94, doi:10.2307/210739.

United Nations Educational, Scientific and Cultural Organization (UNESCO)-Programa Hidrológico Internacional (PHI) (2006) The use of desalination plants in the Caribbean, technical report http://unesdoc.unesco.org/images/0022/002281/228110e.-pdf.

United Nations Office for the Coordination of Humanitarian Affairs (OCHA) 2015: Drought in Central America in 2015: Situation report (as of October 6, 2015). United Nations Office for the Coordination of Humanitarian Affairs (OCHA). [Available online at http://www.redhum.org/uploads/documentos/pdf/Sitrep_OCHA-ROLAC_Drought_in_CA_EN_061015-20151006-AL-17144.pdf.]

van der Schrier G., J. Barichivich, K. R. Briffa, P. D. Jones, 2013: A scPDSI-based global dataset of dry and wet spells for 1901-2009. *J Geophys Res Atmos* 118:4025–4048.

Wells, N., S. Goddard, and M. J. Hayes, 2004: A self-calibrating Palmer drought severity index. *J. Climate*, 17, 2335–2351, doi:10.1175/1520 0442(2004)017,2335:A-SPDSI.2.0.CO;2.

Williams, A. P., R. Seager, J. T. Abatzoglou, B. I. Cook, J. E. Smerdon, and E. R. Cook, 2015: Contribution of anthropogenic warming to California drought during 2012–2014. *Geophys. Res. Lett.*, 42, 6819–6828, doi:10.1002/2015GL064924.

FIGURES

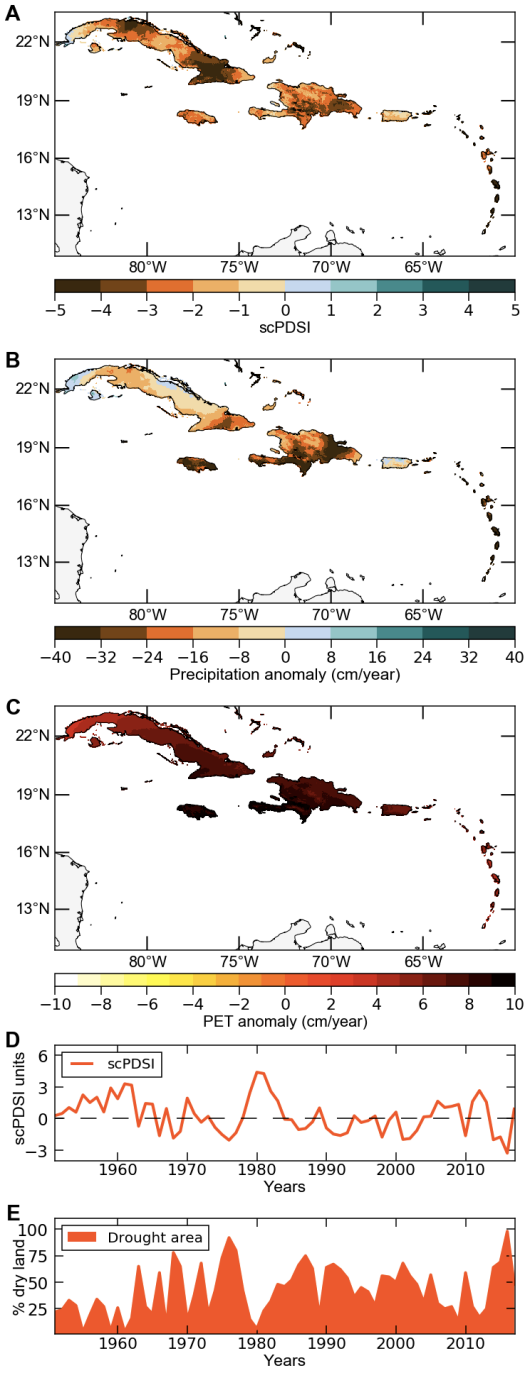

FIG. 1. Spatial and temporal characteristics of the Pan-Caribbean drought: **(A)** scPDSI composite between late 2013 and 2016, panels **(B)** and **(C)** as the same as (A) but with precipitation and Penman-Monteith potential evapotranspiration (PET) anomalies, respectively. Both precipitation and PET anomalies are calculated as departures from

the 1950–1980 climatology. scPDSI time series showing the magnitude of the Pan-Caribbean drought as compared to other droughts between 1950 and 2016 are plotted in **(D)**. Negative scPDSI values indicate drought, while positive values are pluvials. Finally, drought area index between 1950 and 2016 across the Caribbean **(E)**. The Pan-Caribbean drought affected ~98% of land area of the region.

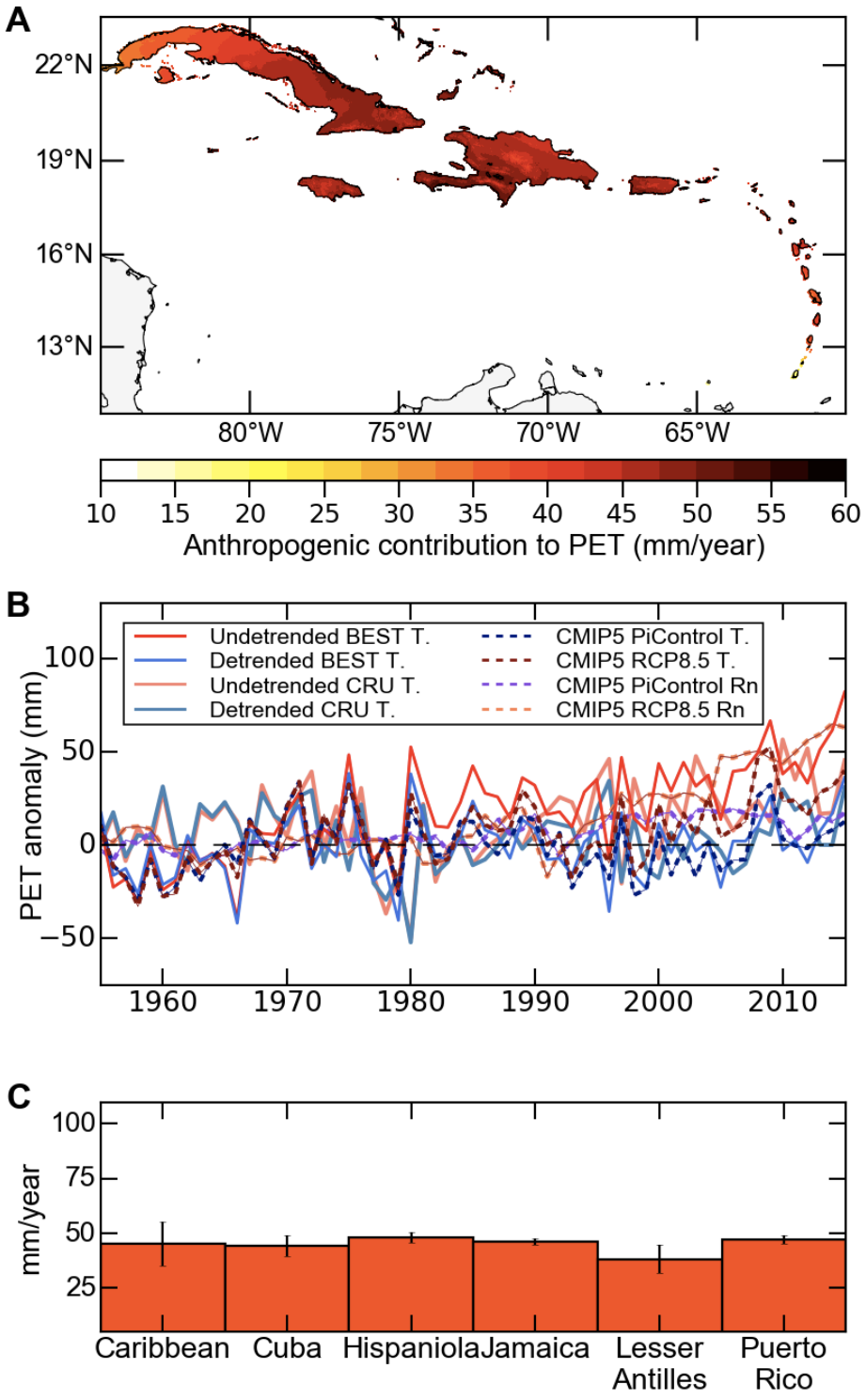

FIG. 2. Anthropogenic contributions to potential evapotranspiration (PET): **(A)** Geographic distribution of anthropogenic contributions to PET anomalies in the Caribbean between 2013 and 2016. **(B)** PET-anomalies time series estimated using

observed and simulated temperature and net radiation data. Reddish colors group PET-anomalies calculated with observed temperature and simulated temperatures with historical plus RCP8.5, while bluish colors group the same anomalies without the anthropogenic warmth. **(C)** contributions to PET by island and the Lesser Antilles.

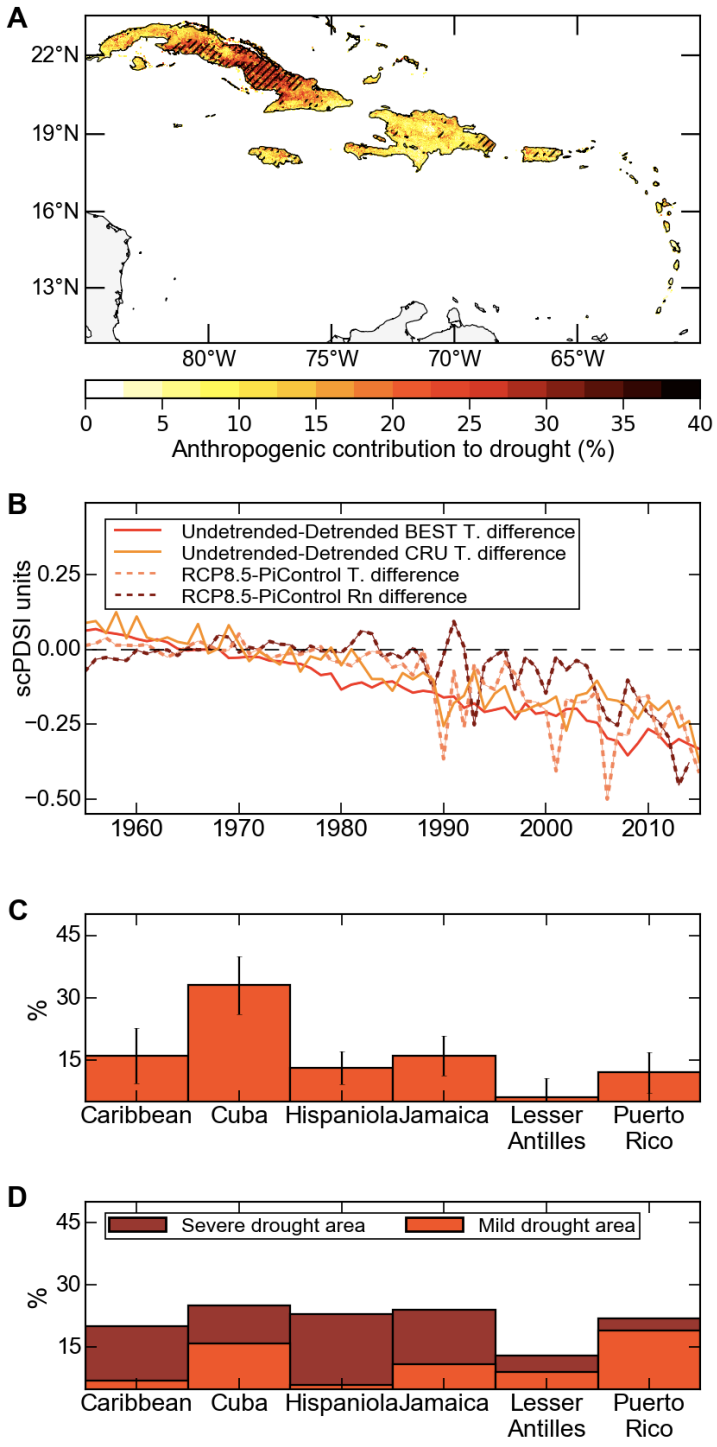

FIG. 3. Anthropogenic contributions to drought severity (scPDSI): **(A)** Anthropogenic contributions to drought severity across the Caribbean. Hatching correspond to statistically significant contributions at the 95% confidence level. **(B)** Changes in drought severity as estimated with scPDSI. The negative trend is the drying contribution

from anthropogenic warmth. **(C)** Anthropogenic contributions (in percentage) to drought severity on each of the Greater Antilles and the Lesser Antilles. **(D)** Anthropogenic contributions to areas under mild (scPDSI between –1.0 and –1.9) and severe drought (scPDSI between –3.9 and –3.0).

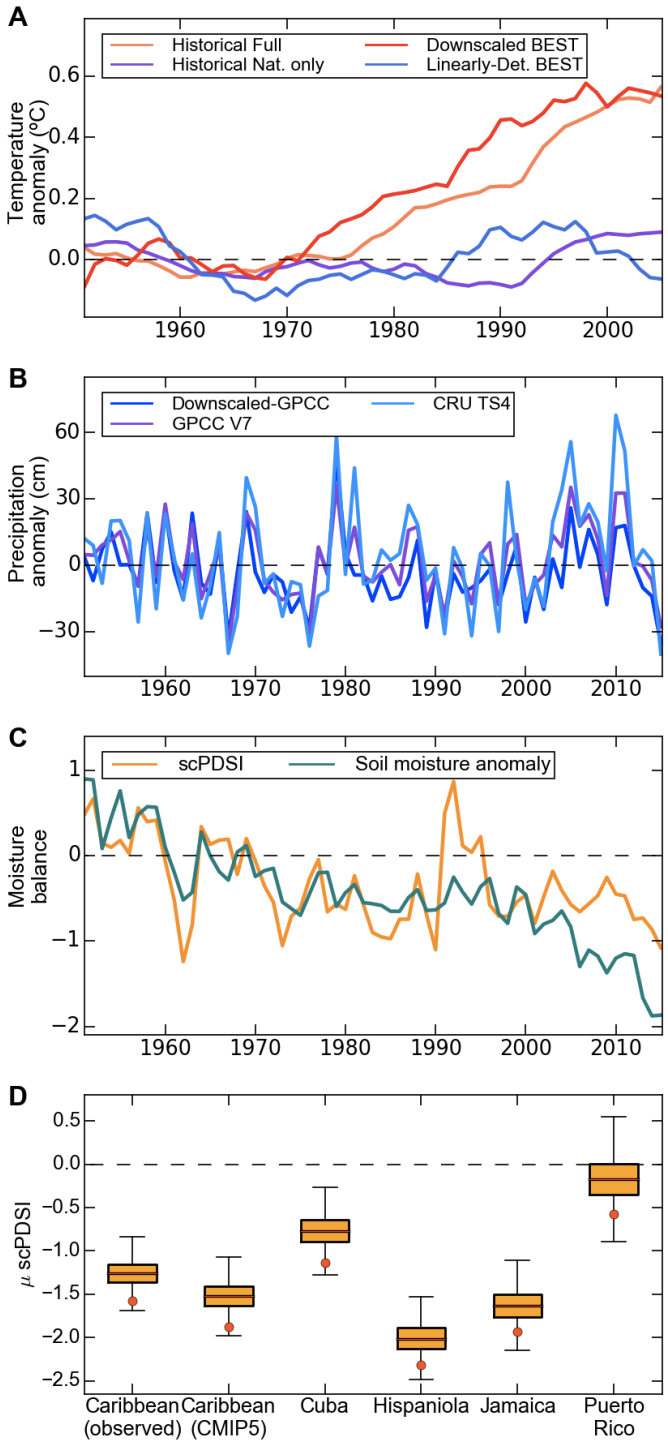

FIG. 4. **(A)** Instrumental and simulated 10-year running mean of temperature anomalies in the Caribbean. Instrumental temperatures (detrended and with the observed trend) come from our statistically-downscaled mean temperature. Simulated temperatures come from a 15-member ensemble of CMIP5 using fully-forced and natural-only forced

historical simulations between 1950 and 2006. **(B)** Annual precipitation anomalies regionally-averaged in the Caribbean. **(C)** Multimodel mean ensemble of simulated scPDSI and soil moisture anomalies during 1950–2016 from CMIP5. **(D)** The distribution of means from the 10000 scPDSI resamples. scPDSI is calculated with detrended temperatures for the Caribbean (using observed and simulated temperatures), for each of the Greater Antilles, and the Lesser Antilles (using observed temperatures). The red dots represent the mean of the observed scPDSI for the Pan-Caribbean drought.

TABLES

TABLE. 1. Relative changes in drought area over land: *"% of land affected"* refers to the percentage of land under each drought category; *"% relative contribution"* refers to the estimated relative anthropogenic contribution to the area of each drought category; while *"Total land area"* is the area of each island/region obtained or calculated from CIA (2013).

Region/Island	**Mild-drought area (scPDSI between –1.00 and –1.99)**		**Severe-drought area (scPDSI between –3.00 and –3.99)**		**Total land area (km^2)**
	Percentage of land affected	***Percentage relative contribution***	***Percentage of land affected***	***Percentage relative contribution***	
Caribbean*	67	7	28	20	239681
Cuba	59	18	22	25	109820
Hispaniola	76	6	33.5	23	76420
Jamaica	65	11	25.9	24	10831
Lesser Antilles*	39	19	37.85	13	9236
Puerto Rico	68	9	13.6	22	8870

* Not including Trinidad and Tobago and Barbados.

SUPPORTING INFORMATION

1. Anthropogenic contributions to drought severity

The contributions of anthropogenic warmth to the Pan-Caribbean drought were estimated using an array of observed gridded climate data, which were combined to validate the consistency of our findings. Specifically, we used the following combinations of (a) precipitation, (b) temperature (T_{min}, T_{mean}, and T_{max}), and (c) net-radiation (if available), total cloud cover, and wind speed to calculate PET and scPDSI:

a. GPCC "combined product", b. BEST, and c. JRA-55 reanalysis.

a. GPCC "combined product", b. BEST, and c. NCEP-NCAR reanalysis.

a., b., and c. CRU TS4.01

a. and b. CRU TS4.01, and c. JRA-55 reanalysis.

From each combination, we obtained the following contributions:

(1) ~14%, (2) ~16%, (3) ~15%, (4) ~13%,

with a mean of ~14.5% and standard deviation of ~1.12%.

2. Validation of downscaled products

As in Herrera and Ault (2017), we validated our downscaled products before using them in our anthropogenic contribution estimations. To do so, we calculated the Pearson correlation coefficient and root-mean-square-errors (RMSE) between 38 weather stations and underlying grid cells for precipitation, and with 20 stations for mean temperature (Fig S3). Most of the weather stations used are from the Global Historical Climatology Network (GHCN), versions 2 and 3. As shown in Fig. S4, correlation coefficients between downscaled monthly precipitation and GHCN station range between $r = 0.76$ and $r = 0.97$, with an average of 0.89 over the Caribbean and northern South America. In terms of RMSE, we found the lowest value with the Maracaibo–Los

Pozos station in Venezuela (RMSE = 27mm), and the highest in Caucagua, also in Venezuela (RMSE = 79mm). In terms of correlation coefficients and RMSE values with temperature fields (T_{min}, T_{mean}, and T_{max}), these were close to what we found with precipitation. The higher biases in mean temperature were found over mountainous regions in Hispaniola Island (RMSE = 0.91ºC), and northern South America (RMSE = 0.89ºC). Similar results were observed with monthly minimum and maximum temperature means, with RMSE ranging from 0.79º to 1.12ºC.

3. ENSO-Caribbean drought

Some of the worst droughts in the Caribbean have been linked to the warm phase of El Niño–Southern Oscillation (ENSO; Peters, 2010; Blunden et al. 2016), including the 1997–1998, 2009–2010, and the 2013–2016 Pan-Caribbean drought. Although the dynamics between ENSO and Caribbean drought is not yet well constrained, previous studies have suggested that a persistent subsidence over northern South America could be responsible of the precipitation deficits observed during El Niño (Giannini et al. 2001a,b). In contrast, the usually wetter conditions observed in northwestern Cuba (e.g., Herrera and Ault, 2017), could be due to an increased intrusion of frontal systems during the boreal winter, when El Niño reaches its maximum intensity (e.g., Schultz et al. 1998; Giannini et al. 2001a,b). However, as described in Jury et al. (2007) and Herrera and Ault (2017), there is a seasonal dependency on ENSO effects to Caribbean precipitation. For example, during El Niño years precipitation deficits in the Caribbean are noticeable in early boreal autumn (ASO), when El Niño usually strengthens. In contrast, spring-summer (MJJ) of the year when El Niño is diminishing, it is usually associated to an even above-normal precipitation (Giannini et al. 2001a; Jury et al. 2007; Herrera and Ault, 2017). In addition, there is also a major geographic variability on ENSO effects to Caribbean precipitation (Jury et al. 2007; Herrera and Ault, 2017) (Fig. S5). ENSO seems to have a stronger influence in Western Caribbean precipitation variability (e.g., Cuba, Jamaica, and western Hispaniola Island), while the North Atlantic Oscillation (NAO)—although weaker—seems to have a more pronounced influence in Eastern-southeastern Caribbean (e.g., SE Lesser Antilles) (Jury et al. 2007). This is consistent

with a recent study, in which the authors have found that ENSO effects to drought variability in Puerto Rico is not significant (Torres-Varcárcel, 2018).

4. Observed surface radiative flux anomalies

Radiative changes during the Pan-Caribbean drought appear to have also played a role in its severity. Between 2013 and 2016, the average downwelling long-wave radiation (RLI) anomaly was 1.03 Wm^{-2}, while the downwelling short-wave radiation (RSI) was 1.84 Wm^{-2}. However, in 2015 when the drought peaked, RLI anomaly averaged 2.59 Wm^{-2} and RSI anomaly 3.22 Wm^{-2}. Above-normal anomalies in upwelling long and short-wave radiative fluxes (RLO and RSO) were also observed during the drought, with 1.2 and 0.11 Wm^{-2}, respectively. Given the relatively short time span covered by CERES (2001–present) it was not possible to assess the direct impact of anthropogenic climate change on surface radiative flux anomalies using this dataset. However, these analyses provide further insights into the radiative characteristics of the Pan-Caribbean drought. Additionally, CERES' cloud's fraction and optical depth reveal a below-normal cloud coverage and a persistent decrease in deep-convection across the Caribbean (Figs. S6 and S7), consistent with observed radiative flux and precipitation anomalies during the Pan-Caribbean drought.

5. Supporting references

Bosart L. F., 1998: Planetary and synoptic-scale signatures associated with Central American cold surges. *Mon Wea Rev* 126:5–27.

Giannini, A., M. A. Cane, and Y. Kushnir, 2001a: Interdecadal changes in the ENSO teleconnection to the Caribbean region and the North Atlantic Oscillation. *J. Climate*, 14, 2867–2879, doi:10.1175/1520-0442(2001)014,2867:ICITET.2.0.CO;2.

——, J. C. Chiang, M. A. Cane, Y. Kushnir, and R. Seager, 2001b: The ENSO teleconnection to the tropical Atlantic Ocean: Contributions of the remote and local SSTs to rainfall variability in the tropical Americas. *J. Climate*, 14, 4530–4544, doi:10.1175/1520-0442(2001)014,4530:TETTTT.2.0.CO;2.Schultz DM, Bracken WE,

Peters E. J., 2015: The 2009/2010 Caribbean drought: A case study. *Disasters* 39:738–761.

Torres-Varcárcel A. R., 2018: Teleconnections between ENSO and rainfall and drought in Puerto Rico. *Int J of Climatol* doi:10.1002/joc.5444.

SUPPORTING FIGURES

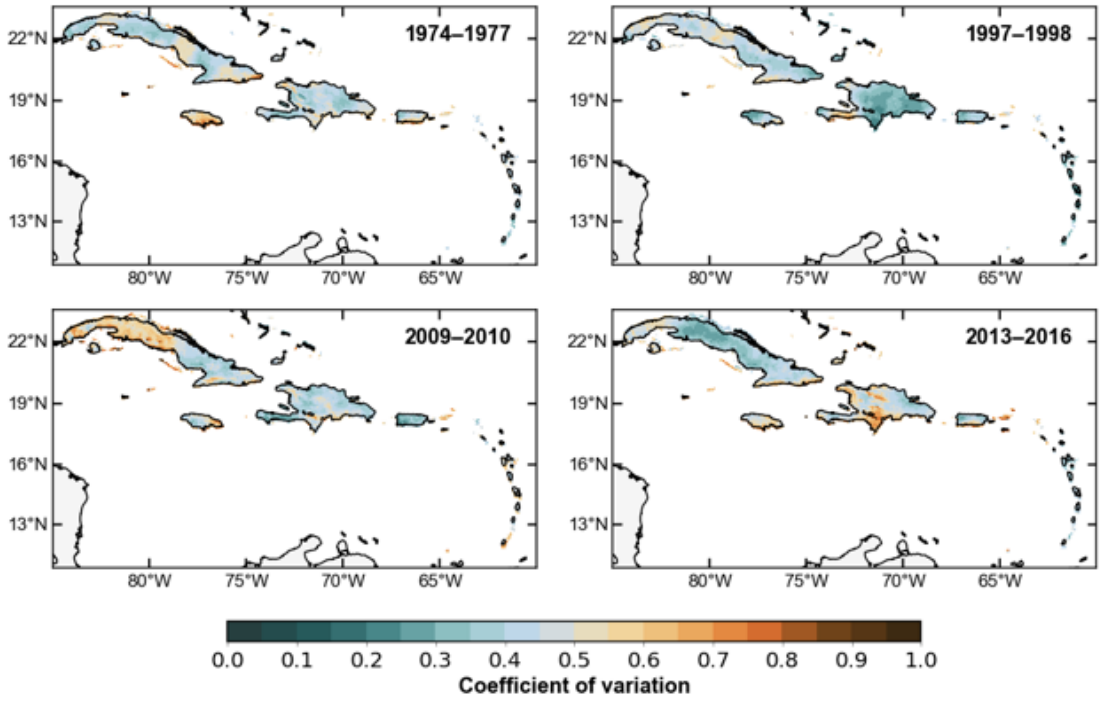

FIG. S1. Coefficient of variation in precipitation anomalies during some of the worst droughts in the Caribbean. In 2013–2016, lower coefficients of variation are observed over the regions with the highest anthropogenic contributions on the drought.

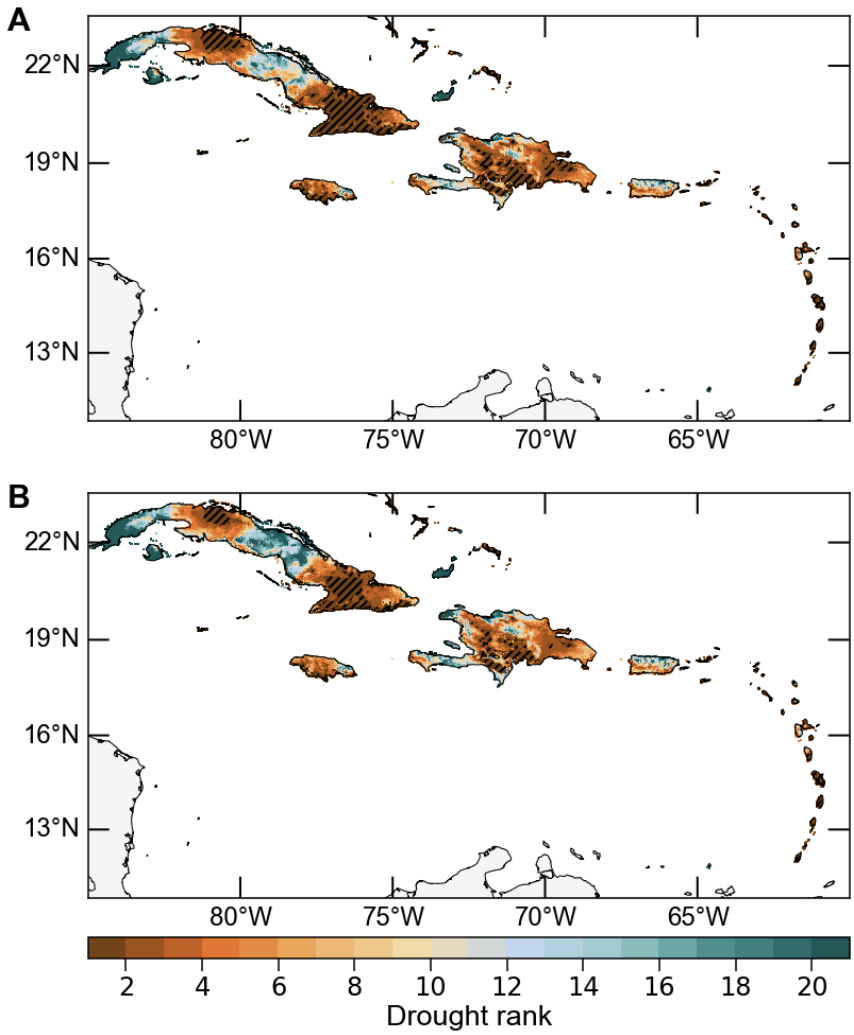

FIG. S2. Drought ranks of scPDSI estimated with the observed trend in temperature and linealy-detrended temperatures. **(A)** Drought rankings of using the observed temperature trend. The hatching refers to the area where the Pan-Caribbean drought was record breaking any year between 2013 and 2016, which is nearly 32%. **(B)** As in (A) but using linearly-detrended temperatures to calculate PET and scPDSI. In this case, the area where the Pan-Caribbean drought was record-breaking is ~21%.

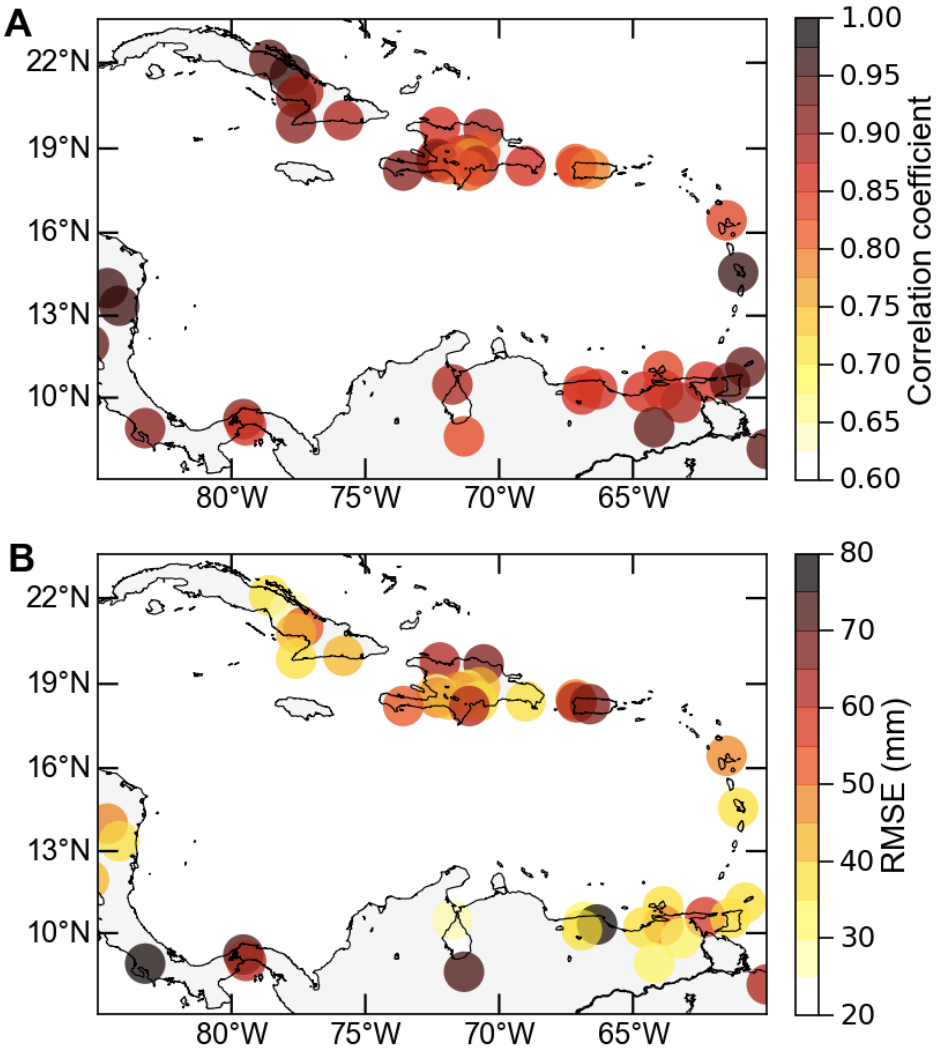

FIG. S3. **(A)** Correlation coefficients and **(B)** RMSE between our downscaled precipitation product and GHCN station data. The intervals of these correlations and RMSEs vary depending on the length of GHCN used. However, we selected stations with at least 20 years of continuous data.

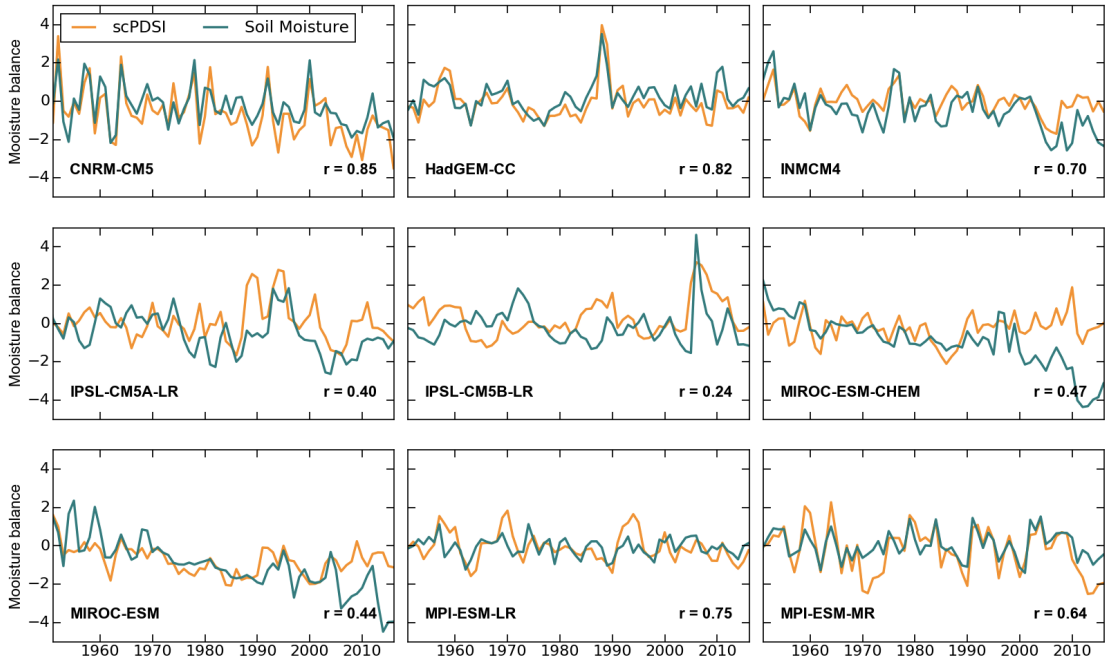

FIG. S4. Simulated scPDSI and soil moisture anomalies during 1950–2016 from CMIP5. scPDSI significantly correlates with soil moisture anomalies in spite of the simple water balance model it uses. The significant correlations between these moisture balance indicators suggest that CO_2 fertilization plays a minor role in affecting PET in the Caribbean during the 1950–2016 interval.

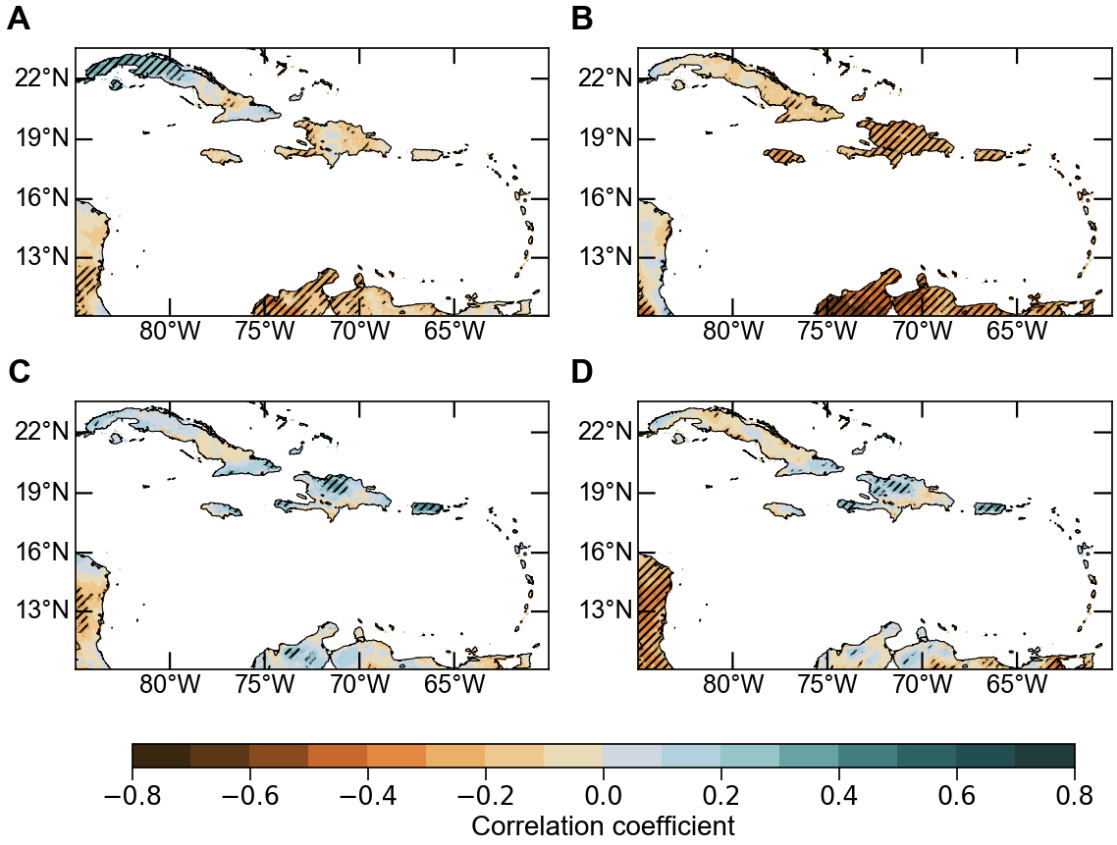

FIG. S5. Correlations coefficients between our downscaled scPDSI and sea surface temperature anomalies (SSTAs) in the Niño-3.4 region. **(A)** In MJJ, **(B)** in ASO. **(C)**, **(D)** As in (A) and (B) but with SSTAs in the tropical North Atlantic. The hatched areas are statistically significant correlations at the 95% level.

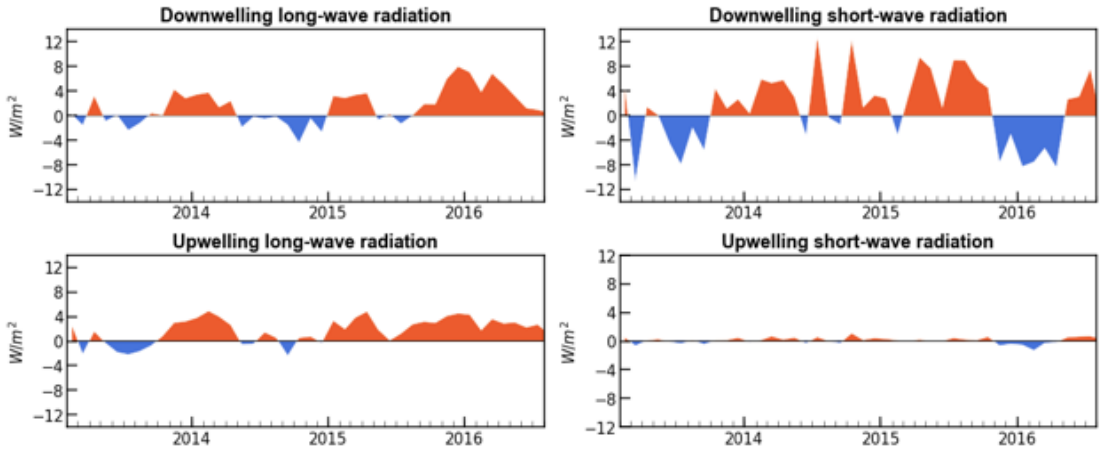

FIG. S6. Radiative flux anomalies during the Pan-Caribbean drought observed from the NASA's CERES data. As expected during dry intervals, there is an increase in incoming short-wave radiation likely due to lower than normal cloud cover. However, during the recent Pan-Caribbean drought anomalously high incoming long-wave radiation was observed, which is mostly due to the rise of anthropogenic greenhouse gas concentrations, with an averaged departure of 0.8 W m^{-2} between January 2013 and December 2016 (as estimated relative to the 2001–2016 CERES climatology).

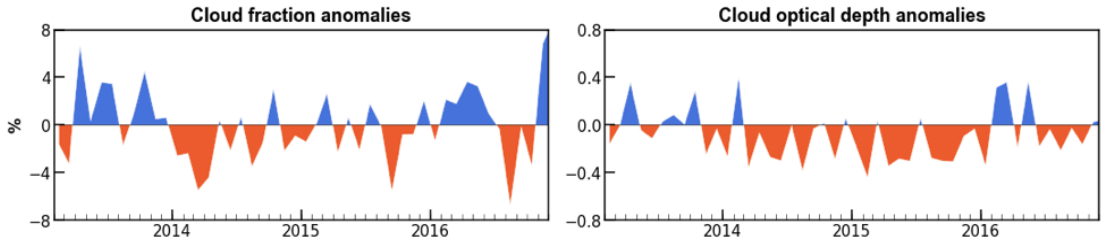

FIG. S7. Cloud fraction and cloud optical depth anomalies during the Pan-Caribbean drought observed from the NASA's CERES data. During the Pan-Caribbean drought a below-normal cloud fraction is observed across the Caribbean. However, the persistent decrease in deep convection, as evaluated from below-normal cloud optical depth anomalies, is the main characteristic of the drought. As in FIG. S6 we estimated these anomalies as departures from the 2001–2016 CERES climatology.

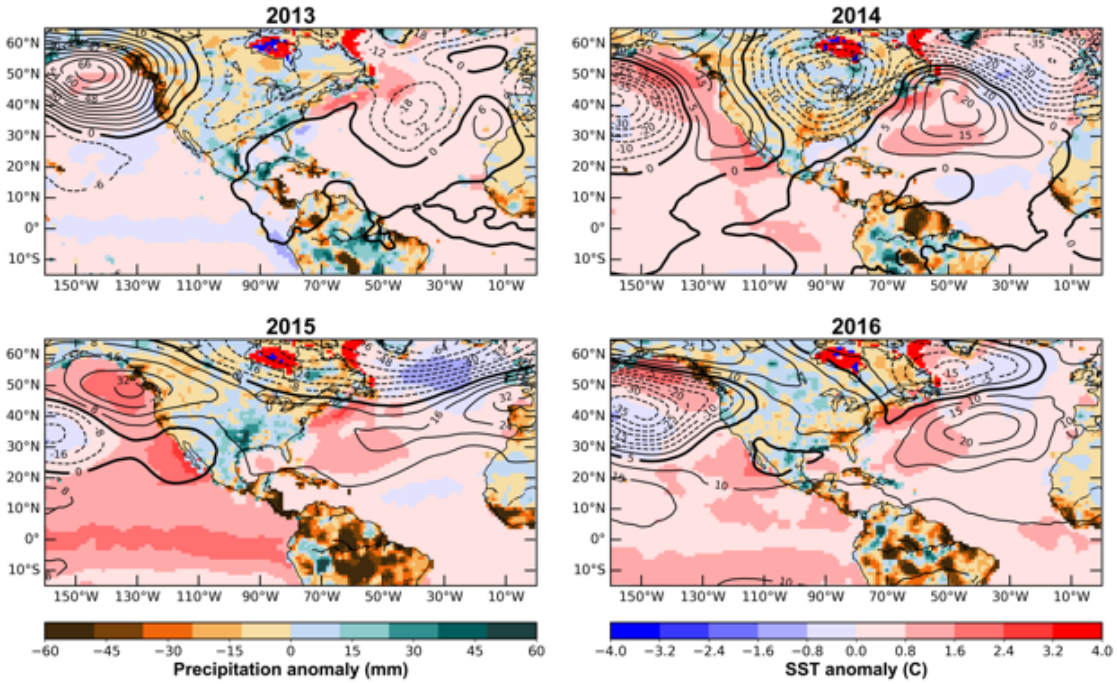

FIG. S8. Observed precipitation, sea surface temperature, and 500-mb geopotential height anomalies during the Pan-Caribbean drought. The period was characterized by persistently cold temperatures in the tropical North Atlantic (0º–20ºN; 60º–20ºW) between 2014 and 2015, and below-normal precipitation in the Caribbean. The drought peaked in severity in 2015, likely related to the onset of El Niño.

SUPPORTING TABLES

TABLE S1. Observed climate datasets.

Variable	Dataset	Native resolution	Period used	Reference
Precipitation	*GPCC	1º	1949–2016	Schneider et al. (2014)
	*CHIRPS	0.05º	1981–2016	Funk et al. (2015)
	*CRU TS4.01	0.5º	1949–2016	Harris et al. (2014)
	WorldClim (Climatology)	~1 km	1950–2000	Hijmans et al. (2005)
	*CHELSA (Climatology)	~1 km	1979–2013	Karger et al. (2016)
Temperature	*BEST	1º	1949–2016	Rohde et al. (2013)
	*NCEP–NCAR Reanalysis	2.5º	1949–2016	Kalnay et al. (1996)
	*CRU TS4.01	0.5º	1949–2016	Harris et al. (2014)
	WorldClim (Climatology)	~1 km	1950–2000	Hijmans et al. (2005)
Net radiation	*JRA-55 Reanalysis	~1.25º	1958–2016	Ebita et al. (2011)
	*NCEP–NCAR Reanalysis	~1.8º	1949–2016	Kalnay et al. (1996)
	*CRU TS4.01	0.5º	(Climatology)	Harris et al. (2014)
	*CERES	1º	2001–2016	Loeb et al. (2012)
Wind speed	*NCEP–NCAR Reanalysis	2.5º	1981–2010 (Climatology)	Kalnay et al. (1996)
	*CRU TS4.01	0.5º	1949–2016	Harris et al. (2014)
Vapor pressure	Derived from *BEST	1º	1949–2016	Rohde et al. (2013)
	*CRU TS4.01	0.5º	1949–2016	Harris et al. (2014)
Elevation	WorldClim	~1 km	- -	Hijmans et al. (2005)
Available Water Holding Capacity	*IGBP–DIS	0.08º	- -	Global Soil Data Task Group (2000)
Radiative fluxes	*CERES	1º	2001–2016	Loeb et al. (2012)

***GPCC: Global Precipitation Climatology Centre Version 7.**
***CRU: Climatic Research Unit version TS4.01**
***CHIRPS: Climate Hazards Group InfraRed Precipitation with Station data.**
***CHELSA: Climatologies at High resolution for Earth's land Surface Areas.**
***BEST: Berkeley Earth Surface Temperature.**
***NCEP–NCAR: National Centers for Environmental Predictions–National Center for Atmospheric Research.**
***IGBP–DIS: International Geosphere-Biosphere Programme Data and Information Services.**
***CERES: Clouds and Earth's Radiant Energy Systems.**
***JRA-55: Japanese 55-year Reanalysis.**

TABLE S2. List of the CMIP5 models used in this work. From these models, we use monthly means of daily maximum and minimum temperature data at 2 m (tasmax and tasmin, respectively), radiation data (rlds, rlus, rsds, and rsus), and soil moisture data (mrso) from historical period (1949–2005), RCP8.5 (2006–2016), and pre-industrial control (1949–2016). We use one member from each model.

Model	Resolution (lat./lon.)	Variables used								
		Tasmax	Tasmin	Pr	Rlds	Rlus	Rsds	Rsus	mrso	sfcWind
BCCM-CSM1-1-M	1.1215º x 1.125º	x	x	x						
BCC-CSM1-1	2.7905º x 2.8125º	x	x	x						
CCSM4	0.9424º x 1.25º	x	x	x						
CESM1-BGC	0.9424º x 1.25º	x	x	x						
CESM1-CAM5	0.9424º x 1.25º	x	x	x						
CNRM-CM5	1.4008º x 1.4063º	x	x	x	x	x	x	x	x	x
CNRM-CM5-2	1.4008º x 1.4063º	x	x	x	x	x	x	x		x
CMCC-CESM	3.711º x 3.75º	x	x	x						
CMCC-CM	0.7484º x 0.75º	x	x	x						
CMCC-CMS	1.8652º x 1.875º	x	x	x						
GFDL-CM3	2º x 2.5º	x	x	x						
GFDL-ESM2G	2.0225º x 2.5º	x	x	x						
GFDL-ESM2M	2.0225º x 2.5º	x	x	x						
GISS-E2-H	2º x 2.5º	x	x	x						
GISS-E2-R	2º x 2.5º	x	x	x						
GISS-E2-H-CC	2º x 2.5º	x	x	x						
GISS-E2-R-CC	2º x 2.5º	x	x	x						
HADGEM2-CC	1.25º x 1.875º	x	x	x	x	x	x	x	x	x
HADGEM2-ES	1.25º x 1.875º	x	x	x	x	x	x	x		x
INMCM4	1.5º x 2º	x	x	x	x	x	x	x	x	x
IPSL-CM5A-LR	1.8947º x 3.75º	x	x	x	x	x	x	x	x	x
IPSL-CM5A-MR	1.2676º x 2.5º	x	x	x	x	x	x	x		x
IPSL-CM5B-LR	1.8947º x 3.75º	x	x	x	x	x	x	x	x	x
MIROC-ESM-CHEM	2.7905º x 2.8125º	x	x	x	x	x	x	x	x	x
MIROC-ESM	2.7905º x 2.8125º	x	x	x	x	x	x	x	x	x
MIROC5	1.4008º x 1.4063º	x	x	x	x	x	x	x		
MRI-CGCM3	1.1215º x 1.125º	x	x	x	x	x	x	x	x	x

MPI-ESM-LR	1.8652º x 1.875º	x	x	x	x	x	x	x	x	x
MPI-ESM-MR	1.8652º x 1.875º	x	x	x	x	x	x	x	x	x
MRI-ESM1	1.1215º x 1.125º	x	x	x	x	x	x	x		x
NORESM1-M	1.8947º x 2.5º	x	x	x						
NORESM1-ME	1.8947º x 2.5º	x	x	x						

CHAPTER 3

DYNAMICAL CHARACTERISTICS OF DROUGHT IN THE CARIBBEAN AND CENTRAL AMERICA DURING 1979–2016

DIMITRIS HERRERA AND TOBY AULT

Department of Earth, and Atmospheric Sciences, Cornell University, Ithaca, New York, 14853.

Abstract

Climate models project a significant drying in the Caribbean during climate change, and the region has recently undergone the worst multi-year drought in the historical period. However, the relative contributions of thermodynamic and dynamic influences on the projected drying, let alone the recent historical droughts, are not well constrained. Here we analyze the dynamical characteristics of contemporaneous droughts in the Caribbean and Central America using observations and model simulations. We found that, at least during El Niño events, there is a strong influence of sea surface temperature anomalies in modulating drought severity in our study domain, by generating an anomalous rising air—and consequently deep convection—in the eastern tropical Pacific Ocean, while promoting a strong subsidence over southeastern Caribbean and northeastern South America. We also found that the Saharan air layer might counteract local and regional dynamics by decreasing precipitation in spite of favorable dynamical conditions. These findings warrant further research to measure the actual contribution of the SAL on drought variation in the Caribbean. We further found that the Community Earth System Model (CESM) Large Ensemble (LENS) suggest a strong influence from the tropical Pacific Ocean on drought severity in the Caribbean, Central America and northern South America.

I. Introduction

The Caribbean Islands and Central America (CA) are prone to relatively short, but intense droughts, that usually cause major losses in agriculture, municipal water shortages, and decreased hydropower generation (Larsen 2000; Mendez and Magaña 2010; Peters 2015). During the unusually prolonged "Pan-Caribbean drought" of 2013–2016 (Herrera et al. [*submitted*]), for example, more than 3 million people were directly affected by food insecurity due to the failure of staple crop production (OCHA 2015). Although partially estimated, losses due to the Pan-Caribbean drought exceed the hundreds of millions of dollars, primarily because of its effects on the agriculture and tourism (FAO 2016; OCHA 2015). Similarly, droughts occurred in 1997–1998 and 2009–2010 reduced crop yields from 20 to over 30%, leading to significant increases in food prices (FAO 2016). In Trinidad and Tobago, fruit prices increased 60.8% in 2010, in part due to the drought (Peters 2015; FAO 2016). These statistics indicate that slow but persistent droughts can also significantly impact the Caribbean and CA.

Because of their tropical setting, the climatology of the Caribbean and CA is characterized by a relatively small seasonal change in temperature, but a pronounced variation in precipitation (Magaña et al. 1999). The annual precipitation cycle of the two regions follows a bimodal pattern characterized by two maxima in May–June and September–October, and a minimum in December–April (Magaña et al. 1999; Gamble and Curtis 2008; Taylor et al. 2002). During the wet season (May–October), a relatively drier period occurs between July and August known as the "midsummer drought" (MSD) (Magaña et al. 1999; Gamble and Curtis, 2008). The dynamics underpinning the MSD are not yet well constrained, but probably different mechanisms operate in the Caribbean as compared to CA (Magaña et al. 1999; Gamble and Curtis, 2008). For instance, Giannini et al. (2001) and Gamble and Curtis (2008) have hypothesized that the expansion of the North Atlantic subtropical high (NASH) in July might play a critical role on the onset of the MSD in the Caribbean. According to this hypothesis, the intensification of the NASH diminishes precipitation in this region by strengthening trade winds and by promoting vertical atmospheric stability (Gamble and Curtis, 2008). In contrast, in CA the MSD might be driven by the latitudinal migration of the

intertropical convergence zone (ITCZ) (Magaña et al. 1999) and changes in the low-level winds in the Pacific coast of CA (Magaña et al. 1999). Regardless the dynamical causes of the MSD, Caribbean drought usually unfolds with an anomalously persistent MSD and subsequent failure of the September–October peak of the rainy season.

Given that some of the worst droughts registered in the Caribbean and CA, including the 2013–2016 Pan-Caribbean drought, have occurred in conjunction with El Niño events (Peters, 2015; Herrera and Ault, 2017), previous studies have linked drought variability in these regions with El Niño-Southern Oscillation (ENSO) (e.g., Giannini et al. 2000; 2001a; 2001b; Jury et al. 2007; Stephenson et al. 2007; Peters, 2015). However, as suggested by Torres-Valcárcel (2018), ENSO impacts on drought are not uniform across the Caribbean. Drought variability in the Caribbean and CA has been further associated with the Madden-Julian Oscillation (MJO), the North Atlantic Oscillation (NAO), and the Atlantic Multidecadal Oscillation (AMO) (Enfield and Alfaro, 1999; Giannini et al. 2000; 2001a; 2001b; Taylor et al. 2002; Gamble and Curtis, 2008; Martin and Schumacher, 2011). NAO impacts to drought in both regions might be modulated by changes in the intensity of the NASH and the Caribbean low-level jet (CLLJ) (Giannini et al. 2000; 2001a; 2001b; Taylor et al. 2002; Martin and Schumacher, 2011). According to Gamble and Curtis (2008), an increased intensity of the CLLJ is associated to lower precipitation rates in central Caribbean, while the opposite has been observed in CA.

Although there are some constraints on the dynamical causes of ENSO-driven droughts in the Caribbean and CA (e.g., Giannini et al. 2000; 2001a; 2001b; Taylor et al. 2002), the occurrence of drought in absence of El Niño (e.g., Herrera and Ault, 2017; Herrera et al. [*submitted*]) indicate that other dynamical and/or thermodynamical processes might also modulate drought variability in these regions. This is especially important for the Caribbean Islands, since topography might further influence drought variation at local scales through thermodynamical processes (e.g., Herrera and Ault, 2017; Torres-Valcárcel, 2018). In addition, most of the "state-of-the-art" global climate models project an increased aridity for the Caribbean and CA due to reduced

precipitation and warming as a result of anthropogenic climate change (e.g., Neelin et al. 2006; IPCC, 2014). Nonetheless, neither the dynamical mechanisms underpinning historical droughts nor the drying projected by climate models are fully constrained. Thus, understanding the dynamical drivers of historical droughts at seasonal, interannual, decadal, and ideally longer timescales is critical to improve drought predictability in these regions, as well as to better understand the causes of the projected drying in models.

In this work we provide insights into the dynamical causes of droughts registered in the Caribbean and CA during the 1979–2016 period using reanalysis and model simulations. Specifically, we use the European Centre for Medium-Range Weather Forecasts (ECMWF) Interim Reanalysis (ERA-Interim) (Dee et al. 2011) to calculate moisture budgets and moisture flux anomalies during three major droughts in the Caribbean: (a)1997–1998, (b) 2009–2010, and (c) the 2013–2016 Pan-Caribbean drought. These droughts are also analyzed in terms of global circulation and sea surface temperature (SST) anomalies, as many droughts in these regions have been linked to SST anomalies in tropical Pacific and North Atlantic oceans (Rogers, 1988; Giannini et al. 2000; 2001a; 2001b; Taylor et al. 2002; Gamble and Curtis, 2008; Martin and Schumacher, 2011; Herrera and Ault, 2017). We further use the National Center for Atmospheric Research (NCAR) Community Earth System Model (CESM) Large Ensemble ("LENS") (Kay et al. 2015) to assess the prevalent dynamical anomalies during drought, with a larger sample size.

2. Data and Methods

2.1. Study Area

As in Herrera and Ault (2017), in this work our target area is located between 7–33º N and 60–90º W, which includes the Caribbean and Central America, and portions of South and North America (Fig. 1). Given that drought variability differs from the subtropical Florida Peninsula to the tropical northern portion of South America (Amador, 1998; Magaña et al. 1999; Gamble et al. 2008; Herrera and Ault, 2017), we

have divided it into four smaller regions to conduct our analysis (Fig. 1). This division allows us to diagnose drought dynamics separately for the following regions: (a) Florida Peninsula, (b) Central America, (c) Northern South America, and (d) the Caribbean.

2.2. Climate Data

2.2.1. ERA-Interim reanalysis

A comprehensive list of the climate datasets used in this work is shown in Table 1. The ERA-Interim reanalysis, which we used, spans from 1979 to near present with temporal resolutions ranging from 3-hourly to monthly time steps, and spatial resolutions varying from 0.125º to 3º lat/lon (Dee et al. 2011). It has a vertical resolution of 60 levels, with the top level at 0.1 mb. In contrast to its predecessor (ERA-40), ERA-Interim includes a 4-dimensional variational assimilation scheme (as compared to the 3-dimensional assimilation used by ERA-40), with an improved low frequency variability, stratospheric circulation, and a better representation of the hydrological cycle (Dee et al. 2011). We used monthly ERA-Interim archives of surface pressure (*Ps*), zonal (*u*) and meridional (*v*) components of the wind, specific humidity (*q*) at 0.5x0.5º to calculate moisture budget anomalies during the 2013–2016 Pan-Caribbean drought (e.g., Herrera et al. [*submitted*]). Since ERA-Interim provides the divergence of the vertically-integrated moisture fluxes, precipitation, and evaporation as data outputs, we compared our budgets against these ERA-Interim outputs. However, as noted in Trenberth et al. (2011) and Seager and Henderson (2013), ERA-Interim divergence does not balance *P*–*E*, which is likely due to the assimilation scheme the model implements (Seager and Henderson, 2013). We further used horizontal wind and geopotential height (*Z*) from ERA-Interim to assess the large scale dynamic anomalies during the droughts studied, but at 1x1º resolution.

We used moisture budget data from the NCAR's Climate and Global Dynamics Laboratory (CGD), which were also calculated with ERA-Interim for the period 1979–2016 (available at: http://www.cgd.ucar.edu/cas/catalog/reanalysis/ecmwf/erai/index.-html). Among other variables, this dataset provides monthly means of the vertically

integrated moisture flux divergence, zonal and meridional moisture fluxes, and *P–E* (originally as *E–P*) at 0.5x0.5º lat/lon resolution. As compared to moisture budgets directly calculated from ERA-Interim fields, the NCAR moisture budgets underwent a T-106 spectral truncation to reduce the "ringing" (i.e., spurious spatial patterns) of the budgets and were further corrected to minimize the mass budget residual (Trenberth and Guillemot, 1995; Trenberth et al. 2011). This step is necessary to assess the long-term trends and variability of moisture transport, because the divergence estimated from reanalyses usually does not balance *P–E* (e.g., Trenberth et al. 2011; Seager and Henderson, 2013). The vertical integrals in this dataset were defined as the mass-weighted sum using 28 model (σ) levels with the top of the atmosphere at $\sigma = 0.0$ and $\sigma = 1.0$ at the surface of the Earth. Monthly means of the divergence and moisture fluxes were calculated before the vertical integrations were computed, as failing to do so could lead to differences in the divergence (e.g., Trenberth et al. 2002).

2.2.2. Observed gridded-climate data

We used observed gridded products of monthly means of precipitation from the Global Precipitation Climatology Project (GPCP) (Adler et al. 2003), the Global Precipitation Climatology Centre (GPCC) (Schneider et al. 2015a), and our statistically-downscaled precipitation product (Herrera and Ault, 2017) (Table S1). We further use sea surface temperature data (SST) from NOAA's Extended Reconstructed Sea Surface Temperature version 5 (ERSSTv5) (Huang et al. 2017) to evaluate SST anomaly patterns associated to droughts in the Caribbean and CA. Although these products span different time intervals, in this work we used them from January 1979 to December 2016 to be consistent with ERA-Interim.

The GPCP product combines rain gauge stations, satellite, and sounding observations to estimate monthly precipitation rates. This product spans from 1979 to near present, at 2.5x2.5º lat/lon (Adler et al. 2003). As compared to other observation-based gridded precipitation products, GPCP has a global coverage, including over oceans, which is advantageous for the purpose of this work (e.g., because the Caribbean is mostly ocean). In addition, GPCC provides the associated precipitation error

estimates. We use GPCP version 2.3 Combined Precipitation dataset, available at: https://www.esrl.noaa.gov/psd/data/gridded/data.gpcp.html.

In addition to GPCP, we also used GPCC v7 to evaluate drought variation in the Caribbean and CA across different rain products. GPCC is a monthly totals of precipitation dataset that uses 75000 quality-controlled rain gauges worldwide (Schneider et al. 2015a), and approximately 400 stations in the Caribbean and CA (Herrera and Ault, 2017). GPCC has spatial resolutions from 0.5º to 2.5º lat/lon, and spans 1901 to 2013. However, the GPCC "combined product" (https://www.esrl.-noaa.gov/psd/data/gridded/data.gpcc.html) that we used, combines GPCC v7 with GPCC v4 monitoring product spanning since 2014 to near present with a spatial resolution of 1x1º lat/lon (Schneider et al. 2015b).

Because of the relatively coarse spatial resolutions of GPCP and GPCC, small islands in the Caribbean nor local—in many cases complex—topography are not resolved by these datasets. We thus used our statistically-downscaled precipitation product with 4 km spatial resolution (Herrera and Ault, 2017). This dataset was constructed by downscaling the GPCC combined product by merging two downscaling procedures that uses WorldClim (Hijmans et al. 2005) and the Climate Hazards Group Infrared Precipitation with Station data (CHIRPS; Funk et al. 2015). This dataset was validated by comparing our gridded product with underlying 58 Global Historical Climatology Network (GHCN) stations across our study area. The details of the downscaling and bias-correction procedures are described in the section 2.b.1 in Herrera and Ault (2017).

To assess global SST anomaly patterns during drought in the Caribbean and CA, we used the newly released ERSSTv5. ERSTTv5 is a global SST dataset spanning 1854 to near present at 2x2º lat/lon. As compared to previous versions (e.g., ERSSTv3 and v4), ERSSTv5 uses a more extensive input data, including the third version of the International Comprehensive Ocean-Atmosphere Data Set (ICOADS), and this version revised the bias correction, interpolation, and quality control procedures (Huang et al. 2017). ERSSTv5 further includes a new estimate of centennial sea ice from HadISST2

(Huang et al. 2017), although in this work we mostly used SST data over the tropical Pacific and North Atlantic.

As a complementary analysis, we used our high-resolution drought atlas for the Caribbean and CA, which is based on monthly estimates of the self-calibrating Palmer Drought Severity Index (scPDSI) (Herrera and Ault, 2017). The atlas spans 1950 to near present, but in this work we used data between 1979 and 2016 to be consistent with the interval analyzed in this paper. The data input used to build the atlas include our statistically-downscaled precipitation and potential evapotranspiration products at 4 km lat/lon (Herrera and Ault, 2017).

2.2.3. Model data

We used climate model archives of 15 members from the National Center for Atmospheric Research (NCAR) Community Earth System Model (CESM) Large Ensemble ("LENS") (Kay et al. 2015) to evaluate if this model realistically simulates drought in the Caribbean and CA. The use of climate models is needed to better understand drought dynamics in our study domain, provided the relatively short interval (and thus, small sample size of drought) that we are able to analyze from observations (e.g., less than 50 years). Therefore, we used LENS to: first, assess the accuracy of this model in simulating drought dynamics in the Caribbean and CA; and second, to increase the sample size of drought to improve our understanding of the robust dynamics linked to drought. LENS is a forty-member ensemble of forced, fully-coupled simulations spanning 1920–2100, at approximately 1º lat/lon resolution (Kay et al. 2015). It further includes two ~1000 year-long preindustrial and control simulations, with the purpose of isolating anthropogenic climate change from the (model) internal variability (Kay et al. 2015). In contrast to what we did with ERA-Interim, we used model outputs of monthly vertically-integrated moisture fluxes, precipitation, and evaporation, rather than diagnostically calculating these fields. Additionally, we calculated scPDSI using each of the 15 members of LENS used here to identify droughts in models, and to further compare their dynamics against the observed drought dynamics. The advantage of using LENS is that, in addition to provide insights into biases of this model to simulate drought

dynamics in our study domain, we can identify and assess the dynamics of more droughts than from observations.

2.3. Methodology

We analyzed the anomalies of moisture budgets and large-scale circulation, which were estimated as departures from the 1979–2016 climatology. We selected the droughts described in Herrera and Ault (2017); however, it was not possible to assess the dynamics of the 1974–1977 because ERA-Interim spans since 1979 (Fig. 2). We also used our Caribbean drought atlas to compare it against the anomalies observed in the moisture budgets and large scale dynamics during the droughts analyzed.

2.3.1. Computation of moisture budgets

The procedure to compute the NCAR's CGD monthly moisture budgets that we used, involves the following steps: (1) Computation of the derived fields, such as moisture fluxes (*uq*, *vq*, and *zq*), at 6-hourly time steps. (2) The monthly means of the same variables are then estimated from 6-hourly data, and incorporates a 29th day in February of the leap years between 1979 and 2016. (3) The resulting monthly means are then used to calculate the vertically integrated fields (e.g., $U = \frac{1}{g}\int_0^{Ps} u dp$, $V = \frac{1}{g}\int_0^{Ps} v dp$). As noted by Trenberth et al. (2002), monthly means should be calculated before the vertical integrations are computed, because inconsistencies in the divergence might arise if the opposite is implemented. (4) Finally, with the vertical integrals *P–E* was obtained following Trenberth and Guillemot (1995) and Newman et al. (2012) as:

$$P - E = -\left[\frac{\partial \langle q \rangle}{\partial t} - \boldsymbol{\nabla} \cdot \mathbf{Q}\right], \quad (1)$$

where

$$\frac{\partial \langle q \rangle}{\partial t} = \frac{1}{g}\int_0^{Ps} q dp,$$

$$\mathbf{Q} = \frac{1}{g}\int_0^{Ps} q\mathbf{v} dp,$$

E is the evaporation from the surface, P is precipitation, and $\mathbf{v}$ is the horizontal wind vector. The term $\langle q \rangle$ is the vertically integrated specific humidity or "precipitable water" (e.g., Trenberth and Guillemot, 1995), $\frac{\partial \langle q \rangle}{\partial t}$ is the precipitable water tendency, and the term $\mathbf{Q}$ is the vertically integrated moisture flux. The computation of the precipitable water tendency in CGD's moisture budgets, however, used 6-hourly data rather than monthly means because tendencies from monthly means are relatively small.

Since Eq. (1) does not separate the moisture converge due to mass convergence from that due to the advection of moisture gradients, we followed Seager and Henderson (2013) to calculate our moisture budgets:

$$P - E = -\frac{1}{g\rho w}\frac{\partial}{\partial t}\int_0^{Ps} q dp - \frac{1}{g\rho w}\frac{\partial}{\partial t}\int_0^{Ps}(q\boldsymbol{\nabla}\cdot\mathbf{v} + \mathbf{v}\cdot\boldsymbol{\nabla}q)dp - \frac{1}{g\rho w}\, q_s\mathbf{v_s}\cdot\boldsymbol{\nabla}P_s, \qquad (2)$$

where g is the acceleration due to gravity, ρw is the density of water, the term $(q\boldsymbol{\nabla}\cdot\mathbf{v})$ is the mass convergence, and $(\mathbf{v}\cdot\boldsymbol{\nabla}q)$ the advection of moisture. The boundary term $-\frac{1}{g\rho w}\, q_s\mathbf{v_s}\cdot\boldsymbol{\nabla}P_s$ is therefore needed as a result of this approximation, but it is usually ignored (Seager and Henderson 2013). However, with this *P–E* formulation we solely focused on calculating the moisture convergence (MC) term with the following equation:

$$\mathrm{MC} = -\frac{1}{g\rho w}\frac{\partial}{\partial t}\int_0^{Ps}(q\boldsymbol{\nabla}\cdot\mathbf{v} + \mathbf{v}\cdot\boldsymbol{\nabla}q)dp, \qquad (3)$$

2.3.2. Large scale dynamics analysis

Large-scale patterns of the NASH, the CLLJ, and global circulation were analyzed by compositing monthly SST, geopotential height, and horizontal wind anomalies of observed droughts. The resulting patterns were then assessed for consistency with moisture flux anomalies from ERA-Interim. Geopotential height anomalies were

detrended to remove the effects of the warming trend on atmospheric expansion (e.g., Williams et al. 2017) during the period analyzed.

2.3.3. Assessment of drought dynamics in LENS

Because of the relatively short time interval of ERA-Interim (i.e., from 1979 to 2016), the number of droughts is also small, and might not fully represent the dynamics underpinning drought in the Caribbean and CA. To circumvent this problem, we used the CESM-LENS model archives to calculate the moisture budget during droughts in the model. To do so, we proceeded as follows: (1) we regionally-averaged soil moisture and precipitation over the Caribbean Islands, and we then calculated their anomalies as departures from the 1920–2006 climatology. (2) Monthly anomalies were averaged to seasonal means (e.g., anomalies for MAM, JJA, SON, and DJF) for each year. (3) We then normalized seasonal precipitation and soil moisture anomalies by calculating z-scores,

$$z = \frac{x-\bar{x}}{\sigma}, \quad (4)$$

where z is the normalized variable, x is the variable seasonal means for each year, $\bar{x}$ is the long-term (i.e., 1920–2006) seasonal climatology, and σ is the standard deviation. (4) We selected normalized droughts of $\sigma \leq -1$. (5) Finally, we composited all seasons to obtain the seasonal climatology of simulated droughts. We repeated this procedure to the first 15 members of LENS used in this work.

Using the droughts identified from soil moisture and precipitation anomalies as reference, we calculated *P–E* directly using model outputs of precipitation and evaporation, while moisture flux anomalies were estimated using specific humidity (q), surface pressure (*P0*), and wind vectors (v, u) as we did with ERA-Interim. The consistency of LENS in simulating drought dynamics in the Caribbean and CA was assessed from two perspectives: (1) by comparing the seasonal climatologies of *P–E* and moisture fluxes against the same climatologies from ERA-Interim, (2) by analyzing anomalies in *P–E* and moisture fluxes during simulated droughts, and (3) by identifying

the NASH and the CLLJ. We finally calculated the advection from CESM-LENS as the residual from moisture convergence and mass convergence.

3. Results

Monthly moisture budgets and large-scale dynamics were analyzed at seasonal time scales to facilitate the interpretation and our findings. This is important because drought dynamics in the Caribbean and CA have a different seasonal response to climate modes of variability such as ENSO (e.g., Herrera and Ault, 2017). For example, the effects of El Niño on precipitation during the boreal summer (June–August) and the autumn (September–November) are the opposite as observed in early spring (March–May), with below normal precipitation in JJA and SON, and positive anomalies in MAM (e.g., Giannini et al. 2000; 2001b; Herrera and Ault, 2017). We therefore analyze drought dynamics for the periods March–May (MAM; spring), June–August (JJA; summer), September–November (SON; autumn), and December–February (DJF; winter).

3.1. Climatology of the vertically integrated moisture transport

The seasonal climatology of the vertically integrated moisture transports in the Caribbean and CA is strongly dominated by changes in the low-level easterly fluxes (mostly represented by the CLLJ), the meridional migration of the intertropical convergence zone (ITCZ), and changes in the position and strength of the NASH (Figs. 3 and 4). Although the ITCZ plays a major role on precipitation seasonality in CA, regional and local features such as moisture transport from the Caribbean Sea and topography also contribute to local precipitation variability in this region, especially during the dry season. At regional scales in the Caribbean Islands, in contrast, the main source of moisture is the North Atlantic carried by the trade winds. The dry season for the Caribbean and CA (from December to May or DJF and MAM) is characterized by dominant divergence over the Caribbean Sea. However, topography enhances convergence at very local scales. This is especially noted in CA, where the Caribbean slope exhibits a relatively strong convergence in DJF, while the opposite is observed in the Pacific coast of CA (Figs. 3 and 4). A similar feature is observed over the Caribbean

Islands, although the magnitude is smaller than in CA. Nonetheless, this might be due to the relatively low resolution of the ERA-Interim we used (0.5x0.5º). The dry season is also dynamically characterized by a stronger CLLJ and the expansion of the NASH.

During the wet season in JJA and SON, there is an appreciable northward migration of the ITCZ accompanied by a relatively small shift in the CLLJ vectors toward northern CA (Figs. 3 and 4). In the wet season, moisture fluxes are relatively large because of the higher water vapor content of the atmosphere (due to warmer temperatures of the summer season and the northward migration of the ITCZ and), but surface winds are slower than during the dry season (Fig. 3). In terms of convergence, there is a pronounced difference between JJA and SON. For example, in JJA there is a persistent convergence in western Caribbean (especially western Cuba), while in the eastern Caribbean Islands a divergence is observed. In contrast, in SON there is predominantly convergence in most of the Caribbean Islands.

3.2. Moisture budget anomalies from ERA-Interim

As in Herrera and Ault (2017), we analyzed the droughts of 1997–1998, 2009–2010, and 2013–2016, which co-occurred with El Niño events. However, because of constrains in the time interval covered by ERA-Interim, it was not possible to analyze the multi-year drought of 1974–1977. These droughts were selected based on their severity in the Caribbean. This means that these droughts might not be the most severe in other subregions such as Florida Peninsula or Northern South America.

The 1997–1998 drought began in the spring of 1997 (MAM), characterized by an anomalous moisture flow divergence in CA and most of the Caribbean Islands (Fig. 5). The western portion of Cuba and northern CA experienced an above normal moisture convergence during this season, which is consistent with precipitation anomaly patterns commonly observed during El Niño events (e.g., Herrera and Ault, 2017). In the summer (JJA) of 1997, the drought intensified in southern CA (e.g., Panama and Costa Rica) as indicated by an anomalous moisture flux divergence of up to 12 mm/day (Fig. 5). In the Caribbean Islands, drought conditions in JJA were similar as in MAM except in Cuba.

There, positive moisture convergence anomalies were observed. In the autumn (SON) there is a noticeable change in moisture fluxes, especially in the eastern Pacific where fluxes changed from a predominantly easterlies to westerlies (Fig. 5). This anomalous moisture flux convergence is consistent with El Niño SSTA in the eastern Pacific Ocean next to South America. In the winter of 1997–1998 (DJF), drought conditions began to diminish in most of the Caribbean Islands and small portions of CA due to an anomalous moisture flux convergence over the Greater Antilles of Caribbean Islands and southeastern North America.

The drought of 2009–2010 was one of the most severe droughts in the Caribbean, but mostly affected the Lesser Antilles and northern South America (Peters, 2015; Herrera and Ault, 2017). During this drought there was a persistent moisture flux divergence over the Caribbean Sea beginning in MAM of 2009 through DJF 2009–2010, with values ranging from 2 to 5 mm/day. Consistent with the rainfall deficits observed in weather stations in the Lesser Antilles (e.g., Peters, 2015), the most intense moisture divergence and negative anomalies in $P–E$ were observed in central-eastern Caribbean basin and northeastern South America. This picture contrast with the average moisture convergence observed in CA, with exception of DJF in 2009–2010 (Fig. 6). In the summer of 2010, the drought has subsided in most of the Caribbean and CA with an average moisture convergence of ~5 mm/day.

In contrast to the previous droughts, the Pan-Caribbean drought of 2013–2016 was characterized by spatial and temporal heterogeneity in terms of moisture flux convergence and divergence (Fig. 7). During this drought, two periods of persistent moisture divergence were observed in the Caribbean with ~3 and ~4 mm/day on average, respectively. The first period spanned from JJA in 2014 to DJF in 2014–2015, and it was characterized by having both moisture flux convergence and divergence in CA. However, during this period there was an appreciable above normal moisture convergence in northern CA (e.g., Yucatan Peninsula) that contrast with the moisture divergence of the Caribbean. The second period occurred from MAM to SON in 2015 when the drought peaked, and was similar as the one observed in 2014 in terms of the

spatial distribution of moisture convergence and divergence anomalies (Fig. 7). During both periods there was a strong moisture convergence anomaly, especially during JJA, in the eastern tropical Pacific near southern CA, reaching more than 10 mm/day (Fig. 7). This pattern is consistent with the strong El Niño of 2015 and the El Niño-like conditions in the summer of 2014. In contrast, beginning in MAM 2016, the pattern is quite the opposite; a strong divergence anomaly (> 12 mm/day) was observed next to southern CA (Fig. 7), probably related to the onset of a weak La Niña in 2016.

During the Pan-Caribbean drought, advection of moisture anomalies contributed to negative values in $P–E$ (suggesting a drying) of -6 mm/day on average in CA and northern South America in 2014 and 2015 (Fig. 8). In the Caribbean region, in contrast, the advection of moisture contributed to a slight wetting of ~2 mm/day, especially over the Greater Antilles; while the opposite was observed on the Lesser Antilles and over the Caribbean Sea during most of the seasons. However, the drying driven by the advection in CA and northern South America was equilibrated by the wetting caused by mass convergence, with values of over 6 mm/day but mostly over the Panama Isthmus (Fig. 9). This is also the opposite of what we observed over the Caribbean Islands, where mass convergence contributed to an average drying of -4 mm/day, although only in JJA. Notably, the spatial patterns in advection and mass convergence anomalies in JJA of 2014 and 2015 were remarkably similar, but anomalies in 2015 were significantly more pronounced.

3.3. Large-scale dynamics during droughts from observations

In addition of assessing the moisture budget anomalies during the 1997–1998, 2009–2010, and 2013–2016 droughts in the Caribbean and CA, we analyzed the global atmospheric and oceanic circulation and precipitation anomalies associated with these droughts. Fig. 10 shows geopotential heights and horizontal wind anomalies at 200 hPa during the 1997–1998 drought. Positive geopotential height anomalies were observed from the Autumn (SON) of 1997 through the Spring (MAM) of 1998 in the Caribbean, CA, and northern South America. In contrast, negative geopotential anomalies were observed at approximately 30ºN (i.e., over Florida Peninsula), separated by a narrow

band of strong westerly wind anomalies. Geopotential and horizontal wind anomalies also indicate a persistent upper-level anticyclonic circulation during the drought over central-eastern Caribbean Islands and CA, which subsequently subsided in the summer of 1998. These patterns are consistent with precipitation and SST anomalies observed during the drought (Fig. 11), characterized by a persistent dryness in CA, eastern Caribbean, and northern South America, and the strong positive anomalies in the tropical Pacific associated with El Niño.

Similarly, during the 2009–2010 drought an anomalous upper-level anticyclonic circulation was observed, but mostly over the eastern Caribbean and northern South America (Fig. 12). Although throughout this drought an El Niño event was present, this was not as strong as the 1997–1998 nor the 2015–2016, and it was characterized by the highest SST anomalies in central-topical Pacific [i.e., an El Niño "Modoki" event (e.g., Ashok et al. 2007)]. These findings are consistent with the precipitation and SST anomalies observed between 2009 and 2010, where a warmer tropical Pacific and cooler tropical North Atlantic was associated with below-normal precipitation rates in the Lesser Antilles, northern South America, and in parts of CA and the Greater Antilles (Fig. 13).

The 2013–2016 Pan-Caribbean drought was atypical in terms of its duration and severity (Herrera and Ault, 2017; Herrera et al. [*submitted*]). Although between 2015 and 2016 this drought is dynamically similar to the previous droughts due to El Niño (Figs. 14 and 15), it unfolded in early 2013 in CA and certain areas of the Caribbean. In 2013, there were not significant anomalies in upper-level winds, but a negative SST anomaly in tropical Pacific and the Caribbean Sea (Fig. 15). This pattern persisted until the winter (DJF) of 2013, when tropical Pacific began warming. In 2014, specifically between JJA and DJF, an El Niño-like pattern was observed as anomalous higher SST and westerly horizontal winds over the tropical Pacific (Fig. 15). It is also noticeable during this period a SST anomaly seesaw between tropical Pacific and tropical North Atlantic and Caribbean Sea, which is observed as a warmer tropical Pacific and colder SST in the tropical Atlantic. This pattern is commonly observed during El Niño (e.g.,

Giannini et al. 2000; 2001a,b; Herrera and Ault, 2017). From MAM to DJF of 2015–2016, there were also observed a 200 hPa westerly wind anomaly over CA and the Caribbean Sea, and a persistent anticyclonic circulation on the Caribbean Islands in SON of 2015 (Figs. 14 and 15). These observations are consistent with the below-normal precipitation registered in the Caribbean, CA and northern South America almost during the whole 2015 (Fig. 15). In the summer of 2016, the drought began to subside in the eastern Caribbean Islands and parts of CA. Nevertheless, certain regions of CA and western Caribbean. In terms of SST anomalies, it was observed a subsequent warming of the Caribbean Sea along the decreasing dry conditions. Since the summer through the winter of 2016, colder SST anomalies over the tropical Pacific were observed, consistent with the onset of a weak La Niña.

3.4. Moisture budget and large-scale anomalies from LENS

As shown in Figs. 16 and 17, the climatology of *P–E*, moisture fluxes, and precipitation from LENS is similar to that observed in ERA-Interim and GPCP. In general, LENS captures the annual northward-southward migration of the ITCZ and the seasonal changes in the NASH and the CLLJ (Figs. 16, 17). However, there is a noticeable difference in the magnitude of total precipitation between LENS and GPCP, which is mostly pronounced over the tropical Pacific Ocean during JJA and SON (Fig. 16). These findings are consistent with the *P–E* climatologies, although LENS has a lower moisture convergence in MAM and DJF than ERA-Interim (Fig. 17).

Seasonal composites of precipitation during drought are characterized by a pronounced positive anomaly over a narrow band in the tropical Pacific, and negative anomalies over the Caribbean, CA, and northern South America during SON (Fig. 18). A similar pattern is also observed in JJA and DJF, although the magnitude is significantly lower than in SON. This pattern is further consistent with the anomalies in *P–E*, although these anomalies are considerably smaller than the anomalies observed in

precipitation. In contrast to precipitation anomalies, the largest moisture convergence anomaly is observed during JJA and DJF rather than in SON (Fig. 19).

As we found from ERA-Interim, in LENS the mass convergence is what appeared to drive drought over the Caribbean and the northern portion of CA, contributing with anomalies of -4 mm/day to *P–E* on average. This is particularly notable in DJF, when mass convergence contributed to drought almost over the entire domain (Fig. 20). Additionally, and consistent with observations, simulated advection of moisture anomalies contributed to negative values in *P–E* mostly in southern CA, ranging from -2 to -5 mm/day on average, and a wetting over the Caribbean Islands of ~3 mm/day (Fig. 21)

Anomalies in SST from LENS suggest a warmer than normal tropical Pacific during JJA, SON, and DJF seasons, while a relatively colder North Atlantic during the same intervals (Fig. 22). The highest SST anomalies during drought in LENS are observed in DJF over the tropical Pacific, whose geographic pattern is similar to that observed during El Niño events from instrumental records.

4. Discussion

4.1. Dynamical causes of the 1997–1998, 2009–2010, and 2013–2016 droughts

Our findings suggest that the historical droughts studied here share some dynamical features in terms of convergence and divergence of the vertically integrated moisture transport, *P–E*, SST, and precipitation anomaly patterns. During the three droughts we analyzed, for example, a persistent moisture divergence anomaly and increased *P–E* were observed in most of the Caribbean basin and CA (Figs. 5–7), suggestive of subsiding air masses. These results are consistent with the reduced precipitation observed from GPCC, in spite of the inherent differences between this dataset and the ERA-Interim reanalysis we used to calculate the moisture budgets. We also found that severe droughts in CA, especially over the Caribbean coast, were associated with an anomalous weaker easterly winds represented by the CLLJ. This was noticeable, for example, in DJF of 1997–1998, MAM of 2009, JJA of 2014, and MAM, JJA, and SON

of 2015 (Figs. 11, 13, 14). In contrast, in JJA of 2010, stronger easterly winds transporting moisture from the tropical North Atlantic were associated with increased precipitation rates in most of CA and the Caribbean Islands (Fig. 13). In addition to these upper-level wind patterns, SST anomalies were characterized by warmer than average SST over the tropical Pacific, and colder SST in the tropical North Atlantic and the Caribbean Sea. Previous studies have called this pattern the "tropical Pacific-tropical North Atlantic seesaw" (e.g., Giannini et al. 2000; 2001a,b), which is usually observed during ENSO events. Nevertheless, since the droughts we have analyzed here occurred during El Niño, these SST anomalies patterns were expected.

The 2013–2016 Pan-Caribbean drought also shared some dynamical characteristics of the previous droughts, especially between JJA of 2014 and DJF of 2015–2016 due to El Niño (Fig. 15). The major difference, however, was its duration, severity, and spatial extent of the drought, which affected over 80% of our study domain, especially the Caribbean, northern South America, and CA (Herrera and Ault, 2017). As we have suggested in Herrera et al. (*submitted*), anthropogenic warming contributed to at least ~16–18% of drought severity (as estimated using scPDSI) and ~7% of dry area over land in the Caribbean by increasing evapotranspiration rates. However, dynamically this drought was also different from previous El Niño droughts probably due to a longer-lasting El Niño-like pattern (Fig. 15). Although the 2015–2016 El Niño unfolded in JJA of 2015 as assessed from SST anomalies, an El Niño-like SST anomaly patterns were observed between JJA and SON of 2014 (Figs. 7 and 15). It was during the periods MAM–SON 2014 and MAM–DJF of 2015–2016 when the highest moisture divergence anomaly was observed over the Caribbean and CA. These patterns were consistent with the precipitation and upper-level wind anomalies observed during the Pan-Caribbean drought. Although during the Pan-Caribbean drought positive precipitation anomalies were observed through certain seasons in the Caribbean and CA (e.g., DJF 2014–2015 and MAM–SON 2016), in many instances these higher precipitation rates were not enough to offset the soil drying of the previous seasons, as evaluated from scPDSI (Herrera and Ault, 2017; Herrera et al. [*submitted*]). enough to offset the soil drying of

the previous seasons, as evaluated from scPDSI (Herrera and Ault, 2017; Herrera et al. [*submitted*]).

During the Pan-Caribbean drought, the advection of moisture anomalies contributed to negative values in $P–E$ during most of the seasons across the Caribbean, CA, and northern South America (Fig. 8). However, it was during JJA of 2014 and 2015 when moisture advection pushed these regions into a significant drying, especially over CA. These findings are consistent with the moisture flux anomalies, which suggest a strong moisture advection (i.e., higher moisture flux anomalies driven by stronger horizontal winds) over these regions (Fig. 8). In addition, mass convergence intensified the drought during JJA of 2014 and 2015, but it slightly contributed to wetting conditions during MAM, SON, and DJF (Fig. 9). Although in many instances the mass convergence wetting was offset by the drying from the advection, this result is consistent with the double peak of the Pan-Caribbean drought observed in the summer-early autumn of 2014 and 2015 in our Caribbean drought atlas, and it was when both the mass convergence and the moisture advection contributed to the drying (Fig. 8, 9). It was also noticeable that the strongest mass convergence anomaly observed over the equatorial eastern Pacific coincided with the highest mass divergence in the Caribbean Sea and tropical North Atlantic, suggesting and confirming the seesaw pattern between both oceanic basins during El Niño-driven droughts in the Caribbean and CA (e.g., Giannini et al. 2000; 2001a,b; Herrera and Ault 2017). This pattern is dynamically explained by an anomalous rising air in the equatorial eastern Pacific and sinking air (subsidence) over the Caribbean Sea and tropical North Atlantic. However, a caveat from these findings is that we used monthly means, rather than daily or sub-daily climate data, to calculate the moisture budgets. Among other things, this could rise errors in the estimation of the advection of moisture gradients, because the advection is not linear (e.g., Seager and Henderson 2013).

4.2. Dynamical characteristics of drought in LENS

The moisture budgets from LENS suggest a major influence of the tropical Pacific Ocean on drought severity across the Caribbean, CA, and northern South America, as

indicated by composites of SST anomalies co-occurring with drought in LENS (Figs. 18–20). The geographic patterns of these SST anomalies are comparable to those during El Niño events from observations. However, while the greatest negative anomalies in precipitation and *P–E* across our study area were observed in SON, the highest SST anomalies were found in DJF (e.g., Figs. 5, 6, 11), which differ from ERA-Interim whose greatest anomaly in rain was identified in JJA (e.g., Figs. 5, 6, 7). This discrepancy may be due to the computation of precipitation anomalies as the difference between the climatology and each month (rather than the ratio or percentage), which leads to higher precipitation anomalies during drought for SON, in the wet season (~386 mm/year [37%]) as compared to DJF in the dry season (219 mm/year [21%]).

Differences in the magnitude of precipitation and *P–E* anomalies between ERA-Interim and LENS arise for various reasons, including that we analyzed seasonal means during droughts occurring between 1920 and 2006 in the model, while from observations we assessed the dynamics of specific droughts. In addition, we examined droughts in LENS using a 15-member ensemble, which also smooths out anomalies in precipitation and *P–E*. We further used outputs of precipitation and evaporation from LENS to calculate *P–E*, rather than using the diagnostically computing these terms with Eq. (1).

Since with LENS we calculated the advection of moisture gradients as the residual from moisture and mass convergence, the resulting computations may be different as calculating those terms separately following Eq. (3). Also, because we used monthly outputs from the model, these computations might not be as accurate as using daily or subdaily climate data (e.g., Seager and Henderson 2013). Regardless this obvious limitations, we found that LENS simulates well the contributions of mass convergence and advection during drought, especially over CA (Figs. 20, 21). For example, LENS suggests a strong moisture advection as the main driver of drought in the western side of CA in JJA and SON (Fig. 21), which is consistent with the mass convergence over the eastern equatorial Pacific observed during El Niño events in ERA-Interim (e.g., Fig. 8). In contrast to what we seen from observations, LENS indicates the mass divergence–

–and thus sinking air—as the main cause of drought during most of the seasons of the year, except in MAM. Nevertheless, as we mentioned above, we should be cautious interpreting these results from LENS, provided the limitations of our calculations and procedures using this model in this work. Future work should be done using subdaily data from LENS, as well as evaluating the dynamics during specific droughts in the model, in addition to analyzing the dynamics of composited events.

4.3. The possible role of the Saharan air layer (SAL) in worsening drought in the Caribbean

We found that during the droughts we studied, in certain areas of the Caribbean and CA the estimated moisture convergence was inconsistent with the observed precipitation anomalies (e.g., in Figs. 5–7). That it, areas with positive moisture convergence did not show negative anomalies in rain. Although this observation might arise from various reasons, including differences between the numerical schemes of GPCC and ERA-Interim, we hypothesize that other thermodynamical features might be responsible of such a discrepancy. As such, we have paid attention to the Saharan Air Layer (SAL) as a potential modulator of drought severity in the Caribbean.

Previous studies have suggested the possible role of the SAL in inhibiting deep convection—and therefore precipitation—in the Caribbean (Dunion, 2011; Jury and Santiago, 2010; Mote et al. 2017). The SAL is a mass of warm, dry, and dusty air that originates in the Sahara and expands toward the North Atlantic and the Caribbean between the boreal spring and early fall (Mote et al. 2017). It is characterized by a temperature inversion from 600 to 800 hPa, which stabilizes the atmosphere and prevents the formation of deep convective clouds (Dunion 2011; Prospero and Mayol-Bracero, 2013). According to Mote et al. (2017), the severity of the Pan-Caribbean drought during MAM of 2015 in Puerto Rico was associated with more intense SAL intrusions into the Caribbean. To gain further insights into this issue, we used cloud optical thickness and total cloud cover data from NASA's Clouds and Earth's Radiant Energy System (CERES; Loeb et al. 2012). However, because CERES only spans 2001–present, we analyzed cloud thickness anomalies during the 2013–2016 Pan-

Caribbean drought. As Fig. 23 shows, during the Pan-Caribbean drought, a lower than average quantity of deep convective clouds were observed. In contrast, even positive anomalies in total cloud cover (suggesting above normal cloud coverage) were observed during the drought. These findings are consistent with our hypothesis, in the sense that, dynamically, cloud formation was possible during the Pan-Caribbean drought, but not deep convective storms likely due to SAL outbreaks. Nevertheless, from these results we cannot assume the SAL as a major contributor to drought variation in the Caribbean. These findings warrant a more comprehensive research, but this not the main purpose of this paper through, for example, idealized model experiments.

5. Conclusions

We have assessed the dynamical characteristics and atmospheric causes of three major droughts in the Caribbean and CA between 1979–2016: (a) in 1997–1998, (b) 2009–2010, and (c) 2013–2016. Although analyzing the dynamical causes of only three dry intervals might not be enough to stablish a causal-effect model of drought in our domain, our results provide further insights into the dynamics underpinning El Niño droughts. Our results indicate, for example, that during these droughts a predominant moisture divergence over the Caribbean Sea and CA, contrasted with a moisture convergence in the tropical Pacific. This is consistent with an anomalous rising air in the eastern tropical Pacific, and subsidence mostly over the Caribbean Sea and northeastern South America. In terms of SST anomalies, we found the typical seesaw pattern between the tropical Pacific and tropical North Atlantic oceans, confirming the oceanic patterns described in previous work during El Niño (e.g., Giannini et al. 2000; 2001a,b).

We also found that the SAL might have contributed to the 2013–2016 Pan-Caribbean drought by suppressing deep convection, as observed from NASA's CERES cloud data. Although this finding warrants a more comprehensive analysis, it emphasizes the role of thermodynamical features in modulating drought severity in the Caribbean. This is especially true for Caribbean Islands because of their complex topography modulates moisture divergence and convergence at local scales. If the SAL has a major role in modulating drought variability in the Caribbean, it should be taken

into account when assessing the risk of drought in the near future during climate change. For example, because of the coarse resolution of most of the "state-of-the-art" global climate models, SAL intrusions into the Caribbean might not be captured. Thus, the drying projected by models might be even worse if, for example, global scale dynamics promote more SAL outbreaks in the Caribbean during the rainy season.

Finally, in general, CESM-LENS does a good job in simulating the dynamics underpinning drought in the Caribbean and CA. Although biases in the magnitude of P–E and moisture flux anomalies, the geographic characteristics of these variables are similar to that observed in ERA-Interim. Furthermore, LENS shows droughts associated to a warmer than normal tropical Pacific, consistent with El Niño events. At least from the results with the 15-member ensemble we used in this work, LENS might be appropriate as a reference to evaluate the dynamics underpinning drought in the Caribbean and CA. However, a more comprehensive assessment should be conducted using the 40 members of LENS, as well as a comparison with other climate models before suggesting this model to evaluate the dynamics of the projected drying in the Caribbean and CA as a consequence of anthropogenic climate change.

REFERENCES

Adler, R. F. and Coauthors, 2003: The version-2 Global Precipitation Climatology Project (GPCP) monthly precipitation analysis (1979–present). *J. Hydromet.*, 4, 1147–1167.

Amador, J. A., 1998: A climatic feature of the Tropical Americas: the trade wind easterly jet. *Top. Meteor. Oceanogr.*, 5, 91–102.

Ashok, K., S. K. Behera, S. A. Rao, H. Weng, T. Yamagata, 2007: El Niño Modoki and its possible teleconnection. *J. Geophys. Res.*, 112, C11007.

Dee, D. P. and Coauthors, 2011: The ERA-Interim reanalysis: configuration and performance of the data assimilation system. *Quat. J. Roy. Met. Soc.*, 137, 553–597.

Dunion, J. P., 2011: Rewriting the climatology of the Tropical North Atlantic and Caribbean Sea atmosphere. *J. Climate*, 24, 893–908.

Enfield, D. B., and E. J. Alfaro, 1999: The dependence of Caribbean rainfall on the interaction of the tropical Atlantic and Pacific Oceans. *J. Climate*, 12, 2093–2103, doi:10.1175/ 1520-0442(1999)012,2093:TDOCRO.2.0.CO;2.

FAO, 2016: Situation report: Dry corridor in Central America. Food and Agriculture Organization of the United Nations, 3 pp. [Available online at http://www.fao.org/-emergencies/resources/documents/resources-detail/en/c/422097/.].

Funk, C., and Coauthors, 2015: The climate hazards infrared precipitation with stations—A new environmental record for monitoring extremes. *Sci. Data*, 2, 150066, doi:10.1038/sdata.2015.66.

Gamble, D. W. and S. Curtis, 2008: Caribbean precipitation: review, model and prospect. *Progress in Physical Geography*, 32, 265–276.

Giannini, A., Y. Kushnir, and M. Cane, 2000: Interannual variability of Caribbean rainfall, ENSO, and the Atlantic Ocean. J. Climate, 13, 297–311, doi:10.1175/1520-

0442(2000)013,0297: IVOCRE.2.0.CO;2.

——, M. A. Cane, and Y. Kushnir, 2001a: Interdecadal changes in the ENSO teleconnection to the Caribbean region and the North Atlantic Oscillation. *J. Climate*, 14, 2867–2879, doi:10.1175/1520-0442(2001)014,2867:ICITET.2.0.CO;2.

——, J. C. Chiang, M. A. Cane, Y. Kushnir, and R. Seager, 2001b: The ENSO teleconnection to the tropical Atlantic Ocean: Contributions of the remote and local SSTs to rainfall variability in the tropical Americas. *J. Climate*, 14, 4530–4544, doi:10.1175/1520-0442(2001)014,4530:TETTTT.2.0.CO;2.

Herrera, D. and T. R. Ault, 2017: Insights from a new high-resolution drought atlas for the Caribbean spanning 1950–2016. *J. of Climate*, 30, 7801–7825.

——, J. T. Fasullo, S. J. Coats, C. M. Carrillo, B. I. Cook, and A. P. Williams: Exacerbation of the 2013–2016 Pan-Caribbean drought by anthropogenic warming. *Submitted.*

Hijmans, R. J., S. E. Cameron, J. L. Parra, P. G. Jones, and A. Jarvis, 2005: Very high resolution interpolated climate surfaces for global land areas. *Int. J. Climatol.*, 25, 1965–1978, doi:10.1002/joc.1276.

Huang, B., Peter W. Thorne, et. al, 2017: Extended Reconstructed Sea Surface Temperature version 5 (ERSSTv5), Upgrades, validations, and intercomparisons. *J. Climate*, 30, 8179–8205.

Jury, M., B. A. Malmgren, and A. Winter, 2007: Subregional precipitation climate of the Caribbean and relationships with ENSO and NAO. *J. Geophys. Res.*, 112, D16107, doi:10.1029/ 2006JD007541.

Jury, M. R. and M. J. Santiago, 2010: Composite analysis of dust impacts on African easterly waves in the Moderate Resolution Imaging Spectrometer era. *J. Geophys. Res. Atmospheres*, 115, D16213.

Kay, J. E. and Coauthors, 2015: The Community Earth System Model (CESM) Large Ensemble Project: a community resource for studying climate change in the presence of internal climate variability. *Bull. Amer. Meteor. Soc.*, 96, 1333–1349.

Larsen, M. C., 2000: Analysis of 20th century rainfall and streamflow to characterize drought and water resources in Puerto Rico. *Phys. Geogr.*, 21, 494–521.

Loeb N. G., and Coauthors, 2012: Observed changes in top-of-the-atmosphere radiation and upper-ocean heating consistent within uncertainty. *Nat Geosci* 5:110–113.

Magaña, V., J. A. Amador, S. Medina, 1999: The Midsummer Drought over Mexico and Central America. *J. Climate*, 12, 1577–1188.

Martin, E. R., and C. Schumacher, 2011: Modulation of Caribbean precipitation by the Madden–Julian oscillation. *J. Climate*, 24, 813–824, doi:10.1175/2010JCLI3773.1.

Méndez, M., and V. Magaña, 2010: Regional aspects of prolonged meteorological droughts over Mexico and Central America. *J. Climate*, 23, 1175–1188, doi:10.1175/-2009JCLI3080.1.

Mote T. L., C. A. Ramseyer, and P. W. Miller, 2017: The Saharan Air Layer as an early rainfall season suppressant in the Eastern Caribbean: the 2015 Puerto Rico drought. *J. Geophys. Res. Atmospheres*, 122, 10966–10982.

Neelin J. D., H. Münnich, H. Su, J. E. Meyerson, C. E. Holloway, 2006: Tropical drying trends in global model and observations. *Proc Natl Acad Sci USA* 103:6110–6115.

Newman, M., G. N. Kiladis, K. M. Weickmann, F. M. Ralph, and P. D. Sardeshmukh, 2012: Relative contributions of synoptic and low-frequency eddies to time-mean atmospheric moisture transport, including the role of atmospheric rivers. *J. Climate*, 25, 7341–7361.

OCHA, 2015: Drought in Central America in 2015: Situation report (as of October 6, 2015). United Nations Office for the Coordination of Humanitarian Affairs (OCHA).

[Available online at http://www.redhum.org/uploads/documentos/pdf/Sitrep_OCHA-ROLAC_Drought_in_CA_EN_061015- 20151006-AL-17144.pdf.].

Peters, E. J., 2015: The 2009/2010 Caribbean drought: A case study. Disasters, 39, 738–761, doi:10.1111/disa.12123.

Prospero, J. M., and O. L. Mayol-Bracero, 2013: Understanding the transport and impact of African dust on the Caribbean Basin. *Bull. Amer. Meteor. Soc.*, 94, 1329–1337.

Rogers, J. C., 1988: Precipitation variability over the Caribbean and tropical Americas associated with the Southern Oscillation, *J. Climate*, 1, 172–182.

Schneider, U., A. Becker, P. Finger, A. Meyer-Christoffer, B. Rudolf, and M. Ziese, 2015a: GPCC full data reanalysis version 7.0 at 1.08: Monthly land-surface precipitation from rain-gauges built on GTS-based and historic data, doi:10.5676/DWD_GPCC/FD_M_V7_100.

——, ——, ——, ——, and M. Ziese, 2015b: GPCC monitoring product: Near real-time monthly land-surface precipitation from rain-gauges based on SYNOP and CLIMAT data, doi:10.5676/DWD_GPCC/MP_M_V5_100.

Seager, R. and N. Henderson, 2013: Diagnostic computation of moisture budgets in ERA-Interim reanalysis with reference of analysis of CMIP-archived atmospheric model data. *J. Climate*, 26, 7876–7901.

Stephenson, T. S., and Coauthors, 2014: Changes in extreme temperature and precipitation in the Caribbean region, 1961– 2010. *Int. J. Climatol.*, 34, 2957–2971, doi:10.1002/joc.3889.

Taylor, M. A., D. B. Enfield, and A. A. Chen, 2002: Influence of the tropical Atlantic versus the tropical Pacific on Caribbean rainfall. *J. Geophys. Res.*, 107, 3127, doi:10.1029/2001JC001097.

Torres-Valcárcel, A. R., 2018: Teleconnections between ENSO and rainfall and drought in Puerto Rico. *Int. J. Climatol.*, doi: 10.1002/joc.5444.

Trenberth, K. E., and C. J. Guillemot, 1995: Evaluation of the global atmospheric moisture budget as seen from analyses. *J. Climate*, 8, 2255–2272.

Trenberth, K. E., D. P. Stepaniak, and J. M. Caron, 2002: Accuracy of atmospheric energy budgets. *J. Climate*, 15, 3343–3360.

Trenberth, K. E., J. T. Fasullo, and J. Mackaro, 2011: Atmospheric moisture transports from ocean to land and global energy flows in reanalyses. *J. Climate*, 24, 4907–4924.

Williams, A. P., B. I. Cook, J. E. Smerdon, D. A. Bishop, R. Seager, and J. Mankin, 2017: The 2016 Southeastern U.S. drought: an extreme departure from centennial wetting and cooling. *J. Geophys. Res. Atmospheres*, 122, https://doi.org/ 10.1002/2017JD027523.

FIGURES

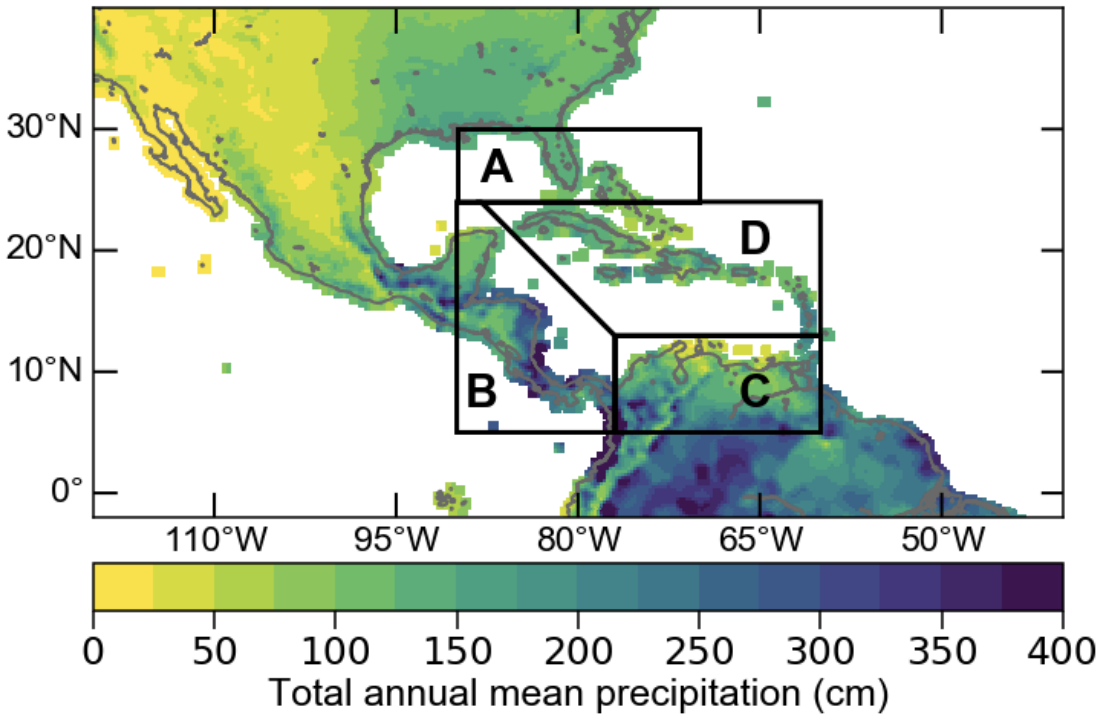

FIG. 1. Long-term annual mean precipitation in our study domain, and the subregions we have divided it in this work: (A) Florida Peninsula, (B) Central America, (C) northern South America, and (D) the Caribbean.

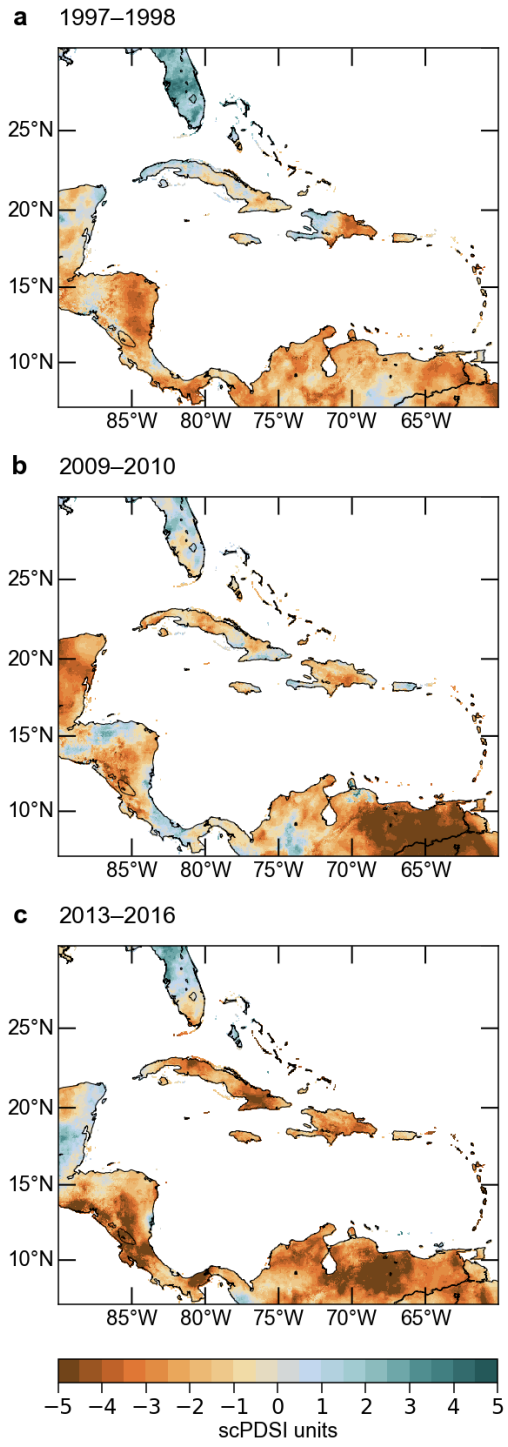

FIG. 2. The most severe and widespread droughts in the Caribbean, as seen in our Caribbean drought atlas (Herrera and Ault, 2017). These droughts co-occurred during two strong El Niño events (1997–1998, 2015–2016), and a "Modoki" El Niño (2009–2010).

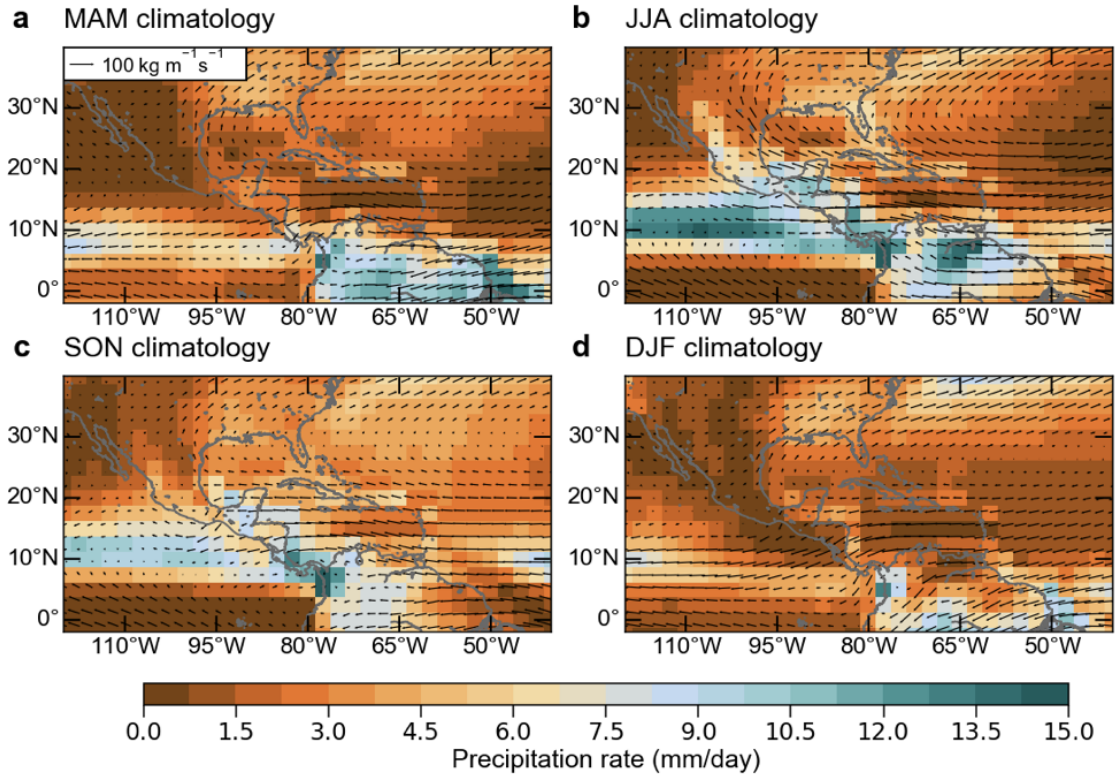

FIG. 3. Seasonal climatologies of precipitation and vertically-integrated moisture fluxes: (a) March–May, (b) June–August, (c) September–November, and (d) December–February.

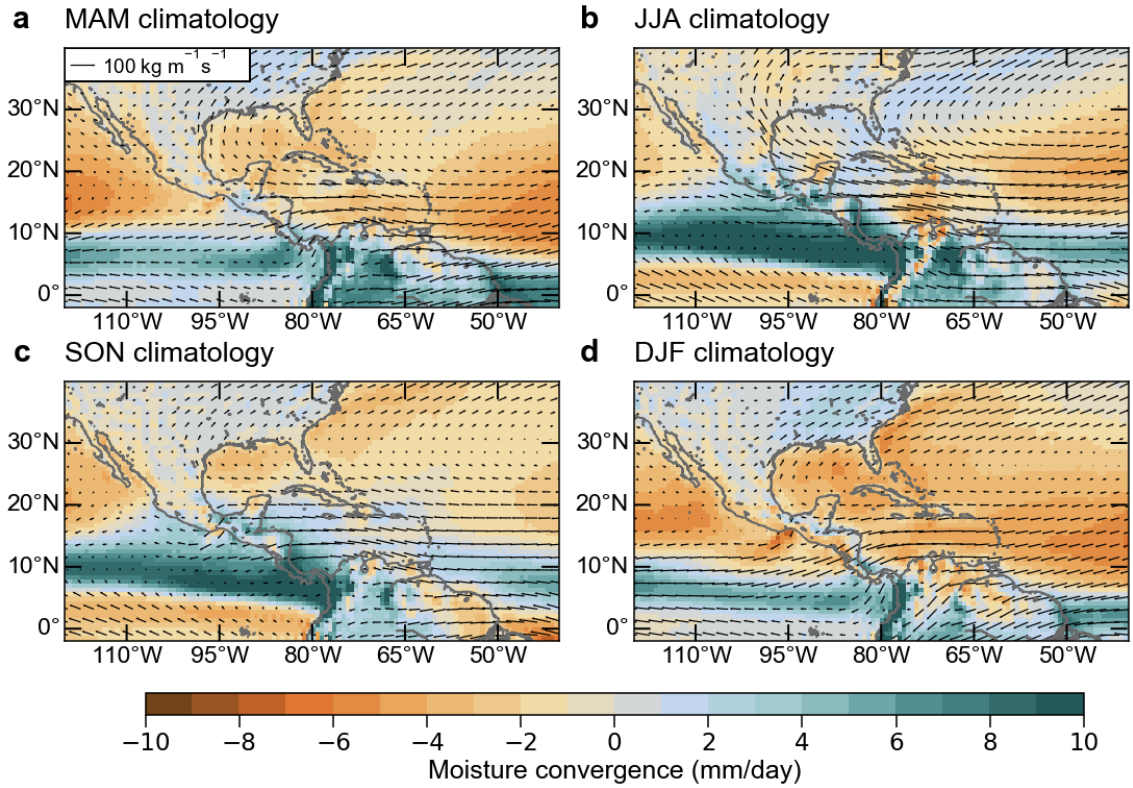

FIG. 4. Seasonal climatologies of precipitation minus evaporation (*P*–*E*) and vertically-integrated moisture fluxes: (a) March–May, (b) June–August, (c) September–November, and (d) December–February.

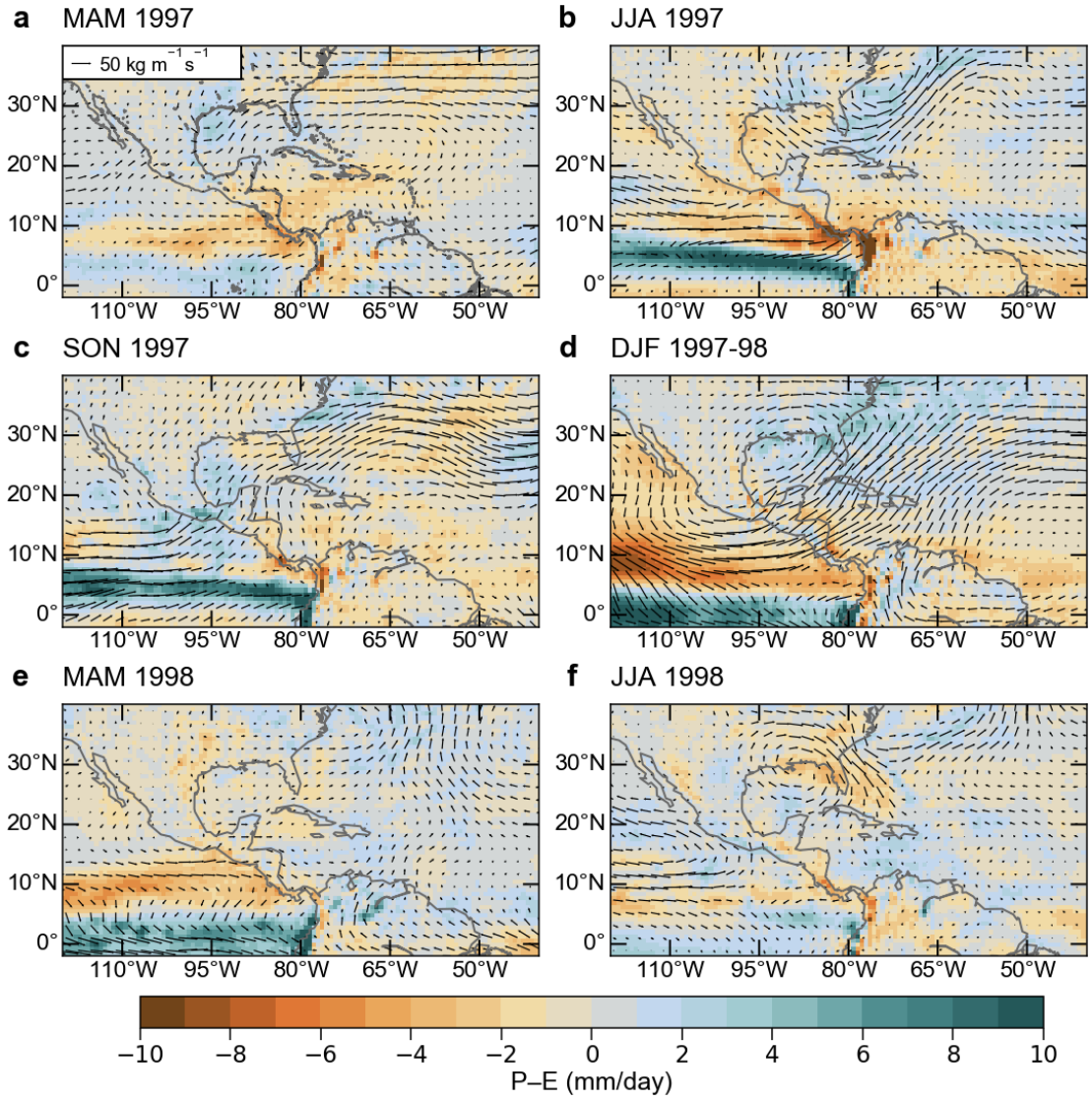

FIG. 5. The 1997–1998 drought *P–E* (shaded) and moisture flux (arrows) seasonal anomalies.

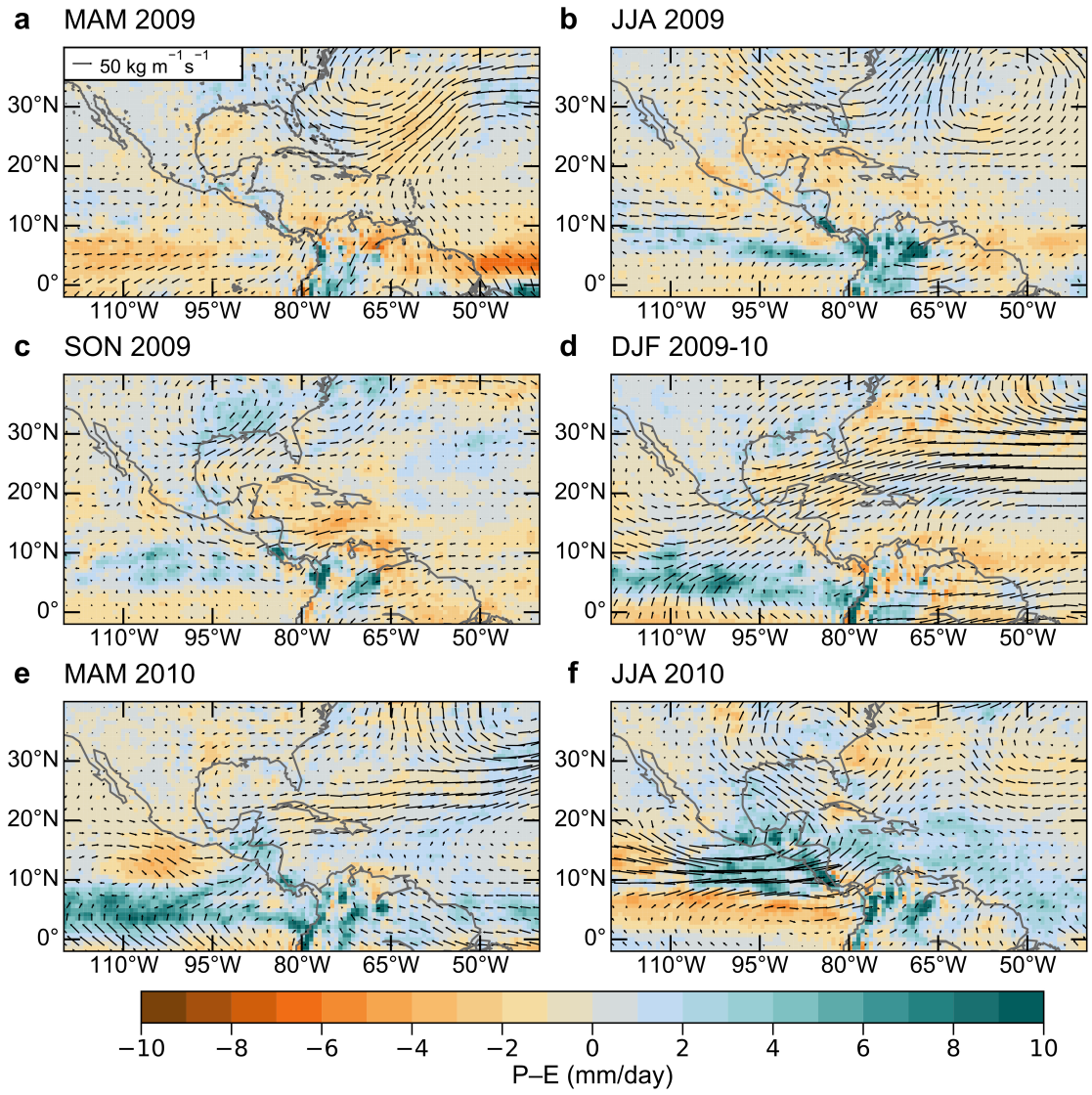

FIG. 6. The 2009–2010 drought *P–E* (shaded) and moisture flux (arrows) seasonal anomalies.

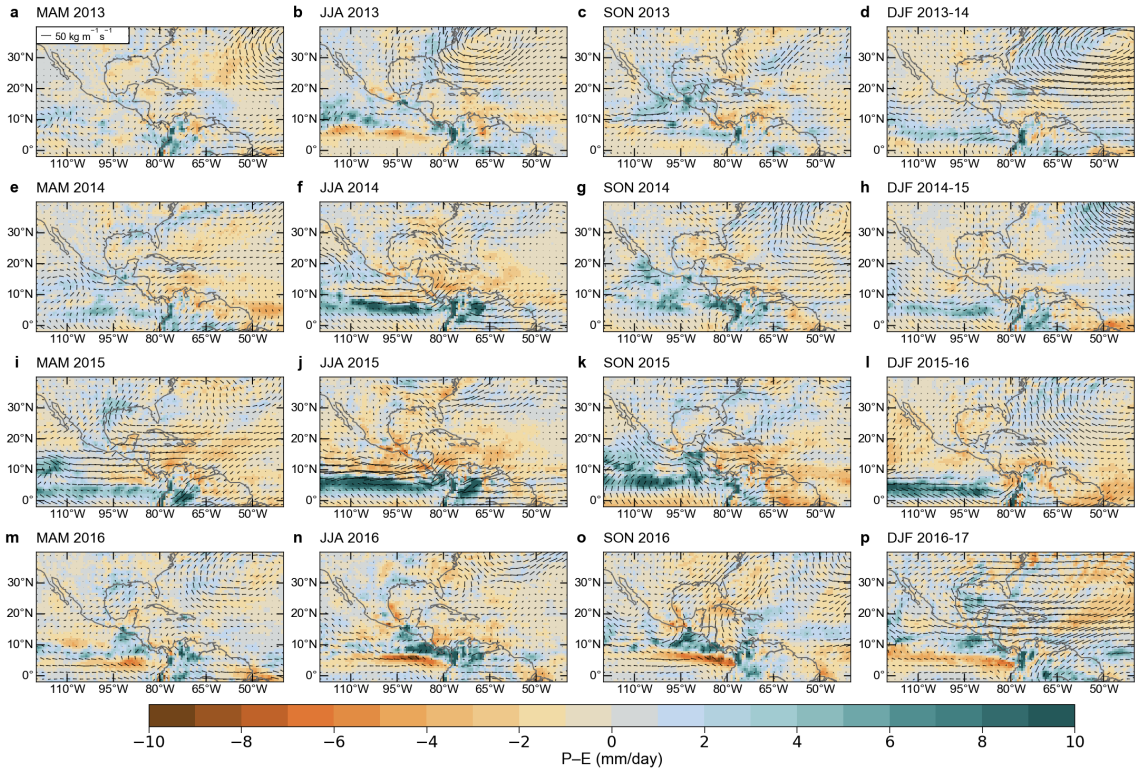

FIG. 7. as in Figures 5 and 6 but during the Pan-Caribbean drought. More panels are included because of the prolonged nature of this drought.

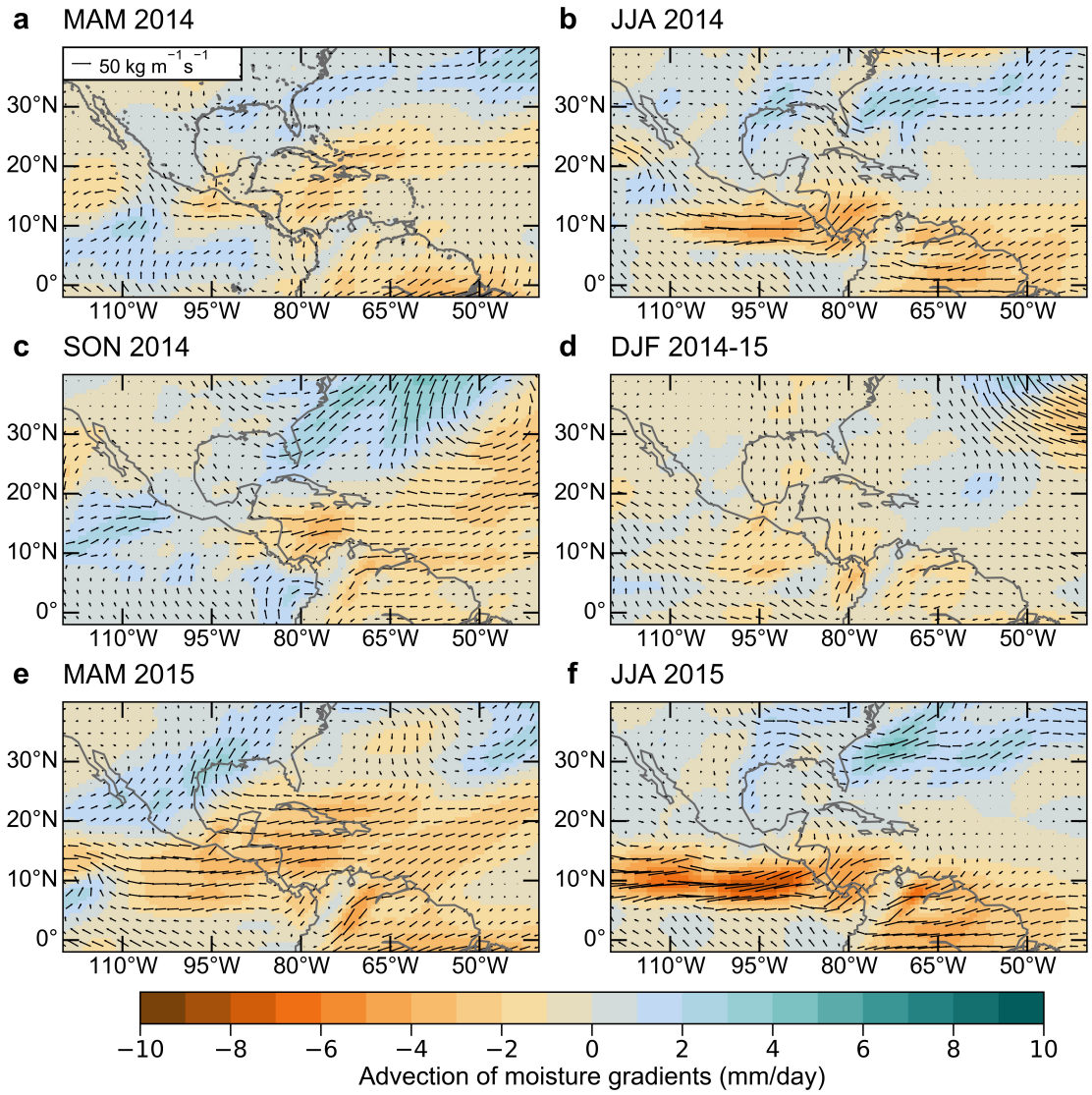

FIG. 8. Advection of moisture gradient anomalies between MAM 2014 and JJA 2015. Advection of moisture contributed to a drying during these years of the Pan-Caribbean drought mostly in CA and northern South America.

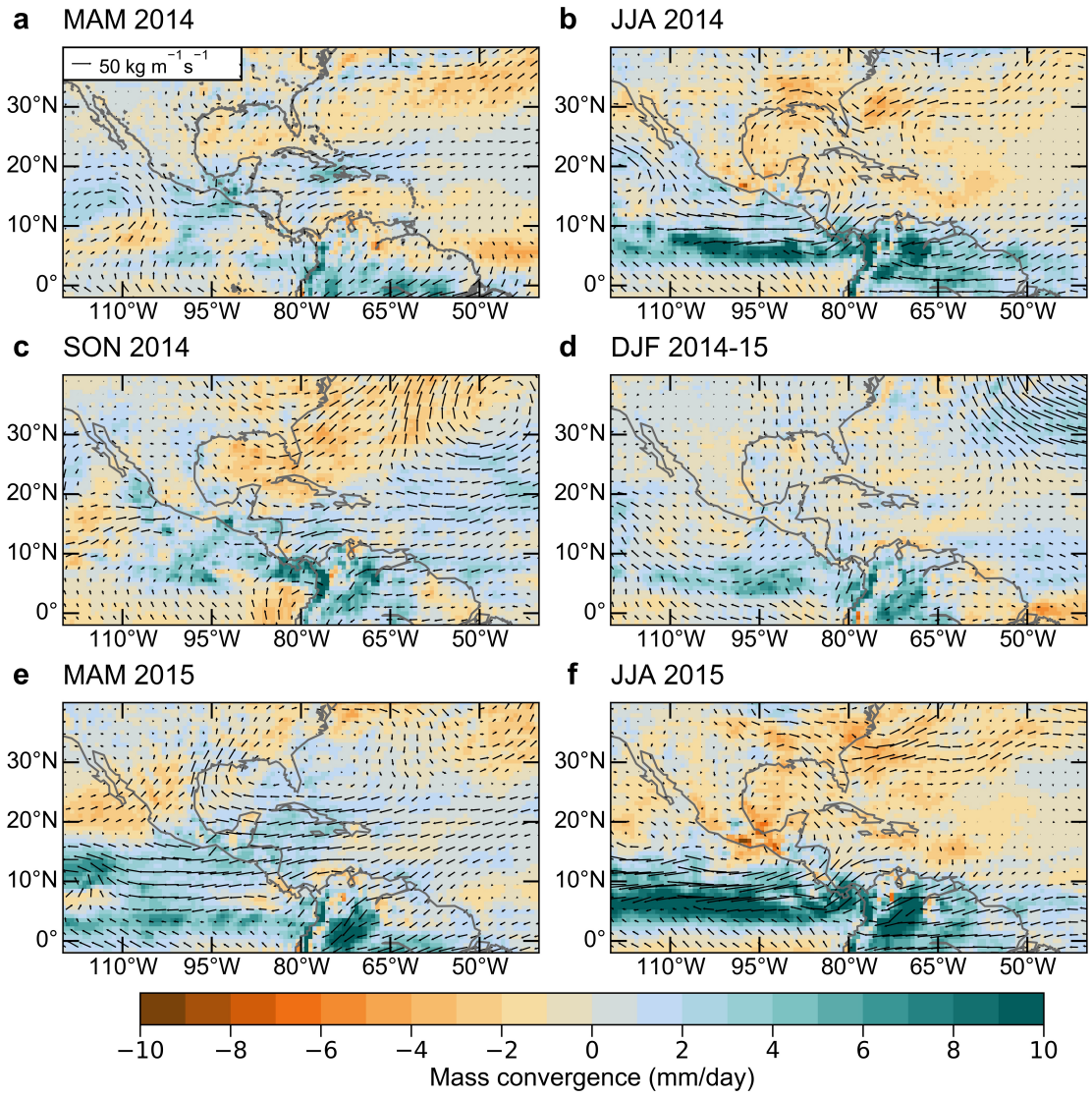

FIG. 9. As in Fig. 8 but for mass convergence anomalies. As opposed to the moisture advection, mass convergence contributed to wetting the eastern equatorial Pacific and northern South America. In some cases, mass convergence offset the drying from the advection, especially over Panama and northwestern South America.

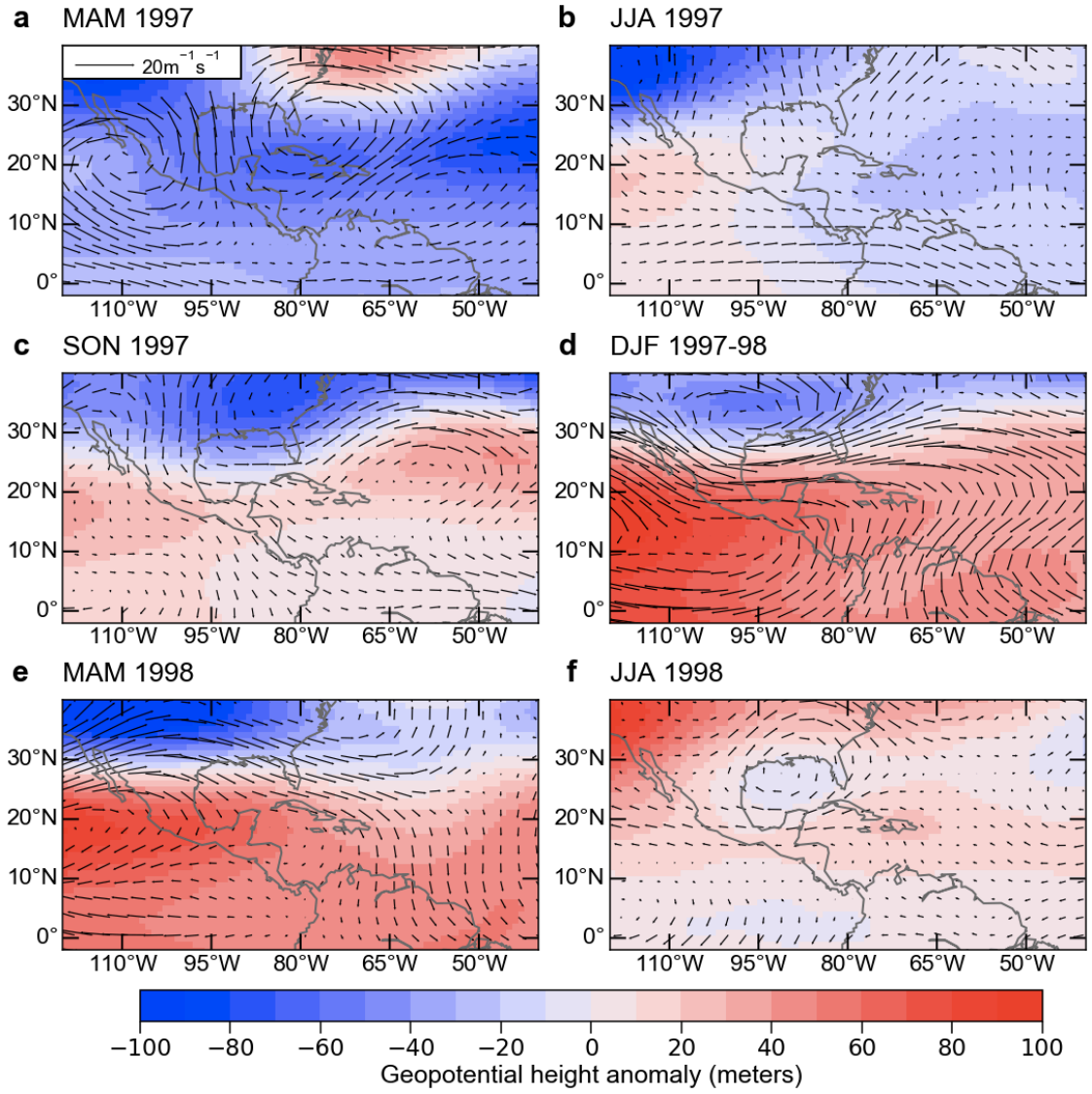

FIG. 10. ERA-Interim horizontal wind and geopotential height anomalies during the 1997–1998 drought in the Caribbean and CA. During the peak of El Niño in DJF of 1997–1998, there was a predominantly positive geopotential heights anomalies, which is consistent with the anomalous warm of El Niño in the tropical Pacific Ocean.

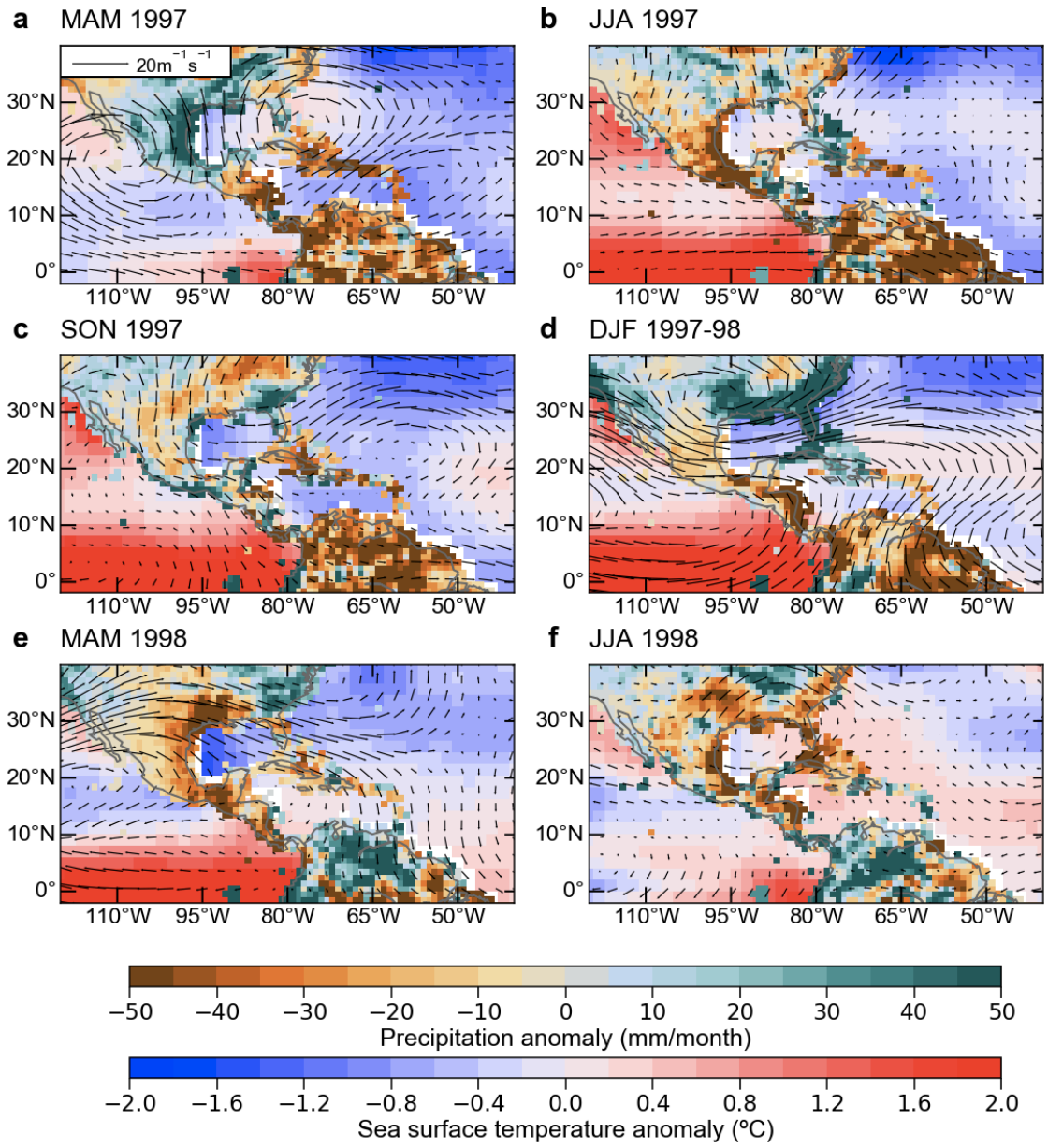

FIG. 11. Sea surface temperature (SST) and precipitation anomalies during the 1997–1998 drought in the Caribbean and CA. The characteristic positive SST anomalies over the eastern tropical Pacific was observed between the summer of 1997 (JJA) through the Spring (MAM) of 1998.

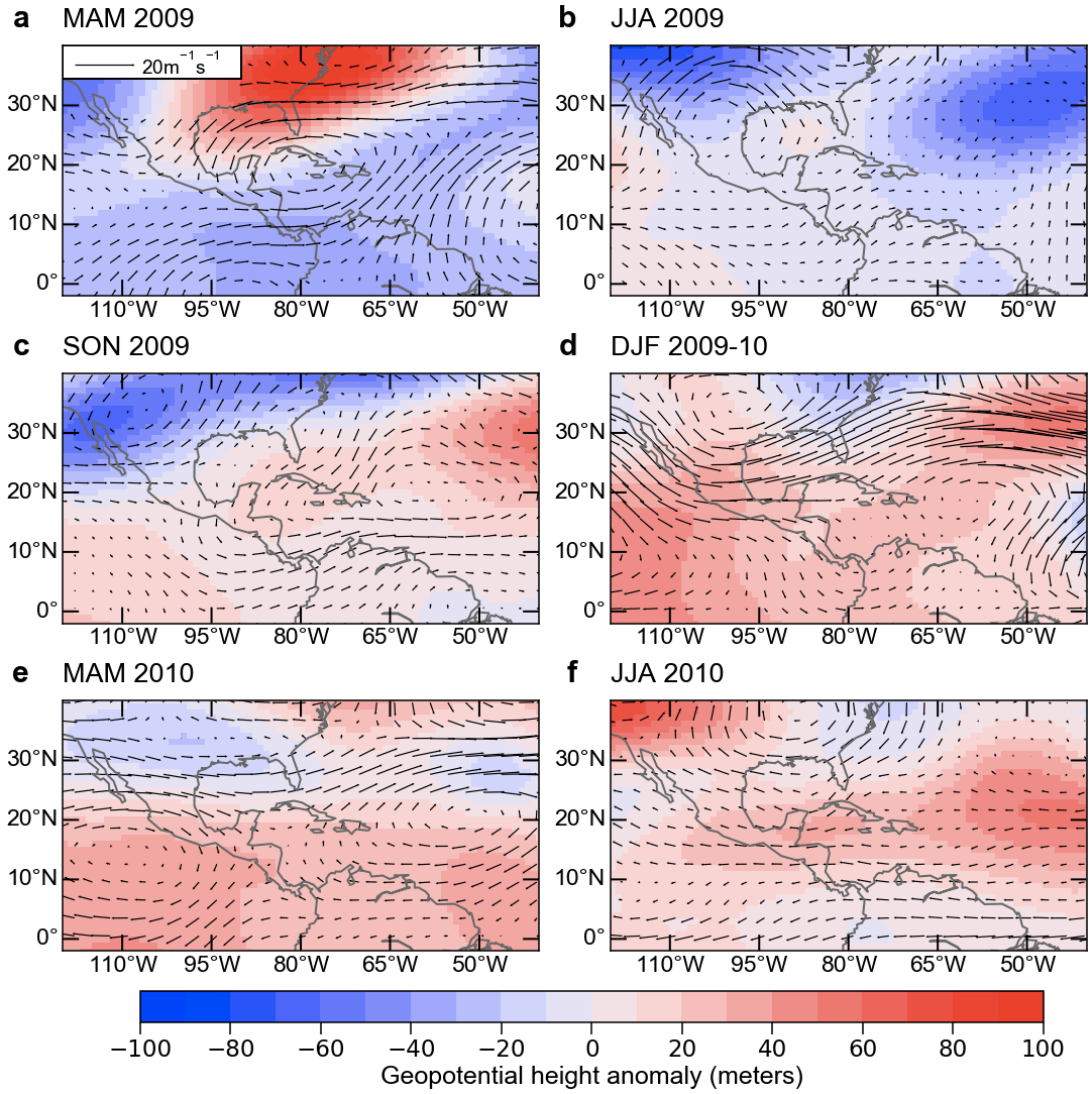

FIG. 12. As in Figure 10 but for the 2009–2010 drought.

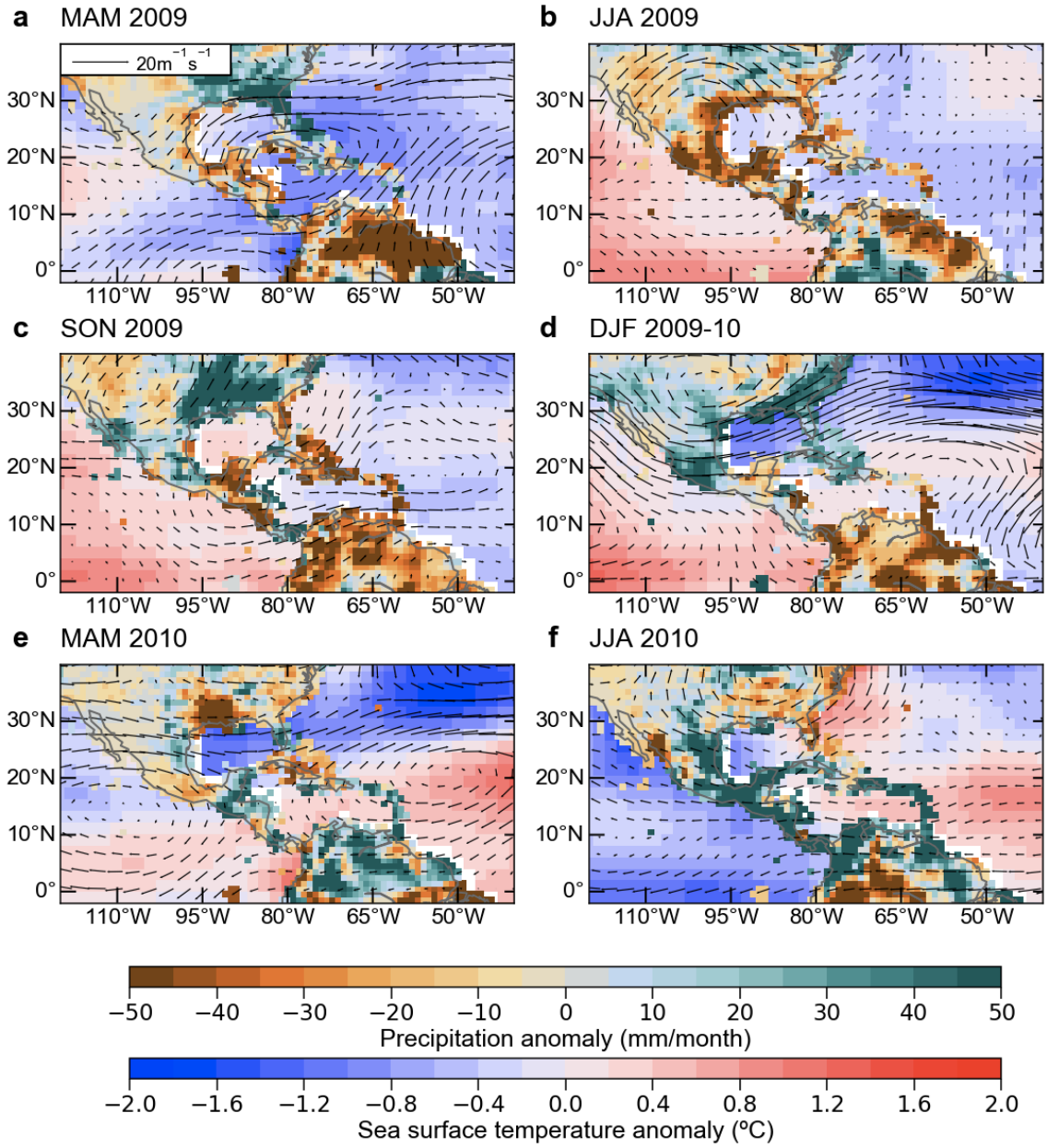

FIG. 13. As in Figure 11 but for the 2009–2010 drought.

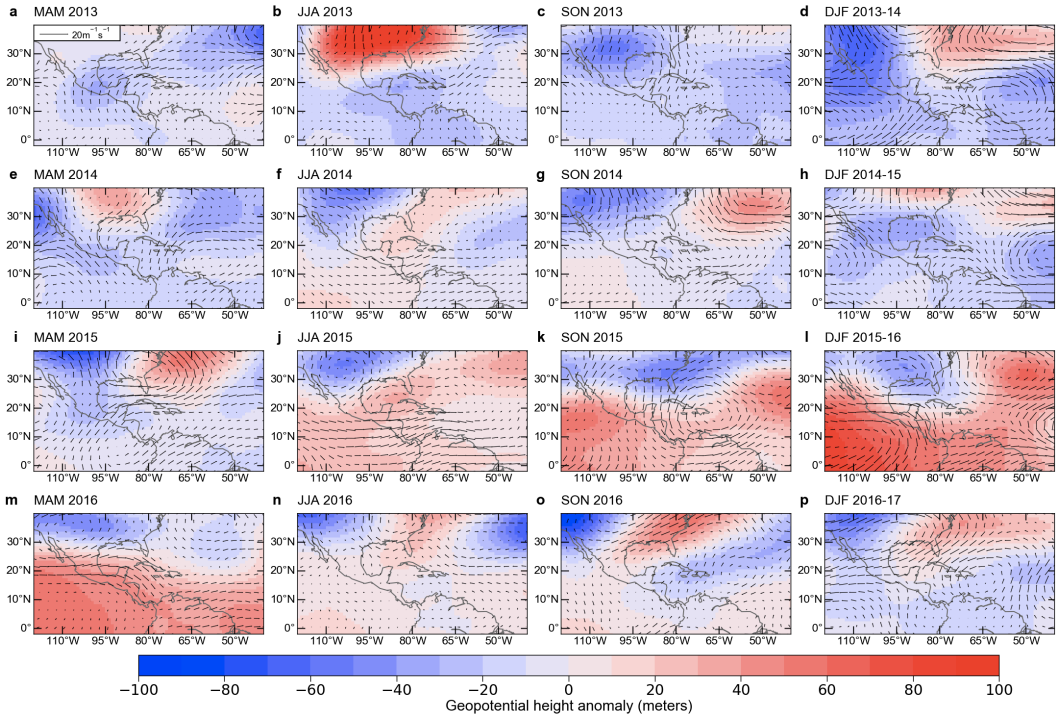

FIG. 14. As in Figure 10 but during the 2013–2016 Pan-Caribbean drought.

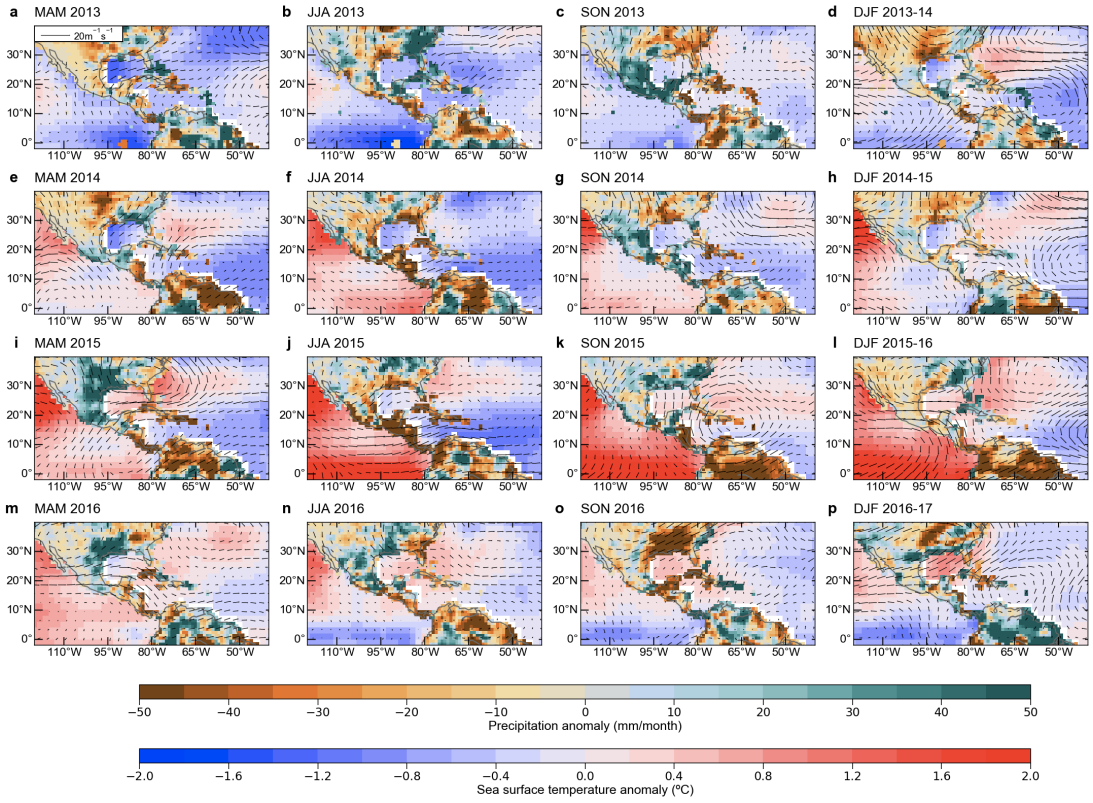

FIG. 15. As in Figure 11 but during the 2013–2016 Pan-Caribbean drought.

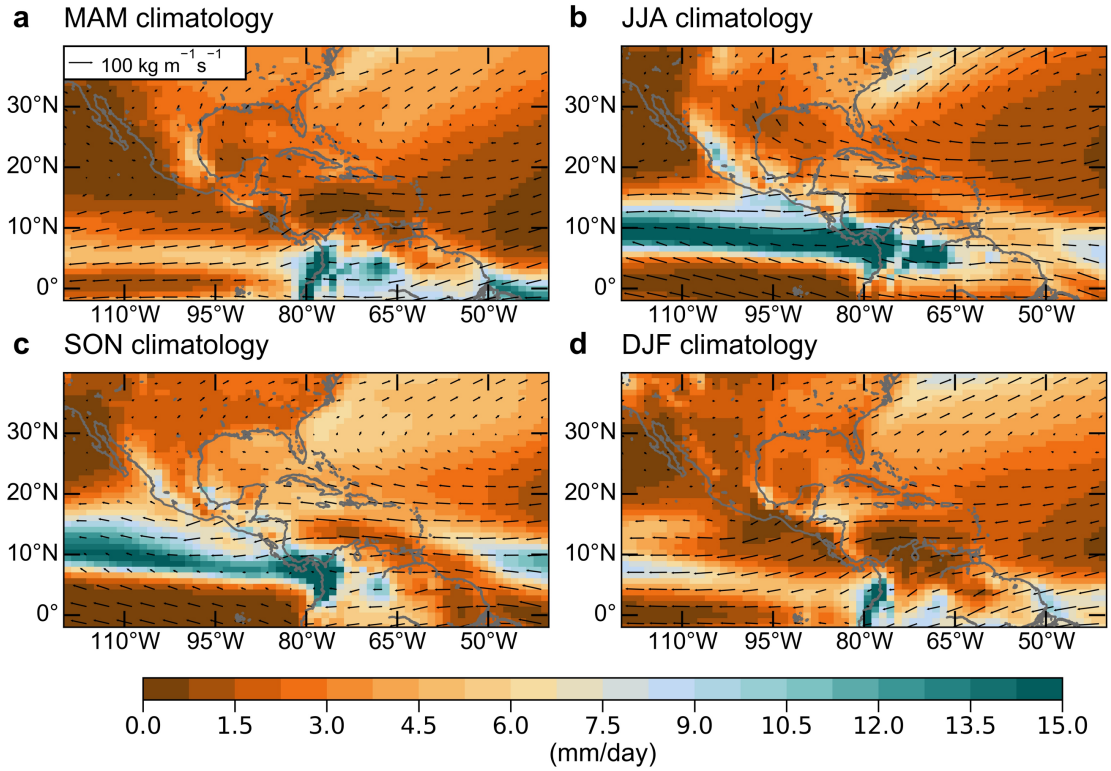

FIG. 16. Precipitation and moisture flux climatologies from LENS. The climatology was calculated from the full 1920–2006 interval.

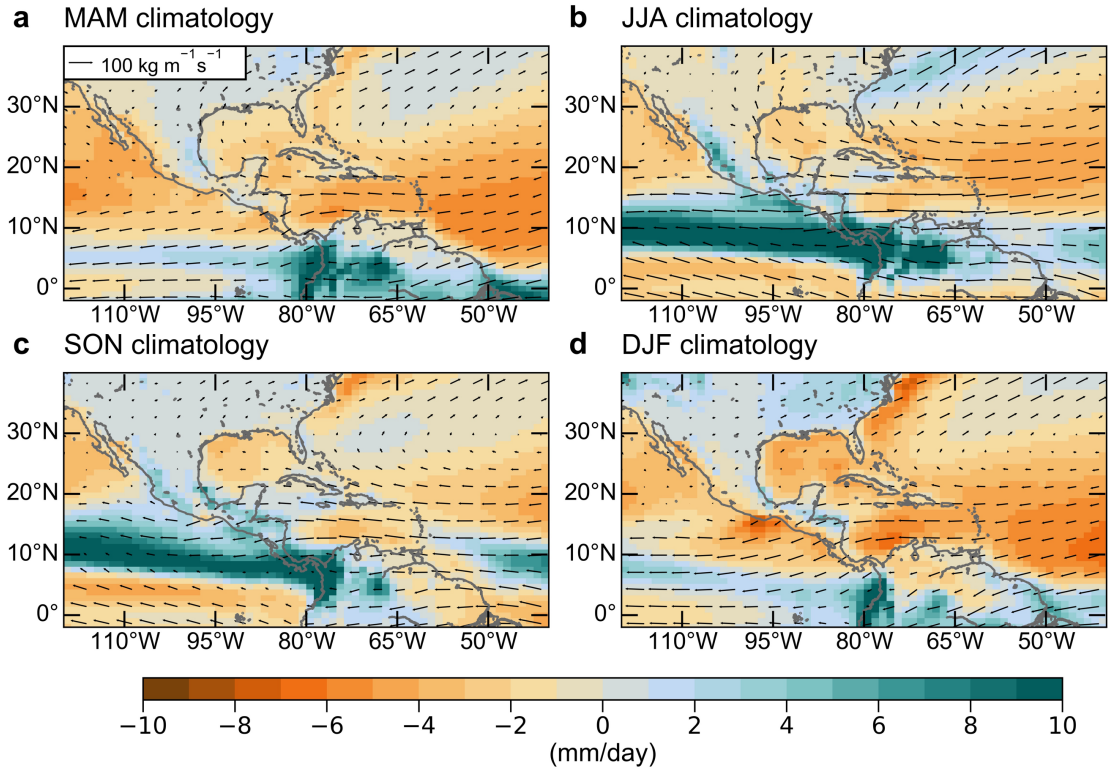

FIG. 17. As in Fig. 16 but for *P*–*E*.

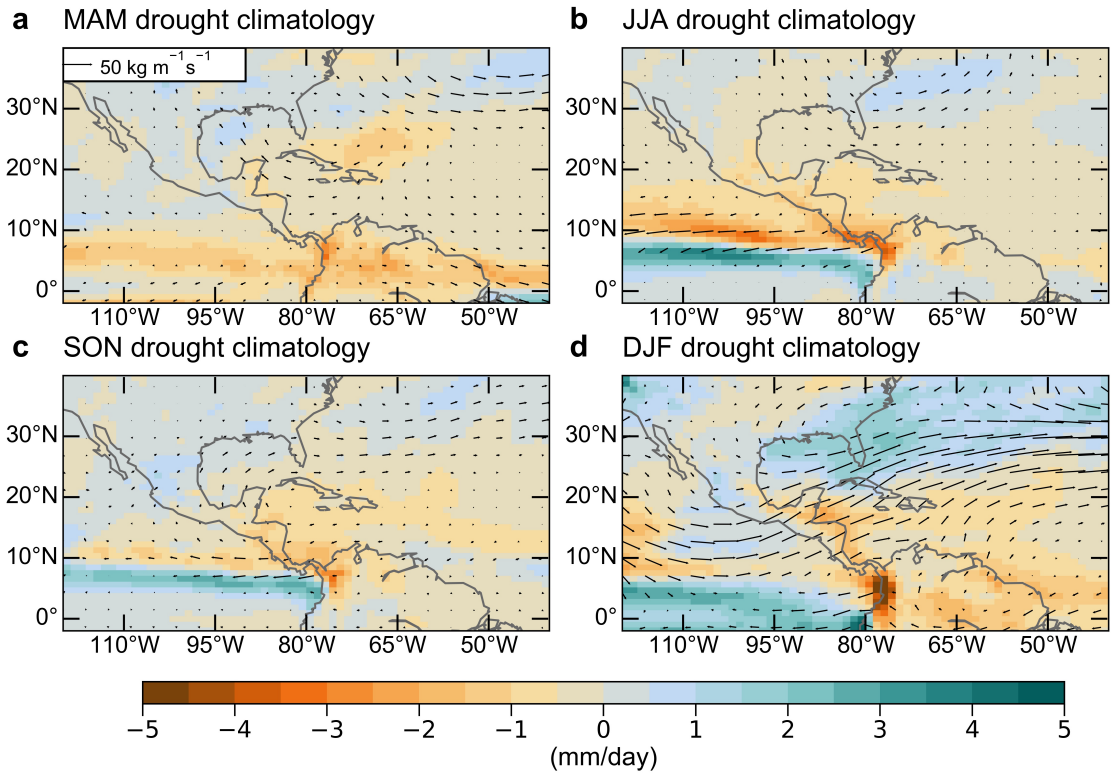

FIG. 18. Precipitation anomalies during drought in LENS.

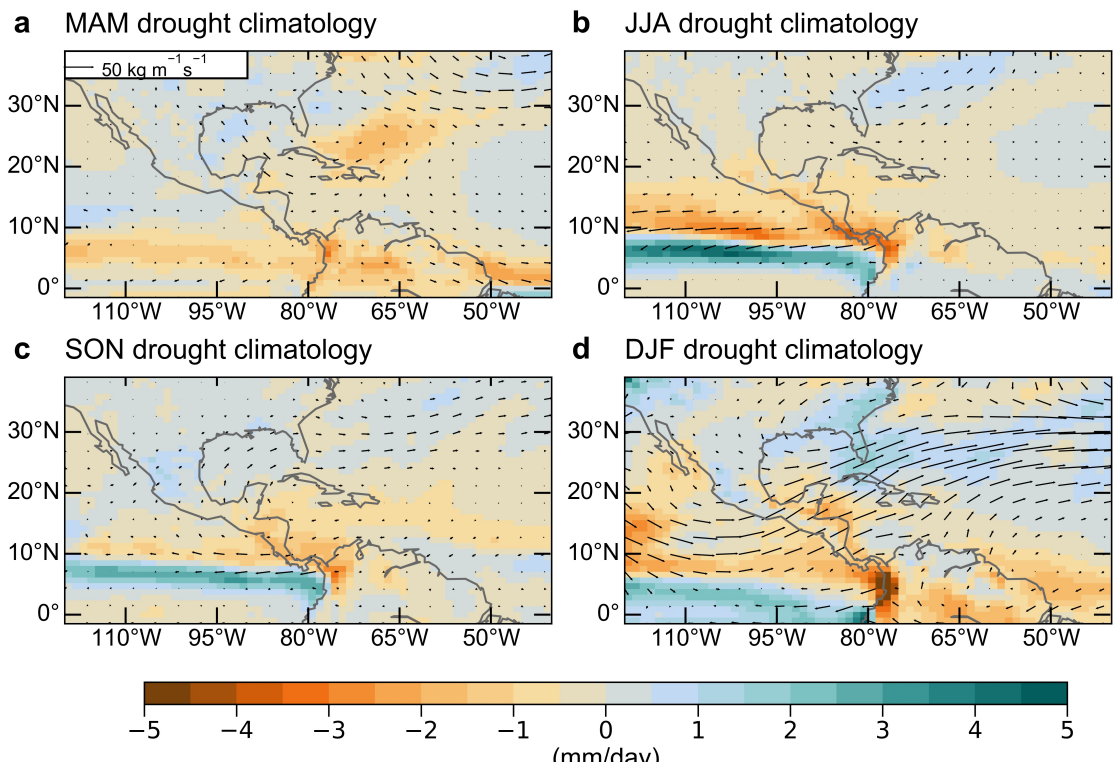

FIG. 19. As in Figure 18 but for *P*–*E* in LENS.

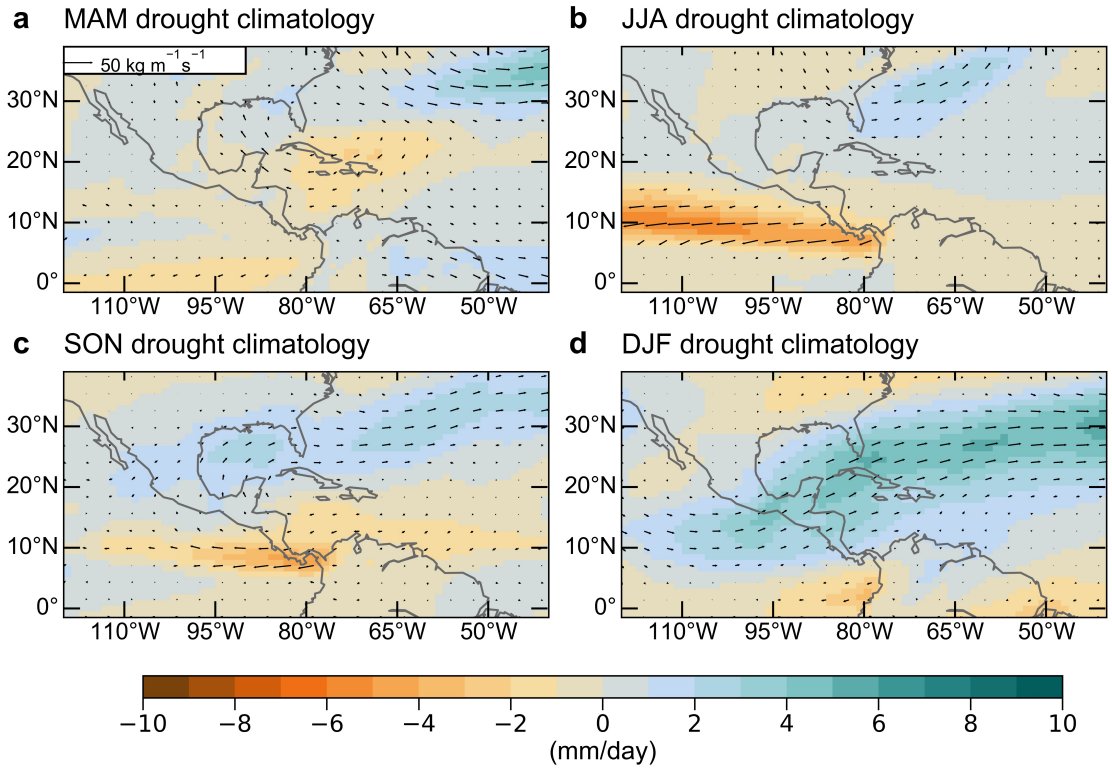

FIG. 20. Advection of moisture gradient anomalies from LENS. Consistent with observations, advection contributes to the drying over the eastern equatorial Pacific, just the north of the strong mass convergence associated with El Niño events.

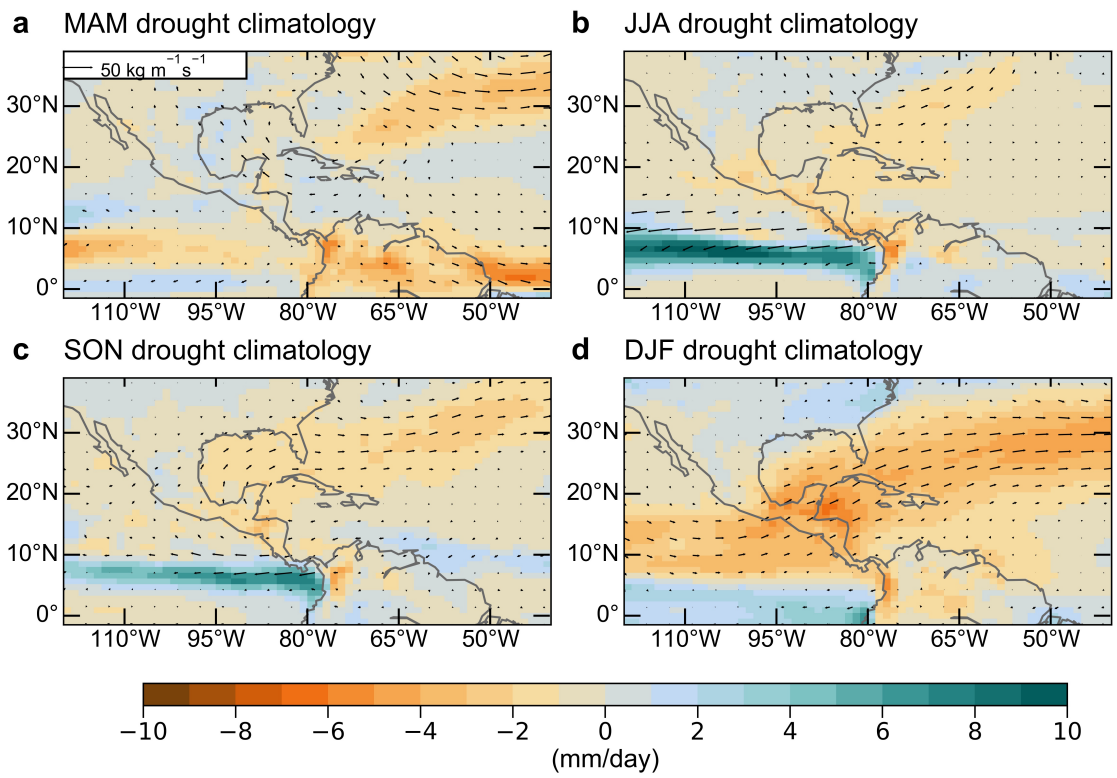

FIG. 21. As in Fig. 20 but for mass convergence anomalies. Notice the strong mass convergence over the eastern equatorial Pacific during JJA and SON, consistent with El Niño events from observations.

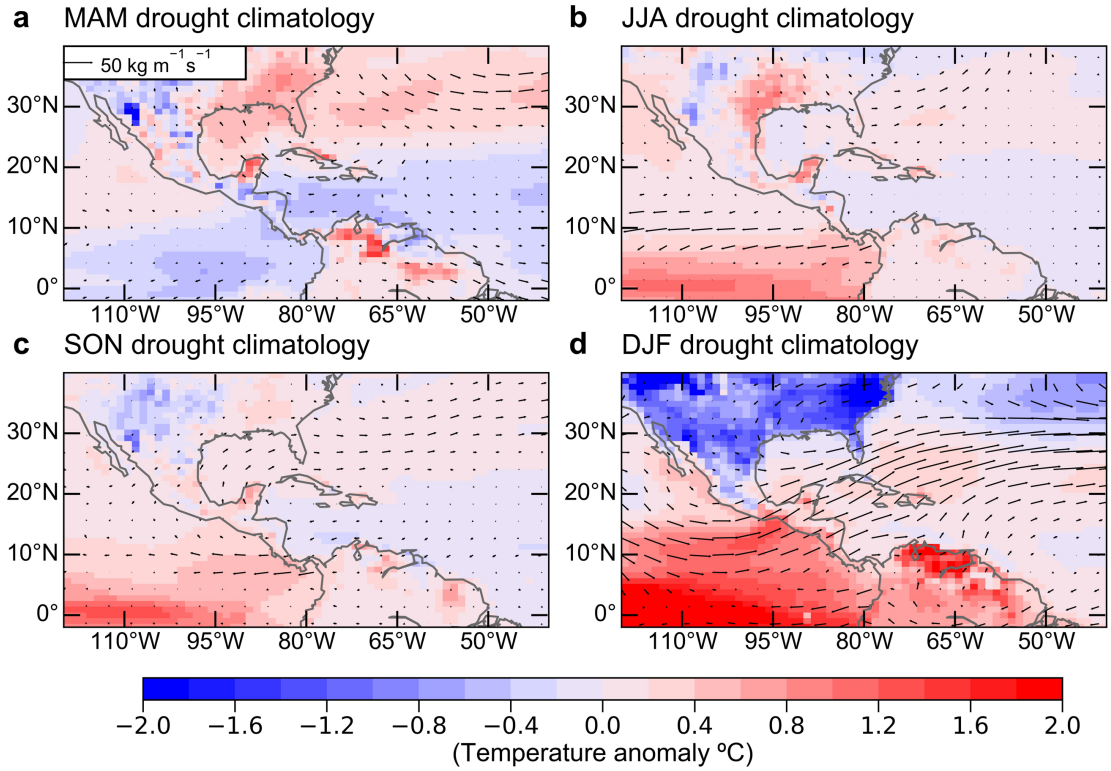

FIG. 22. Seasonal skin temperature anomalies during drought in LENS.

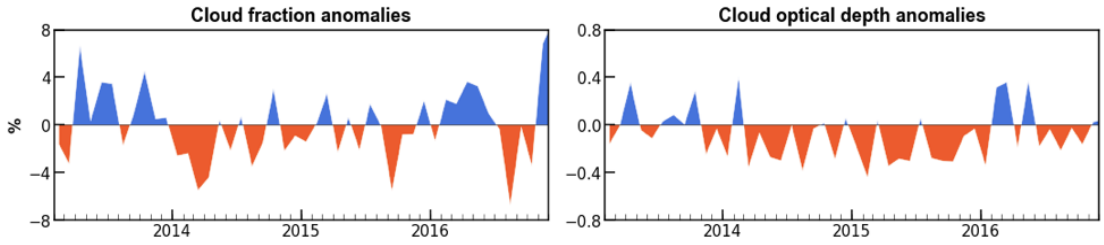

FIG. 23. Cloud fraction and cloud optical depth anomalies during the Pan-Caribbean drought observed from the NASA's CERES data. During the Pan-Caribbean drought a decreased deep convective clouds were observed, as evaluated from below-normal cloud optical depth anomalies.

TABLES

TABLE 1: Observed climate datasets used in this work.

Variable	Dataset	Native resolution	Period used	Reference
Precipitation	*GPCC	1º	1979–2016	Schneider et al. (2014)
	*GPCP	2º	1979–2016	Adler et al. 2003
Drought data	*CarDrought	4 km	1979–2016	Herrera and Ault (2017)
Sea surface temperature	*ERSST v5	2º	1958–2016	Huang et al. (2017)
Specific humidity	*ERA-Interim Reanalysis	0.5º	1979–2016	Dee et al. (2011)
Zonal wind component	*ERA-Interim Reanalysis	0.5º	1979–2016	Dee et al. (2011)
Meridional wind component	*ERA-Interim Reanalysis	0.5º	1979–2016	Dee et al. (2011)
Surface pressure	*ERA-Interim Reanalysis	0.5º	1979–2016	Dee et al. (2011)
Geopotential height	*ERA-Interim Reanalysis	0.5º	1979–2016	Dee et al. (2011)
Radiative fluxes	*CERES	1º	2001–2016	Loeb et al. (2012)
Surface pressure	*ERA-Interim Reanalysis	0.5º	1979–2016	Dee et al. (2011)

***GPCC: Global Precipitation Climatology Centre Version 7.**
***GPCP: Global Precipitation Climatology Project Version 2.3**
***CarDrought: Caribbean drought atlas**
***ERSST v5: Extended Reconstructed Sea Surface Temperature Version 5.**
***CERES: Clouds and Earth's Radiant Energy Systems.**

CONCLUSIONS AND IMPLICATIONS

In this work we have provided insights into the nature of drought variability, its trends, and its dynamics in the Caribbean and Central America between 1950 and 2016. We have introduced the first high-resolution (4 km) drought atlas for these regions using monthly estimates of the "self-calibrating" Palmer Drought Severity Index (scPDSI). This atlas served as the basis for assessing and diagnosing drought variability in the Caribbean during the period studied in this work, and it is currently available to the public through our lab's website: http://ecrl.eas.cornell.edu/products/caribbean-drought/index.html. To construct the atlas, we further used the UN Food and Agriculture Organization (FAO) reference potential evapotranspiration method (Allen et al. 1998), rather than the Thornthwaite formulation used in the original PDSI. Furthermore, to gain insights into the dynamical characteristics of drought in the Caribbean, we calculated the moisture budgets using monthly climate data from the ERA-Interim reanalysis and model outputs from the Community Earth System Model (CESM) Large Ensemble ("LENS"). We summarize our major findings with the following conclusions:

- Using our Caribbean drought atlas, we found that the 2013–2016 "Pan-Caribbean drought" was the most severe and widespread event seen in the Caribbean between (at least) 1950 and 2018. This drought not only affected the entire Caribbean Islands, but it also severely impacted northern South America and Central America, especially Guatemala, El Salvador, Honduras, and Panama. The Pan-Caribbean drought was also unprecedented because it affected portions of the Caribbean that usually receive above normal precipitation during El Niño events, such as western Cuba and Florida Peninsula.
- We also found that three of the four major droughts analyzed in this work (e.g., in 1974–1977, 1997–1998, 2009–2010, and 2013–2016) co-occurred in conjunction with El Niño events. However, El Niño effects at local scales are modulated by topography, especially in Central America and the Greater Antilles. For example, correlation coefficients calculated between sea surface temperature (SST) anomalies over the El Niño 3.4 region (5ºN–5ºS; 170º–

120ºW) and our drought atlas, in which we found significant negative correlations (suggesting drought with higher SST anomalies) between the eastern equatorial Pacific and the pacific coast of Central America. In contrast, positive correlations were observed with the Caribbean coast of the same region. At the same time, drought in the Caribbean was associated to colder SST over the tropical North Atlantic, which is also usually observed during strong El Niño events. Nevertheless, the signal of the eastern equatorial Pacific on hydroclimate variability in the Caribbean and Central America is further complicated by the interplay of the tropical North Atlantic variability, which also has a strong influence on Caribbean rain variation.

- We have found that climate change is already increasing drought risk in the Caribbean through temperature effects on evapotranspiration. For example, during the Pan-Caribbean drought, in addition to the precipitation deficits observed, higher temperature anomalies contributed to greater evapotranspiration rates. Because we do expect even warmer temperatures in the near future due to anthropogenic climate change, these findings provide insights into the nature of drought that the Caribbean might experience at higher frequency in the coming decades. Despite the simplicity of the linearly-detrended method we used to evaluate such anthropogenic warming contributions to the Pan-Caribbean drought severity, our results were consistent with those estimated from model outputs of temperature and net radiation from the fifth phase of the Coupled Model Intercomparison Project (CMIP5) during the period analyzed in this work (i.e., 1950–2016).
- Although the scPDSI does not account for increased CO_2 effects on plant physiology, using CMIP5 outputs of soil moisture and scPDSI we found that these vegetation feedbacks did not significantly reduced the anthropogenic contribution to the Pan-Caribbean drought. However, from this analysis, and because of the native resolution of most of the CMIP5 models, we cannot argue that these vegetation feedbacks will not play a role in future drought risk in the Caribbean. Regardless, we found that anthropogenic climate change certainly

contributed to the severity and spatial extent of the Pan-Caribbean drought by increasing the evaporative demand of moisture by the atmosphere, which agrees with previous work suggesting an increased drought risk in the region as anthropogenic greenhouse gas concentrations increase in the atmosphere.

- Finally, drought dynamics in the Caribbean is characterized by a strong moisture divergence over the Caribbean Sea and northeastern South America (especially during El Niño events), which further occurs along with an anomalously high moisture convergence in the eastern equatorial Pacific Ocean. Furthermore, a "seesaw" pattern is also noticeable between the tropical Pacific and North Atlantic during drought in these regions. That it, a warmer than normal tropical Pacific is associated with drought in the Caribbean (especially the eastern portion) and Central America, and this usually occur along with colder temperatures in the tropical North Atlantic. Although with biases in the magnitude of *P–E* and moisture flux anomalies, LENS does a good job in simulating the overall dynamics underpinning drought in the Caribbean. Nevertheless, using subdaily outputs from this model would provide a more accurate evaluation of LENS on simulating the dynamics of drought in this region.